APERTURE AVERAGING EFFECTS ON SCINTILLATION AND THE TEMPORAL-FREQUENCY POWER SPECTRUM

Howard Robert Hall

NAVAL POSTGRADUATE SCHOOL
Monterey, California

THESIS

APERTURE AVERAGING EFFECTS ON SCINTILLATION AND THE TEMPORAL-FREQUENCY POWER SPECTRUM

by

Howard Robert Hall

June 1976

Thesis Advisor: A. W. Cooper

UNCLASSIFIED

SECURITY CLASSIFICATION OF THIS PAGE (When Data Entered)

REPORT DOCUMENTATION PAGE		READ INSTRUCTIONS BEFORE COMPLETING FORM
1. REPORT NUMBER	2. GOVT ACCESSION NO.	3. RECIPIENT'S CATALOG NUMBER
4. TITLE (and Subtitle) Aperture Averaging Effects on Scintillation and the Temporal-Frequency Power Spectrum		5. TYPE OF REPORT & PERIOD COVERED Master's Thesis; June 1976 6. PERFORMING ORG. REPORT NUMBER
7. AUTHOR(s) Howard Robert Hall		8. CONTRACT OR GRANT NUMBER(s)
9. PERFORMING ORGANIZATION NAME AND ADDRESS Naval Postgraduate School Monterey, California 93940		10. PROGRAM ELEMENT, PROJECT, TASK AREA & WORK UNIT NUMBERS
11. CONTROLLING OFFICE NAME AND ADDRESS Naval Postgraduate School Monterey, California 93940		12. REPORT DATE June 1976 13. NUMBER OF PAGES 134
14. MONITORING AGENCY NAME & ADDRESS(if different from Controlling Office) Naval Postgraduate School Monterey, California 93940		15. SECURITY CLASS. (of this report) Unclassified 15a. DECLASSIFICATION/DOWNGRADING SCHEDULE

16. DISTRIBUTION STATEMENT (of this Report)

Approved for public release; distribution unlimited.

17. DISTRIBUTION STATEMENT (of the abstract entered in Block 20, if different from Report)

18. SUPPLEMENTARY NOTES

19. KEY WORDS (Continue on reverse side if necessary and identify by block number)

Aperture Averaging
Marine Boundary Surface Layer
Temporal-Frequency Power Spectra
Turbulence
Avalanche Detector
Scintillation

20. ABSTRACT (Continue on reverse side if necessary and identify by block number)

Aperture averaging effects on the measurement of scintillation and on the temporal-frequency power spectrum have been examined in the marine boundary surface layer using a He-Ne (6328 Å) laser beam propagating over various path lengths and under varying turbulence conditions. Two significant results have been obtained: (1) For scintillation measurements, a vanishingly small receiver can best

DD FORM 1 JAN 73 1473 (Page 1) EDITION OF 1 NOV 65 IS OBSOLETE S/N 0102-014-6601

UNCLASSIFIED

SECURITY CLASSIFICATION OF THIS PAGE (When Data Entered)

be approximated by using an aperture of diameter $D_{min} = (Z/k)^{1/2}$. (2) The aperture averaging correction factor for an aperture diameter $D > D_{min}$ decreases as the level of turbulence increases.

Data have also been obtained supporting the theoretical prediction that an increase in aperture diameter reduces the high frequency power content of the temporal-frequency power spectrum.

Aperture Averaging Effects on Scintillation and the Temporal-Frequency Power Spectrum

by

Howard Robert Hall
Lieutenant, United States Navy
B.S., United States Naval Academy, 1970

Submitted in partial fulfillment of the
requirements for the degree of

MASTER OF SCIENCE IN PHYSICS

from the

NAVAL POSTGRADUATE SCHOOL
June 1976

ABSTRACT

Aperture averaging effects on the measurement of scintillation and on the temporal-frequency power spectrum have been examined in the marine boundary surface layer using a He-Ne (6328 Å) laser beam propagating over various path lengths and under varying turbulence conditions. Two significant results have been obtained: (1) For scintillation measurements, a vanishingly small receiver can best be approximated by using an aperture of diameter $D_{min} = (Z/k)^{1/2}$. (2) The aperture averaging correction factor for an aperture diameter $D > D_{min}$ decreases as the level of turbulence increases.

Data have also been obtained supporting the theoretical prediction that an increase in aperture diameter reduces the high frequency power content of the temporal-frequency power spectrum.

TABLE OF CONTENTS

I. INTRODUCTION

Scintillation is the term used to describe the atmospherically induced intensity fluctuations of a constant power output laser source as seen from a distant detection device. The precise manner in which a detector's aperture size affects the measured value of the variance of the intensity fluctuations as a function of distance from the source and lasing wavelength has not been satisfactorily established. Several aperture averaging experiments have been conducted under various turbulence conditions to examine this effect along with an analysis of the frequency power spectrum effects of aperture size.

A. PROJECT HISTORY

Since 1971 an interdisciplinary group of professors principally from the Departments of Physics and Chemistry, Meteorology, and Mechanical Engineering have been investigating under a Navy research contract various aspects of laser beam propagation over the marine boundary layer. Data has been gathered thus far on (1) Modulation Transfer Function (MTF) at wavelengths of .4880 μm, .6328 μm, 1.06 μm and 10.6 μm, (2) scintillation at .4880 μm, .6328 μm and 10.6 μm, (3) extinction at .6328 μm, (4) beam wander and (5) beam spread.

The stated general objectives of the project are: (1) to develop an understanding of the factors affecting the propagation of optical radiation through the atmosphere, particularly

the marine boundary surface layer, the lowest 30 meters above the ocean surface; (2) to develop the capability of predicting optical system performance on the basis of point meteorological measurements.

Previous thought had been that the sea surface might present a smooth, isothermal layer, giving rise to little turbulence effect on a propagating light beam. However, early experiments in the project proved that this was not the case.

B. SCINTILLATION

1. Description

The twinkling one sees when observing distant light sources is a physical realization of scintillation. This appears as fluctuation in the output from a small photo-detector illuminated by a distant source.

In the general case of finite beam propagation, measured intensity fluctuation can be caused by any or all of the following: (1) source output power fluctuations, (2) beam wander, (3) detector motion through a plane perpendicular to the optical axis, (4) a temporal wavefront breakup within the beam caused by small-scale spatial and temporal variations of the dielectric constant (or index of refraction) of the lower atmosphere. Of these, the most critical for experimentation or information transmission are the turbulence effects of scintillation, beam wander and beam spread, since they cannot be overcome by system refinement.

2. The Effects of Turbulence on a Propagating Wavefront: Physical and Theoretical Models

a. Kolmogorov Model of Turbulence

Currently the only well-developed model of atmospheric turbulence is that of Kolmogorov. It is basically a velocity turbulence model that assumes homogeneous, isotropic turbulence. The turbulence is assumed to be composed of small turbulent eddies, or turbules, each of characteristic temperature and density (hence index of refraction), as illustrated in Figure 1. In this homogeneous turbulence model, often referred to as "frozen-in turbulence," fluctuations in the dielectric constant over a vanishingly small volume element are due to atmospheric temperature variations produced by the turbules being swept past the reference point by the mean wind.

Let $n(\underline{r},t)$ be the refractive index at point $\underline{r}$ in space at time t. Then

$$(1) \qquad n(\underline{r},t) = \frac{1}{\tau}\int_{o}^{\tau} n(\underline{r},t')dt' + n_1(\underline{r},t',\tau)$$

$$= \langle n(\underline{r},t)\rangle_{\tau} + n_1(\underline{r},t',\tau)$$

where $n_1(\underline{r},t',\tau)$ is the deviation from the average value at point $\underline{r}$ and time t.

The refractive index structure function gives the mean square variation in the refractive index between

two points in space:

$$(2) \qquad D_n(\rho) = \langle [n_1(\underline{r}_1) - n_1(\underline{r}_2)]^2 \rangle ,$$

where $$\rho = |\underline{r}_1 - \underline{r}_2| .$$

The cross-correlation function of refractive index fluctuations is defined as

$$(3) \qquad B_n(\rho) = \frac{1}{\tau} \int_0^\tau n_1(\underline{r}_1, t') n_1(\underline{r}_2, t') dt'$$

$$= \langle n_1(\underline{r}_1) n_1(\underline{r}_2) \rangle$$

Under the assumption that homogeneous turbulence is present and the appropriate statistical averages for $B_n(\rho)$ and $D_n(\rho)$ are stationary in time and locally constant in space, one finds that

$$(4a) \qquad D_n(\rho) = 2[B_n(0) - B_n(\rho)]$$

$$(4b) \qquad B_n(\rho) = \frac{1}{2}[D_n(\infty) - D_n(\rho)] .$$

As ρ becomes smaller, correlation increases while the structure function decreases.

According to the Kolmogorov theory of turbulence, for $\ell_o << \rho << L_o$, that is, within the "Inertial Subrange" of scales,

(5) $$D_n(\rho) = C_N^2 \rho^{2/3} ,$$

and the corresponding temperature structure function for meteorological measurements is

(6) $$D_T(\rho) = C_T^2 \rho^{2/3} .$$

ℓ_o and L_o are the inner and outer scales of turbulence in the Inertial Subrange (Figure 2), and C_N and C_T are the refractive index structure constant and temperature structure constant, respectively. If ℓ (or L) represents the diameter of a turbulent eddy, ℓ_o is the scale size below which viscous effects cause the conversion of turbulent energy into heat, and subsequent destruction of the eddy ensues. L_o, the outer scale size, is the minimum scale at which energy enters the turbulent system from wind shear and heat flux.

For Kolmogorov turbulence, an analytical form (the von Karman form) of the power spectrum (the three-dimensional Fourier transform of the cross-correlation function), which illustrates its approximate dependence on ℓ_o and L_o, is

(7) $$\Phi_n(K) = 0.033 C_n^2 (K^2 + L_o^{-2})^{-11/6} \exp[-(K\ell_o)^2] .$$

For $K >> L_o$, this reduces to the more common form used by Tatarski,

$$(8) \qquad \Phi_n(K) = 0.033\, C_n^2 K^{-11/3} \exp[-K^2/K_m^2] \ ,$$

where $$K_m = \frac{2\pi}{\ell_o} \ .$$

b. Physical Models

(1) Tatarski's Geometrical Optics Approach. The physical mechanism through which turbulence induces beam breakup is by the focusing of sections of a wavefront produced by the inhomogeneities in the index of refraction over the propagation path. Tatarski uses a plane wave incident upon a series of closely packed refractive spheres of various sizes. Using the paraxial approximation, a sphere acts as a lens with focal length $f = \frac{a}{2n_1}$, where n_1 is the index of refraction perturbation within the sphere. For a = 1mm, ℓ_o of the Inertial Subrange, and $n_1 = 10^{-6}$, f = 500m. For a = 1m, the lowest L_o limit, f = 500 Km. Thus, for most applications in a turbulent medium, a detector will appear to be closer to the "lens" than to the focal plane. The fractional intensity change induced per sphere will be small. Over a long path, perturbation effects will be multiplicative and the resulting wavefront at the receiver will be neither coherent nor of constant intensity. In addition, diffraction effects, important at distances

greater than the Rayleigh range, $Z_R = ka^2$, limit the ability of the sphere to focus the incident wave. The amplitude fluctuation induced by a sphere at a distance Z from a detector is estimated [Ref. 1] as

$$(9) \qquad \frac{\delta A}{A_o} \approx \frac{Z}{f} = \frac{2|n_1|Z}{a} , \quad Z << f .$$

From equation (9) it is seen that the largest fluctuations are produced by the smallest turbules. By the geometrical optics approach [Ref. 1], within the Rayleigh range, amplitude fluctuations increase as the cube of the distance, are dominated by the smallest turbules, and are independent of wavelength:

$$(10) \qquad \langle (\frac{\delta A}{A_o})^2 \rangle \approx C_N^2 \, \ell_o^{-7/3} \, Z^3 .$$

However, this model does not take into account diffraction effects, important for smaller turbules that contribute most toward amplitude fluctuations.

(2) Diffraction Effects. Diffraction effects are taken into account by assuming that spheres of radius $a_i \approx (\lambda Z')^{1/2}$, where Z' is the distance from the center of the turbule to the receiver, contribute very weak, diffracted waves with no focusing effects at the receiver. Substituting $(\lambda Z)^{1/2}$ for ℓ_o in equation (10), the mean square amplitude fluctuations become

$$(11) \qquad \left\langle \left(\frac{\delta A}{A_o}\right)^2 \right\rangle \simeq C_N^2 \, k^{7/6} \, Z^{11/6} \quad , \quad k\ell_o^2 \leq Z \leq kL_o^2 \; .$$

Now defining $\frac{\delta A}{A_o} \equiv \chi_1$ where χ_1 is the first order log-amplitude for $|\chi_1| << 1$, Tatarski has calculated the first order log-amplitude variance with diffraction effects considered for plane waves as

$$(12) \qquad \langle \chi_1^2 \rangle = 0.31 \, k^{7/6} \, C_N^2 \, Z^{11/6} \quad ,$$

and for spherical waves as

$$(13) \qquad \langle \chi_1^2 \rangle = 0.13 \, k^{7/6} \, C_N^2 \, Z^{11/6} \quad ,$$

both restricted to $Z >> k\ell_o^2$. Lutomirski and Yura [Ref. 1] state that one would expect the behavior of a beam wave to lie between that of the plane and spherical waves. Therefore, one may use equations (12) and (13) as bounds for weak scintillation. For inhomogeneous turbulence, equations (12) and (13) can be expressed in the form

$$(14) \qquad \langle \chi_1^2 \rangle^{(P)} = 0.56 \, k^{7/6} \int_o^Z (Z-Z')^{5/6} \, C_N^2(Z') dZ' \quad , \quad \text{and}$$

$$(15) \qquad \langle \chi_1^2 \rangle^{(S)} = 0.56 \, k^{7/6} \int_o^Z (Z-Z')^{5/6} \left(\frac{Z'}{Z}\right)^{5/6} C_N^2(Z') dZ' \quad ,$$

where Z is the distance from source to receiver and Z' from turbule to receiver. For plane wave propagation, the fluctuation effects are weighted by the factor $(Z-Z')^{5/6}$, which has its maximum value near the source and approaches zero at the receiver. The spherical wave weighting factor, $[(Z-Z')(\frac{Z'}{Z})]^{5/6}$, has its maximum value at the midpoint of the path and approaches zero at both ends.

c. Theoretical Models, The Scalar Wave Equation

Numerous attempts have been made to solve the scalar wave equation to relate the electric field E(r) of an optical wave passing through a turbulent medium to the refractive index fluctuations. Three approaches currently in use for solving this problem are: (1) Geometrical Optics, (2) The Born Approximation, and (3) The Rytov Approximation. Below is a brief resumé of the approaches, their assumptions, highlights, methods of approach and restrictions. All three methods start with the scalar wave equation,

$$\nabla^2 E + k^2 n^2 E = 0 \quad . \tag{16}$$

The derivation of this has assumed a medium with no free charges or current density, with the permeability of free space, that correlations between the components of the field polarized in different directions can be neglected, and that $\lambda << \ell_o$.

(1) Geometrical Optics Approach

(a) Amplitude fluctuations are attributed to the focusing and defocusing of the rays by the curvature of the turbulent eddies along the path.

(b) Phase fluctuations are calculated from the changes in velocity as a ray passes through regions of different refractive index.

(c) Diffraction effects are ignored.

(d) The major restriction is $(\lambda Z)^{1/2} << \ell_o$. This reduces the applicability of this model to extremely short ranges. Note: When $(\lambda Z)^{1/2} \geq \ell_o$, diffraction effects become important.

(2) The Born Approximation

(a) This is a perturbation technique to incorporate diffraction effects into the scalar wave equation. $n = \langle n \rangle + n_1$ is substituted into the scalar wave equation, which is solved for the first order solution for E. The result is

$$E_1 = \int_V 2k^2 n_1(\underline{r}')E_o(\underline{r}')G(|\underline{r}-\underline{r}'|)dv' \quad , \tag{17}$$

where $G(|\underline{r}-\underline{r}'|)$ is the free space Green's function.

(b) The perturbation technique used is valid as long as the amplitude fluctuations remain small.

(c) It is assumed that the field at the receiver is the sum of the original incident field and the field scattered one time from a turbule.

(d) It requires that $(\lambda Z)^{1/2} \geq \ell_o$.

(e) Restrictions: In the optical wavelength range, amplitude fluctuations often become very large compared to the average value of the amplitude. Multiple scattering effects cannot be ignored (but are). References 2, 3 and 4 contain details on multiple scattering effects.

(3) The Rytov Approximation (Method of Smooth Perturbations)

(a) This is a perturbation technique applied to a transformation of the scalar wave equation using the exponential notation:

$$E(r) = e^{\psi(r)} \quad , \quad \psi(r) = \chi(r) + i\phi(r) \quad .$$

$\psi(r)$, the "complex amplitude," contains both the amplitude and phase terms. Using this, the scalar wave equation takes the form of the non-linear Ricatti Equation,

$$\nabla^2\psi + \nabla\psi\cdot\nabla\psi + k^2(1 + \delta n) = 0 \quad . \tag{18}$$

Now applying the perturbation technique $\psi = \psi_o + \psi_1$, where ψ_1 is the perturbation to the average value of ψ_o, one obtains the solution,

$$\psi_1(r) = \frac{1}{E_o(r)} \int_V G(\underline{r}-\underline{r}')[\nabla\psi_1\cdot\nabla\psi_1 + k^2\delta n]E_o(\bar{r}')dV' \quad . \tag{19}$$

The "Rytov Approximation" is $\nabla\psi_1 \cdot \nabla\psi_1 = |\nabla\psi_1|^2 = 0$, and results in

$$(20) \qquad \psi_{10}(r) = \frac{k^2}{E_o(r)} \int_V G(\underline{r}-\underline{r}')\delta n(\underline{r}')E_o(\underline{r}')dV' \ ,$$

the "first order complex phase." A higher order solution for ψ_1 can be obtained by iteration.

(b) This approach includes multiple scattering effects. Caveat--these effects are included in an inflexible way which does not depend on the turbulence or other correlated parameters [Refs. 5 and 6].

(c) The method requires that the perturbations of the log-amplitude, the real part of the complex phase $[\chi_1 \equiv \log_e(\frac{A}{A_o})]$, and of the phase, ϕ_1, be small, i.e., $\lambda|\chi_1| << 1$ and $\lambda|\phi_1| << 1$.

(d) Restrictions: $\lambda << \ell_o$, $|\nabla\psi_{10}| << |k^2\delta n|$, $\frac{\lambda^3 L}{\ell_o^4} << 1$.

(e) This method includes both the Geometrical Optics approach and Born Approximation as special cases.

(f) Theoretical evidence indicates the equation derived for amplitude fluctuations is valid as long as $\langle\chi^2\rangle \leq 0.8$ (Saturation Condition) [Refs. 7-10].

3. The Form of the Probability Distribution for Amplitude Fluctuations

The application of the Central Limit Theorem in the derivation of the log-amplitude equation leads to a

prediction of a log-normal distribution of the amplitude fluctuations, or equivalently, a normal distribution for log-amplitude. Some authors [Refs. 11 and 12], taking a different approach, argue for a Rayleigh distribution. The Rayleigh distribution arises when the field at the receiver is the sum of the electric field components from randomly scattered wavefront elements. This occurs in line-of-sight propagation when the effects of the turbulent medium are far from the receiver. In line-of-sight propagation where the receiver is located within the region in which turbulent effects are being introduced, the field at the receiver is the result of multiplicative effects on a single wavefront. Strohbehn [Ref. 2] shows that $\psi_r(t)$, representing the amplitude and phase terms of a single wavefront, is composed of the sum of a large number of independent components, and from the Central Limit Theorem, has a normal or Gaussian distribution.

For long enough paths, however, both the multiplicative effects on a single wavefront and additive effects from different wavefronts may be important, and Strohbehn indicates that it is difficult to tell which effect will be predominant. Empirical results thus far support a log-normal distribution [Refs. 14, 15 and 16 and Figure 9]. However, extremely long-range experiments have not as yet been conducted.

C. THE SATURATION OF SCINTILLATION

1. Description

For plane and spherical waves (only) in homogeneous turbulence and for weak fluctuations,

$$\sigma_n^2 = \frac{\sigma_I^2}{\langle I \rangle^2} \approx 4 \langle \chi_1^2 \rangle = \sigma_{\ell I}^2 , \tag{21}$$

where σ_n^2 is the normalized variance and $\sigma_{\ell I}^2$ the log-intensity variance. In terms of the log-intensity variance, equations (12) and (13) become

$$\sigma_{\ell I}^2 = 1.24\, k^{7/6} Z^{11/6} C_N^2 , \text{ (Plane Wave)} \tag{22a}$$

$$\sigma_{\ell I}^2 = 0.52\, k^{7/6} Z^{11/6} C_N^2 , \text{ (Spherical Wave).} \tag{22b}$$

Empirical results [Refs. 14, 32-34] have shown that when the optically measured $\sigma_{\ell I}$, $\sigma_{\ell I}^{(OM)}$, is plotted against Tatarski's theoretical values of equation (22), $\sigma_{\ell I}^{(t)}$, calculated from the temperature structure constant, the measured scintillations reach their maximum value for $\sigma_{\ell I}^{(t)}$ of the order of 1 to 3, then decrease slowly and tend to level off with increasing $\sigma_{\ell I}^{(t)}$. This approximately constant value for $\sigma_{\ell I}^{(OM)} \geq 1$ is called the saturation effect. Yura [Ref. 17] states that the log-amplitude covariance function differs both quantitatively and qualitatively in the saturation region from that under unsaturated conditions.

The actual value of $\sigma_{\ell I}^2$ at which saturation begins has not yet been strictly established. Strohbehn [Ref. 2] indicates that saturation begins for $\sigma_{\ell I}^2 > 0.8$, while de Wolf [Ref. 18] and Lutomirski and Yura [Ref. 1] maintain it occurs for $\sigma_{\ell I}^2 > 1$.

2. Theory

De Wolf has defined the saturation region in terms of $\sigma_{\ell I}^2$ as

$$1 < \sigma_{\ell I}^2 << \frac{kL_o^2}{Z} , \tag{23}$$

or equivalently,

$$1 < K_m^{1/2}\, kZ^2\, C_n^2 << \frac{kL_o^2}{Z} . \tag{24}$$

De Wolf [Ref. 18] improves upon the Rytov approximation by introducing a directional correction factor, $\cos[\underline{K}\cdot\underline{\rho}(Z)]$, to allow rays being refracted by a turbule to be deflected by more than one Fresnel zone size off the optical axis. This directional factor eliminates the focusing effect of turbules close to the detection point and introduces serious interference effects and therefore amplitude changes.

De Wolf has calculated the log-amplitude variance in the saturation region based on plane wave theory to be

$$\langle \chi_1^2 \rangle = 0.41(K_m^{7/3}\, Z^3\, C_n^2)^{-1/6} , \quad K_m = \frac{2\pi}{\ell_o} , \tag{25}$$

and derives the result that the irradiance distribution remains log-normal in the saturation regime. However, to verify this equation, K_m must be determined empirically, which is difficult to do.

Other authors have attempted to describe the saturation effect by carrying higher order terms through the wave equation. The efforts have been extremely complex mathematically and have resulted in little success.

D. TEMPORAL-FREQUENCY SPECTRUM ANALYSIS

1. Description

Like any other time-varying signal, a fluctuating voltage response from the output of a photodetector possesses an autocorrelation function. The power spectrum of the signal can be found (1) manually by computing the Fourier transform of the signal's autocorrelation function, or (2) electronically by feeding the fluctuating voltage signal into a Spectrum Analyzer, which performs the transform. The power spectrum shows the frequencies composing the signal and their relative magnitudes. Current theories (described below) indicate that the maximum frequency that will be present will be directly proportional to the mean wind speed normal to the propagation path and inversely proportional to the square root of the wavelength used and distance of propagation. Theories differ significantly on the effects of aperture diameter on the power spectrum.

2. Theories

a. Lutomirski and Yura

It is assumed that all refractive index inhomogeneities of the turbulent medium move convectively with mean wind speed $\bar{v}$ everywhere along the propagation path. Intensity fluctuations will be dominated by the velocity component normal to the propagation path, $\bar{v}_n$. If the transverse intensity correlation length is ρ_ℓ, then the correlation period of the intensity fluctuations at a point is of the order of $\tau_o \simeq \rho_\ell/\bar{v}_n$, giving a characteristic frequency of

$$f_o = \frac{\bar{v}_n}{2\pi\rho_\ell} . \tag{26}$$

Using Lutomirski and Yura's [Ref. 1] model of $\rho_\ell \simeq (Z/k)^{1/2}$, the maximum frequency cutoff for scintillation effects at a point is given by

$$f_c = \frac{\bar{v}_n}{(2\pi\lambda Z)^{1/2}} \tag{27}$$

The normalized photodetector signal at time t is given by

$$S'(t) = \frac{S(t) - \langle S(t)\rangle}{\langle S(t)\rangle} = \int \frac{I(\underline{P}_1,t) - \langle I\rangle}{\langle I\rangle} d^2\underline{P}_1 , \tag{28}$$

and from the frozen-in turbulence assumption,

$$(29) \qquad S'(t+\tau) = \int \frac{I(\underline{P}_2 - \bar{v}_n\tau, t) - \langle I\rangle}{\langle I\rangle} d^2\underline{P}_2 \ .$$

The autocorrelation function of S'(t) is

$$(30) \quad R_{s'}(\tau) = \langle s'(t)s'(t+\tau)\rangle = \frac{1}{\langle I\rangle^2} \int C_I(|\underline{P}_1 - \underline{P}_2 + \bar{v}_n\tau|) d^2\underline{P}_1 d^2\underline{P}_2 \ .$$

The power spectrum is the Fourier transform of $R_{s'}(\tau)$ and is given by

$$(31) \quad \Phi_{s'}(\omega) = \frac{8\pi}{\langle I\rangle^2 \omega} \int_0^\infty C_I\left(\frac{\omega}{\bar{v}_n}\sqrt{1+x^2}\right)\left[\frac{2J_1\left(\frac{\omega}{\omega_D}\sqrt{1+x^2}\right)}{\frac{\omega}{\omega_D}\sqrt{1+x^2}}\right]^2 dx.$$

Aperture averaging effects on the spectrum are seen through the ω_D term, $\omega_D = \frac{2\bar{v}_n}{D}$, where D is the aperture diameter. J_1 is a first-order Bessel function and $C_I(K)$ is the two-dimensional power spectrum of the intensity fluctuations. The square bracketed term falls off rapidly for $\omega > \omega_D$, displaying the filtering action of the aperture diameter.

When plotting a normalized power spectrum, $\Phi_n(f)$, versus log f, a change in λ, Z, $\bar{v}_n$ or D effects a shift of $\Phi_n(f)$ along the log f axis.

b. Clifford [Ref. 19]

A theoretical solution for the temporal-frequency spectrum of scintillation at a vanishingly small aperture is given as shown for plane and spherical waves in Figure 3. The corresponding asymptotic forms are given

for plane waves as

$$\Phi(f) = 0.44\ (\sigma_{\ell A}^2)\left(\frac{1}{f_o}\right)(1 + 0.27\ \Omega^{4/3}) \quad , \ \Omega << 1 \ , \tag{32}$$

$$\Phi(f) = 1.44\ (\sigma_{\ell A}^2)\left(\frac{1}{f_o}\right)\ \Omega^{-8/3} \quad , \ \Omega >> 1 \ , \tag{33}$$

and for spherical waves as

$$\Phi(f) = 0.245\ (\sigma_{\ell A}^2)\left(\frac{1}{f_o}\right)[1 + 0.119\ \Omega^{4/3}] \quad , \ \Omega << 1 \ , \tag{34}$$

$$\Phi(f) = 2.81\ (\sigma_{\ell A}^2)\left(\frac{1}{f_o}\right)\ \Omega^{-8/3} \quad , \ \Omega >> 1 \ , \tag{35}$$

where $\Omega = \frac{f}{f_o}$ and $f_o = \bar{v}_n(2\pi\lambda Z)^{-1/2}$.

II. NATURE OF THE PROBLEM

A. APERTURE AVERAGING EFFECTS ON SCINTILLATION

1. Description

A photodetector placed at the image point of a lens illuminated with a plane wave responds to the square of the integrated amplitude over the convergent wavefronts. Having passed through a turbulent medium, the wavefront of incoming light for an ideal spherical or plane wave is no longer coherent nor of equal amplitude across the surface at the detector aperture. The random-sized turbules of different refractive indices along the propagation path have perturbed the wavefront creating a buildup of amplitude in some areas and a cancellation in others. A transverse correlation distance, ρ_ℓ, is defined as the distance in which intensity fluctuations remain correlated on the traveling wavefront at the point of observation, and in general is a function of path length Z and wavelength of the source. If a detector of diameter D is used to measure the intensity fluctuations at a point distant from the source, then the variance of the log-amplitude measured will depend on the value of D as compared to ρ_ℓ. For $D > \rho_\ell$, the wavefront incident upon the detector will not be strongly correlated, cancellations from the amplitudes of different parts of the wavefront being out of phase will occur, and intensity fluctuations measured will be less than for a correlated

wavefront, i.e., $D \leq \rho_\ell$. This observed decrease in the variance of the log-intensity fluctuations due to increasing aperture size is called the aperture averaging effect.

2. Theories

a. Lutomirski and Yura [Ref. 1]

For small scintillations and homogeneous turbulence, the transverse correlation distance of the intensity fluctuations is given as

$$\rho_\ell \approx (Z/k)^{1/2} = .399\ (\lambda Z)^{1/2} \quad . \tag{36}$$

For strong scintillation, no reliable estimate of ρ_ℓ exists. If the aperture diameter $D < \rho_\ell$, then the intensities measured at all points r_1 within the aperture, $I(r_1,t)$, are correlated at time t, and the photodetector current s(t) is proportional to

$$s(t) \approx \frac{\pi D^2}{4} I(0,t) \quad , \tag{37}$$

i.e., an effective point detector. As D becomes greater than ρ_ℓ, s(t) fluctuates less and for $D >> \rho_\ell$, the average incident intensity becomes constant and we have

$$\langle s \rangle = \frac{\pi D^2}{4} \langle I \rangle \quad . \tag{38}$$

The signal variance is given by

$$\sigma_s^2 = \int C_I(|\underline{p}_1 - \underline{p}_2|) d^2p_1 d^2p_2 \tag{39}$$

where $C_I(\rho)$ is the covariance of irradiance. Lutomirski and Yura state that aperture averaging "...is the ratio of σ_s^2 in (equation 39) to what the variance would have been if the intensity over the whole aperture varied as it did at a point." At a point,

$$\sigma_{s_o}^2 = \left(\frac{\pi D^2}{4}\right)^2 C_I(0) \; . \tag{40}$$

The aperture averaging factor, A, is defined as:

$$A \equiv \frac{\sigma_s^2}{\sigma_{s_o}^2} = \left(\frac{4}{\pi D^2}\right)^2 \int \frac{C_I(|\underline{p}_1 - p_2|)}{C_I(0)} \, d^2\underline{p}_1 d^2p_2 \; . \tag{41}$$

Reference 1 shows that if:

$\rho_\ell >> D$, then $A = 1$, i.e., there is no aperture averaging factor;

$\rho_\ell << D$, then $A \approx 4\left(\frac{\rho_\ell}{D}\right)^2$;

$\rho_\ell \approx D$, then the value of A requires a detailed knowledge of $C_I(\rho)$. $C_I(\rho)$ varies with source diameter, propagation slant path and meteorological conditions. For homogeneous turbulence and plane wave propagation, $C_I(\rho)$ is not known for strong scintillation. It is recommended that

(42) $$A = \frac{1}{1 + \left(\frac{D}{2\rho_\ell}\right)^2}$$

be used for homogeneous turbulence when the scintillation is small.

b. Fried [Ref. 21]

Using the statistics of propagation of an infinite plane wave over a horizontal path, Fried derives equation (37), then develops an expression for the signal variance,

(43) $$\sigma_s^2 = 2\pi \int_0^D \rho K_o(\rho,D)\, C_I(\rho)\, d\rho \ ,$$

where $K_o(\rho,D)$ is the area of overlap of two circles of diameter D whose centers are displaced a distance ρ, and is given by

(44) $$K_o(\rho,D) = \begin{cases} \frac{D^2}{2}\left\{\cos^{-1}\left(\frac{\rho}{D}\right) - \left(\frac{\rho}{D}\right)\left[1 - \left(\frac{\rho}{D}\right)^2\right]^{1/2}\right\} , & \rho \leq D \\ 0, & \rho > D. \end{cases}$$

Fried then derives the same aperture averaging factor as given in equation (41) but labels the factor Θ. He states that the normalized log-amplitude covariance, $C_\ell(\rho)/C_\ell(0)$, is a function of $\rho(4Z/k)^{-1/2}$ only, for the horizontal propagation case, and gives for an aperture diameter

normalization factor,

$$(45) \qquad (4Z/k)^{1/2} = .798\ (\lambda Z)^{1/2} \ .$$

Fried's theoretically calculated dependence of Θ upon the normalized aperture diameter, $D/(4Z/k)^{1/2}$, is shown in Figure 4 for various values of $C_{\ell}(0)$.

c. Tatarski [Ref. 20]

This theory on aperture averaging effects gives the amplitude correlation distance as being "on the order of" the first Fresnel zone size, $(\lambda Z)^{1/2}$. For this model then, the aperture normalization factor is simply $(\lambda Z)^{1/2}$. Tatarski was the first to define the aperture averaging factor $G(R) = \frac{Q(R)}{Q(0)}$, where $Q(R) = \frac{\sigma_s^2}{\langle s \rangle^2}$ and $Q(0) = \frac{\sigma_{s_o}^2}{\langle s \rangle^2}$, which Lutomirski and Yura have labeled "A" and Fried "Θ."

3. Published Experimental Data

a. Homstad and Heneghan [Ref. 22]

Measurements were made on a mesa near Boulder, Colorado, over a horizontal (statistically homogeneous) path at distances of 200-1600m using a He-Ne (6328 Å) laser. $G(R)$ vs. $R/(\lambda Z)^{1/2}$ was compared with Fried's theoretical curve of Figure 4. $G(R)$ is the aperture averaging factor, equivalent to A in equation (41). The result was that good agreement with theoretical calculations was observed

"...in the region of weak fluctuations (i.e., at shorter path lengths)...data in the region of strong fluctuations ...show a trend toward larger G(R) for $R/(\lambda Z)^{1/2} > 1.0$, in agreement with Kerr" [Refs. 23 and 24]. This is consistent with recent theoretical predictions [Refs. 25 and 26] and with Kerr's experimental work which found the correlation radius to be longer in the region of strong fluctuations [Refs. 23, 24, 35 and 36].

Homstad and Heneghan point out that a reason that experimental data collected by Fried [Ref. 16] did not support his theoretical predictions may have been that the apertures he used for the 8 km path length were not large enough to extend beyond the correlation radius and hence gave a relatively constant G(R) as reported by Fried.

b. Strohbehn and Homstad [Ref. 27]

In an experiment conducted over land, good agreement with Fried's model in the region of weak fluctuations is confirmed.

c. Kerr [Ref. 23]

States that the predicted value of the aperture averaging factor should vary as D^{-x} for diameters much larger than $(\lambda Z)^{1/2}$, where different authors have assigned values of 2, 7/3 or 3 to x, and that he did not observe this.

d. Previous NPS Work [Ref. 28]

Schroeder observed that "Significant aperture averaging was observed in an enclosed laboratory for apertures less than the first Fresnel zone size." From

two field experiments (both conducted at the same path length and with the same wavelength) Schroeder stated that the aperture averaging factor may be dependent on C_N and that "...a 4.8 mm aperture can approximate a vanishingly small receiver and should be used whenever possible." The two field experiments were conducted transmitting across Monterey Bay with receiver and source located on shore. Path length was 4.05 km, 98 percent of which was over the ocean surface at 4.9 meters. Aperture sizes used varied from .3 cm to 2.3 cm. By graphing "$<\sigma_{\ell A}(D) - \sigma_{\ell A}(23mm)>$ vs. Aperture Diameter D," Schroeder's data indicated that the largest average difference in $\sigma_{\ell A}$ values was seen for a 4.8 mm aperture.

B. APERTURE AVERAGING EFFECTS ON THE TEMPORAL-FREQUENCY POWER SPECTRUM

1. Tatarski's Theoretical Model

With increase in aperture size, Tatarski predicts a loss in the high frequency components of the normalized spectrum. By the addition of the factor

$$\left[\frac{2J_1(R\sqrt{K^2 + 4\pi^2 f^2/v_n^2})}{R\sqrt{K^2 + 4\pi^2 f^2/v_n^2}}\right]^2$$

in the kernal of the integral for the plane wave model of W(f), the spectral density of intensity fluctuations, a

partial suppression of the normalized intensity fluctuations as seen by an aperture of radius R is accounted for. For $f >> \frac{v_n}{2\pi R}$, this correction factor is a very small number, which corresponds to a suppression of high frequencies. As the aperture size is increased, the frequency at which the suppression occurs decreases. The low frequency portion of the spectrum will remain unaffected [Ref. 20].

Using the frozen-in turbulence model, the relationship between large spatial frequencies, K, and large temporal frequencies is given by $\omega = \underline{K} \cdot \underline{v_n}$. This implies that a receiver of diameter D will pass only temporal frequencies of $\omega \leq \frac{\overline{v}_n}{D}$.

2. Published Data

a. Höhn [Ref. 29]

A He-Ne (6328Å) source was used over path lengths of 4.5 km and 14.5 km. Various aperture sizes from .5 cm to 8 cm were used. Wind speed values were obtained from a meteorological center near the test site. Normalized spectrum curves were deduced from the data taken and the results were that "No systematic correlations of U(f)... or $f_{1/2}$ were found with changing aperture diameter D of the photometer." A second result was that the theoretical relation $f_c \propto Z^{-1/2}$ did not appear to hold empirically.

b. Schroeder's NPS Work [Ref. 28]

An aperture averaging frequency analysis sequence was conducted during each of the two field experiments

previously mentioned. Schroeder noted that changes in wind velocity could produce a different spectrum if two data samples at different aperture sizes were not conducted simultaneously. General wind speed conditions were measured at the transmitting location and assumed to be the same over the propagation path. The spectrum was obtained by passing a recorded scintillation signal through a wave analyzer with a bandwidth of 10 Hz at 10 Hz intervals from 20 to 100 Hz, then at 100 Hz intervals from 100 to 1000 Hz. The power was determined by integrating the output curves with a planimeter. Results were that for $f < 90$ Hz, the aperture averaging effect on the relative power spectrum was "unpredictable," while for $f > 90$ Hz, the smaller apertures show a larger contribution to relative power, as predicted by Tatarski's theoretical model. A second result is that for the same aperture size, the power spectrum relative to the power at 20 Hz measured on a day when wind speed was estimated to be 16 knots over the path, was overall higher in magnitude at all frequencies above 20 Hz than for the day with wind speed estimated at one knot.

C. C_{NO} vs. C_{NT}

As stated previously, one of the goals of the project is to be able to predict, through meteorological measurements, optical propagation conditions. A common indicator of this is the refractive index structure constant, C_N, which is related to the log-amplitude variance through

equations (12) and (13). C_N can be computed from the temperature structure constant, C_T [equation (6)], through the relationship

$$C_T^2 = \left(79 \times 10^{-6} \frac{P}{T^2}\right)^{-2} C_{NT}^2 , \tag{46}$$

where C_{NT} is the refractive index structure constant predicted from temperature fluctuations. Agreement between the structure constant C_{NO} obtained from long-path measurements of the log-intensity variance with C_{NT} may be taken as an indication that the optical fluctuations are not saturated and that the point-measured temperature fluctuations are characteristic of the path.

III. EXPERIMENTAL PROCEDURE

A. GENERAL EQUIPMENT DESCRIPTION

1. Detectors

To compensate for the time dependence of the variance, in measurement of effects of aperture size, a United Detector Technology PIN-5DP photodetector (Noise Equivalent Power 5 x 10^{-13} watts) with fixed aperture size was used as a reference. This was operated without bias voltage with the circuit shown in Figure 5.

For the variable aperture detector, a TIXL69 silicon avalanche photodiode (operated at its optimum S/N reverse bias voltage of 159V) was used to provide the high sensitivity at low S/N needed for measurement at very small aperture sizes. The characteristics of the TIXL69 are given in Appendix B.

For the first series of experiments conducted in the enclosed corridor laboratory, both detectors operated without field lens systems. The field lens images the entrance aperture on the detector so that the light entering the aperture is spread over the surface of the detector. This avoids fluctuations due to the image wandering over the detector active area which may vary in sensitivity [Ref. 28]. For the field experiments, the following field lens systems were installed:

(a) Avalanche Detector (Figure 6). A 50 cm focal length objective lens with a diameter of 4.9 cm focused the beam onto a 1.5 cm focal length, 9.5 mm microscope objective lens. Between the lenses a clear glass beam splitter reflected a portion of the image into an eyepiece for alignment purposes. The field lens magnification was designed so that the image of the aperture filled the detector active area (1.8×10^{-2} cm^2). A 4.9 cm, 30 Å filter centered at 6328 Å with a 77 percent peak transmission coefficient preceded the lens system, and an 18 leaf iris, adjustable from 1.5 mm to 42 mm aperture diameter, was placed in front of the filter.

(b) PIN-5DP Photodiode Detector (Figure 7). This field lens system is fundamentally the same as that for the avalanche detector with the exception that a 33.3 cm focal length, 2.54 cm diameter objective lens and 1.8 cm focal length, 9 mm diameter field lens were used to cover the detector active area of .05 cm^2.

2. Fan-Scan Mode of Laser Operation

A CW Radiation 5 mWatt 6328 Å laser operating in the TEM_{oo} mode was used for the aperture averaging experiments. The NPS "Fan-Scan" transmitter optics developed for ship-to-shore measurements was used. This system broadens the circular beam cross-section horizontally by reflection from a variable-radius cylindrical mirror, then scans this "fan" vertically by reflection from an oscillating output mirror. Thus the narrow uniform beam scans vertically twice each

cycle over a detector within a square field of view of order 20 meters side at 1500 meters (variable). Ship motion and background compensation are provided by measuring the difference between maximum and minimum irradiance values.

3. Electronic Components

Figure 8 is a block diagram of the electronic components used in all aperture averaging and frequency analysis experiments. The voltage signal from each detector package was sent to a PAR 113 (Princeton Applied Research) low noise differential pre-amplifier with maximum gain of 10 K. The outputs from the two PAR's were connected to a single switch box, from which the selected output passed to the demodulator. This switch box enabled the operator to rapidly record alternate scintillation signals from the two detectors. The demodulator stretched the voltage peak and sampled the stretched value, sampled the noise voltage 100 microseconds later in between peaks, and sent the difference to the Log Converter. The log-converted difference was then sorted by the PIP into the appropriate voltage channel as one count. The demodulator provides a trigger pulse for a signal monitoring oscilloscope and the PIP.

The calibration box provides calibration voltages of .5, 1, 2, 4 and 8 volts to the Log Voltmeter/Converter, and from there into the appropriate voltage channel on the PIP 400 Multichannel Pulse Height Analyzer (MPHA). A readout of the counts in each channel during calibration is used by the HP9810A Calculator and Plotter to scale the

voltage. The PIP 400 MPHA records the number of times a particular voltage value (i.e., log-intensity) is measured from the fluctuating signal during a run. This information is displayed during collection and can be stored indefinitely for subsequent printout and analysis as long as no other data is recorded further on that channel. The scintillation signal for frequency analysis was recorded from the output of the Log Voltmeter/Converter.

4. Shipboard Detector Stabilization

The avalanche and PIN photodiode detectors were mounted on a feedback-controlled gyrostabilized platform. The system is designed to compensate for ship motion and keep the critical detector alignment stable. Currently this system's performance is adequate at short ranges (less than 2000 m) and fairly calm sea states, but is degraded rapidly by increased distances or moderate sea states. In these instances the detector (gyroscope) alignment must be controlled manually by keeping the laser signal image in the center of two crosshairs of an eyepiece mounted on the gyro support. Gyroscope nutation, inability to keep the detectors aligned properly, and movements of the ship all contribute errors to a measured value of signal variance.

B. APERTURE AVERAGING EXPERIMENTS

1. Propagation Paths and Turbulence Conditions Present

a. Corridor Laboratory

Aperture averaging experiments were conducted in a long basement corridor by locating a 5 milliwatt He-Ne

(6328 Å) laser at one end of the corridor, propagating the beam the length of it, reflecting it back down the length of the corridor using a plane mirror and measuring the scintillation near the location of the source. Total path length was 280 m. The avalanche and PIN photodiode detectors were clamped to a vertical support. Once aligned, the detectors were not subject to any of the inherent motions from platform instability which are present when conducting the same experiment on board a ship. The experiments were conducted during early morning hours (with the exception of that on 7 April) to eliminate rapid variances in turbulence conditions due to persons opening and closing exterior doors. Turbulence was provided by ventilation system openings and building heating ducts located near the propagation path. Earlier measurements on the nature of the turbulence in this corridor indicated that the turbulence present did not represent homogeneous (Kolmogorov) turbulence conditions. However, the non-homogeneous turbulence did produce an intensity distribution that proved to be log-normal as predicted from theory. A sample log-intensity distribution taken during a corridor experiment is shown in Figure 9.

b. Over Land

To complete an aperture averaging sequence in homogeneous (Kolmogorov) turbulence before going to sea, where the ship's motion can affect the measured signal variance, an aperture averaging sequence was conducted on the Naval Postgraduate School Annex grounds on which the

Fleet Numerical Weather Central is located. The site selected to conduct the experiment consisted of a level terrain, three fourths of which was a blacktop covered road, the remainder a level dirt road. There were buildings and trees within 50 m of the propagation path; however, no forced draft blowers, heating systems or machinery was present to disturb the apparent homogeneity of the path. Winds were negligible; hence no eddy effects from winds curling around buildings or trees were present. The 5 mW He-Ne (6328 Å) source was mounted on a large telescope frame in a small, open-end trailer. It transmitted a Fan-Scan signal over a path length of 336 m to the avalanche and PIN photodiode detectors mounted on a metal plate affixed to a manually trained telescope. The equipment setup of Figure 8 was used and a frequency analysis experiment was conducted in conjunction with the aperture averaging. Again, intensity distributions over the path proved to be log-normal.

c. Over Water (Land to Land)

Two experiments were conducted over different path lengths and under different turbulence conditions.

Experiment I: Coast Guard Wharf to Spanagel Roof. The optical path, of length 2335 m, was highly irregular. The propagation path was slanted downwards, going from the roof at an altitude of about 75 m above sea level down to the Mobile Optical Research Laboratory at the Coast Guard Station parking lot at about 10 m above sea level.

About one third of the path was over water, the remainder over several commercial and residential structures. During the course of the experiment there were intermittent rain squalls. Data revealed that this entire sequence was conducted under saturation conditions for $\sigma_{\ell I}$.

Experiment II: Monterey Holiday Inn to Hopkins Marine Station. The second experiment, conducted over a propagation path length of 4230 m, was 97 percent through the marine boundary layer. The laser beam was transmitted over a horizontal path at about 10 m above sea level. The sky was clear on 11 March with average wind speeds during the experiment of about 7 m/sec. The He-Ne (6328 Å) laser source was located in the rear of the open-end trailer and was operated in the Fan-Scan mode. The trailer was located at the Monterey Holiday Inn parking lot, about 100 m from the water's edge. The terrain between the ocean and the trailer consisted of a low, sandy incline sloping downwards from the trailer's position towards the ocean. The detection devices and processing system were located in the bus (Mobile Optical Research Laboratory) stationed on the Hopkins Marine Station grounds about 10 m above the ocean surface and 20 m from the water's edge with an unobstructed view of the signal source.

Experiments measuring MTF being conducted simultaneously with aperture averaging precluded the PIN photodiode detector's being available for use as the fixed aperture system on this occasion. For this experiment a

HgCdTe detector with an aperture size of 23.6 mm was used as the fixed aperture system. The HgCdTe detector measured scintillation from a (10.6 μm) CO_2 laser. It is assumed that C_N^2 measured at 10.6 μm varied temporally in the same way as measured at .6328 μm, as indicated by the consistency of multiwavelength measurements of C_N^2.

d. Over Water (Land to Ship)

The He-Ne Fan-Scan transmitter on the bus was located at Pt. Pinõs (Figure 10) as near to the shoreline as possible (about 50 m away), with the detectors and data processing system on board the Research Vessel ACANIA. Only those runs were recorded in which detector alignment was maintained for periods of at least two to three minutes. Path lengths used during these runs were 1442 m, 1550 m, and 1625 m; the maximum range was limited by the failure of the tracking system to lock-on automatically at ranges greater than 2000 m. Path lengths were determined by base-line triangulation methods on shore using surveyor's transits. The optical paths were about 98 percent over the ocean surface.

2. Data Reduction

Data reduction, i.e., determining the refractive index structure constant and the log-intensity variance from a fluctuating voltage signal, was accomplished within minutes of the completion of a data collection run through the use of the Victoreen PIP 400 Multichannel Pulse Height Analyzer and the Hewlett Packard 9810A Calculator and

Plotter. As described previously, the PIP 400 stored the log-intensity distribution of the irradiance measured. An interface was developed between the PIP 400 and the HP9810A to allow the calculator/plotter to print out the log-intensity distribution and determine C_N and $\sigma_{\ell I}$ from it. The algorithm the computer followed [Ref. 31] was to apply a best-fit Gaussian curve to the distribution to obtain $\sigma_{\ell I}$, and then determine C_N through the relation

$$C_N = \frac{\sigma_{\ell I}}{k^{7/12} Z^{11/12} (.476)^{1/2}} . \tag{47}$$

An example of the printout is shown in Figure 9. The three markers near channels 60, 116 and 173 are calibration points of .5 V, 2 V and 8 V respectively, which are equally spaced on the log scale.

3. Aperture Averaging Factor G(D)

a. Description

To determine the aperture size that best approximates a point receiver, i.e., that size at which $\sigma_{\ell I}$ reaches a maximum for a given path length and C_N value and does not decrease significantly for further reduction of aperture size, the following aperture averaging factor was used:

$$(48) \quad G(D) \equiv \frac{C_N[V(D_o,t_o)]}{C_N[F(D_o,t_o)]} \cdot \frac{C_N[F(D_o,t)]}{C_N[V(D,t)]} = \frac{C_N[V(D_o,t)]}{C_N[V(D,t)]} .$$

$C_N[V(D_o,t_o)]$ is the value of C_N measured using the variable aperture detector at the maximum diameter D_o and the time t_o. Similarly, F denotes the fixed aperture detector which is used to measure the change in C_N due to variables other than a change in aperture size. The first factor $C_N[V(D_o,t_o)]/C_N[F(D_o,t_o)]$, compares the initial C_N value measured (at time t_o) with the variable diameter set at D_o to that measured by the fixed diameter at time t_o. $C_N[F(D_o,t)]/C_N[V(D,t)]$ reflects the change in that ratio produced by a reduction in aperture diameter from D_o to D. If the two apertures (fixed and variable) measure $\sigma_{\ell I}$ simultaneously at times t_o and t, and the variable aperture size is not changed between the two measurements, then G(D) will ideally equal 1.00. This was tested in conjunction with two corridor experiments conducted on 10 February and 5 March 1976. The comparison runs produced G(D) values of .9818 and .9981, indicating an average error of about one percent for G(D) values at different aperture sizes due to experimental variances.

b. Reason for Use; Relation to Fried's $\Theta(D)$

By starting with the largest experimental variable aperture diameter, D_o, for which $G(D_o) = 1.00$, then progressively reducing it until the minimum variable

aperture D_{min} is reached, the aperture size that best approximates a point detector can be determined by noting at which aperture diameter the lowest value of G(D) occurs. Empirical results (Section IV.A.) show that G(D) does not remain linear from D_o down to the smallest possible aperture size, D_{min}, but levels off and reaches a minimum value, $[G(D)]_{min}$, well before it.

Fried [Ref. 21] defined an aperture averaging factor $\Theta(D)$ [equivalent to A in equation (41)] based upon a vanishingly small receiver (D → 0 mm). Fried's theory states that all apertures of diameter D > 0 will measure a signal variance of smaller magnitude than would be measured using a vanishingly small detector. When using an aperture of diameter D, the measured variance must be multiplied by the correction factor $\frac{1}{\Theta(D)}$ to allow for aperture averaging. $[G(D)]_{min}$ identifies the aperture diameter, D_{min}, that best approximates a vanishingly small receiver. G(D) is related to Fried's aperture averaging factor in the following manner:

$$(49)\quad \frac{G(D)}{[G(D)]_{min}} = \frac{C_N[V(D_o,t)]}{C_N[V(D,t)]} \cdot \frac{C_N[V(D,t)]}{C_N[V(D_{min},t)]} = \frac{C_N[V(D_o,t)]}{C_N[V(D_{min},t)]} = \frac{1}{\Theta(D)}$$

C. APERTURE AVERAGING EFFECTS ON TEMPORAL-FREQUENCY SPECTRUM ANALYSIS

1. Experimental Conditions

a. (7-9) April 1976, Basement Corridor

The electronic equipment setup used in aperture averaging sequences is shown in Figure 8 and the procedure

followed in obtaining and processing signals on this date is described in Sections III.B.1.a, IV.A.1, and IV.A.2.a.(3). For frequency analysis, the scintillation signal was recorded from the output of the Log Voltmeter/Converter with a Precision Instruments, Model No. PI-6204, four-channel recorder at 37.5 ips. Performance characteristics of the recorder are contained in Appendix C. Signals were recorded for a period of about 75 seconds each at aperture sizes of 40, 30, 20, 15, 10, 7, 5, 3, 2 and 1.5 millimeters.

b. 20 April 1976, Navy Annex

Experimental conditions are as described in Sections III.B.1.b, IV.A.1, and IV.A.2.c. Frequency analysis data was recorded as described above for the (7-9) April run. Aperture diameters examined were of 40, 30, 20, 15, 10, 7, 5 and 3 millimeters. Power to operate the equipment on the bus was provided by a portable gasoline-powered motor generator.

c. (29-30) April 1976, R/V ACANIA

Experimental conditions on this date and procedures followed for aperture averaging are described in Sections III.B.1.d, IV.A.1, and IV.A.3.(d and e). The signal to be frequency analyzed was recorded from the output of the Log Voltmeter/Converter (Figure 8) on a Sanborn HP-3914, 14-channel Analog Tape Recorder, operated by the meteorology team recording micrometeorological data

for C_N comparison. Operating characteristics of the HP-3914 Recorder are included in Appendix C. Time reference signals were recorded on the tape for identification.

2. Data Reduction

The recorded scintillation signal was frequency analyzed by playing back the signal into an EMR Schlumberger Instruments 1510 Digital Spectrum Analyzer. The spectrum analyzer was operated in the continuous mode over a frequency range of 10 Hz to 2.56 KHz. The signal was sampled by the spectrum analyzer for a period of 25.6 seconds. The resulting spectrum was plotted on a Hewlett Packard Moseley 7035B X-Y Recorder. Frequency was plotted linearly along the X-axis from 42 Hz to 2.56 KHz. The Y-axis was a 0 to -60 dB linear scale.

For evaluation of the aperture averaging effects on the spectral density, relative power spectra were obtained directly by aligning the -60 dB line of the spectrum of each different aperture to a common new reference axis and plotting each spectrum manually. Points of local minima were plotted on each spectrum, thereby avoiding abnormal magnitudes due to noise spikes.

IV. EXPERIMENTAL RESULTS

A. APERTURE AVERAGING EFFECTS ON SCINTILLATION

1. Commonalities

In addition to the electronic equipment setup (Figure 8), detectors, and laser source previously described, the following items were common to all aperture averaging experiments: (1) The Hewlett Packard 9810A Calculator and Plotter was used for immediate data reduction. (2) Aperture sizes for the variable aperture system were set by inserting a micrometer caliper set at the proper diameter size within the aperture and closing the iris upon it. Both horizontal and vertical dimensions were checked. The aperture size was rechecked at the end of the run.

2. Preliminary Investigations

a. Corridor Experiments

(1) 2235, 7 February 1976 - 0515, 8 February 1976

This initial aperture averaging sequence was conducted to examine the validity of the assertions made by Schroeder [Ref. 28] that a 4.8 mm aperture diameter best approximates a vanishingly small receiver. For this experiment, the laser was operated in the Scan mode only and a neutral density filter of .5 was used to decrease the signal strength. The field lens detector systems of Figures 6 and 7 had not been constructed at this time. Each detector consisted of the photodiode placed at the focal plane of an

objective lens in a narrow cylinder of diameter 22.6 mm with a 10 Å filter centered at 6328 Å at the cylinder front. This made the largest variable aperture size available 22.6 mm. Aperture sizes of 22.6, 20, 17, 14, 12, 10, 7, 6, 5, 4, 3 and 2 millimeters were used. G(D) values calculated from the measured log-intensity distribution standard deviations, $\sigma_{\ell I}$, are given in Table I with the plotted "G(D) vs. Aperture Diameter, D" shown in Figure 11. The last column of Table I gives $\frac{1}{\Theta(D)} = \frac{G(D)}{[G(D)]_{min}}$, the correction factor for aperture averaging.

In Figure 11, the curve bottoms out at an aperture size of about 5 mm and the corresponding value of G(D) does not significantly decrease from its value at that point as the aperture diameter is further reduced.

(2) 1655-1820 and 2100-2240, 10 February 1976

It was noted from the experiment of 7 February that although the log-intensity distributions were for the most part Gaussian, on several of the larger aperture runs double peaks occurred near the top of the log-intensity curve. It was believed that this was due to the laser being in the Scan mode only so that the detector would see one average intensity peak as the beam swept up and a slightly different one as the beam swept down. In an attempt to alleviate this, a second aperture averaging sequence was conducted with the laser in the Fan-Scan mode. By spreading the beam out and scanning it, it was felt that a more uniform intensity might be seen by the detector, and

TABLE I

D (mm)	$\sigma_{\ell I}[V(D,t)]$	$\sigma_{\ell I}[F(D_o,t)]$	G(D)	$G(D)/[G(D)]_{min}$
22.6	.218	.426	1.000	2.17
20	.251	.419	.854	1.86
17	.258	.414	.821	1.78
14	.228	.325	.729	1.58
12	.258	.361	.716	1.56
10	.265	.331	.639	1.39
7	.267	.273	.523	1.14
6	.280	.276	.504	1.10
5	.292	.267	.468	1.02
4	.306	.281	.470	1.02
3	.308	.277	.460	1.00
2	.324	.306	.483	1.05

the double peaks eliminated. A Fan-Scan divergence setting of seven milliradians was used and a neutral density filter of optical density .5 was inserted in the beam to reduce the signal intensity at the detector. With the beam reflected off a 625 cm^2 mirror at a distance of 140 m, the estimated signal strength at the position of the detector is 1.7×10^{-9} $Watts/cm^2$, which is of the order of the signal intensity for the at-sea experiments, described later, at a path length of 1600 m.

Aperture sizes used were identical to those used during the 7 February run. Log Intensity distributions on this day revealed that the double peaks were eliminated in all but one distribution by use of the Fan-Scan, and this mode was therefore adopted as the standard laser operation mode for future aperture averaging sequences. Figure 12 shows "G(D) vs. Aperture Diameter, D" for this experiment. Although this experiment was conducted identically to that on 7 February with the exception of the Fan-Scan operation, three significant differences stand out in the results. First, the curve bottoms out at the 6 mm aperture size vice the 5 mm size of 7 February. Secondly, G(D) values at all aperture sizes are in general larger than they were on 7 February, even though the same value of D_o(22.6 mm) was used to calculate G(D) values. Thirdly, the shape of the curve following the bottoming out at 6 mm is different from that seen on 7 February. In comparing the data, the

average $\sigma_{\ell I}[F(D_o,t)]$ is seen to be significantly different on the two days, implying a larger C_N. On 7 February $\langle\sigma_{\ell I}[F(D_o,t)]\rangle$ = .330, while on 10 February $\langle\sigma_{\ell I}[F(D_o,t)]\rangle$ =.428. An increasing $\langle\sigma_{\ell I}\rangle$ seems to increase G(D) values, as can be seen by comparing Table II with Table I.

(3) (7-9) April 1976

An aperture averaging frequency analysis experiment was conducted. The aperture averaging results are included for comparison with runs conducted on 7 February and 10 February. The same He-Ne (6328 Å) laser was operated in the Fan-Scan mode with a divergence setting of seven milliradians and a neutral density filter of .5 was inserted in the beam.

Prior to this run the largest aperture size available on the variable aperture detector was 22.6 mm. To increase the largest aperture size available and improve signal detection capability, the field lens systems of Figures 6 and 7 had been constructed and were in use for this experiment. The significance here is that with a larger D_o available, one would expect to see a smaller $[G(D)]_{min}$ for this sequence. This proved accurate, as shown in Figure 13. A much lower $[G(D)]_{min}$ resulted using the 40 mm aperture as D_o vice 22.6 mm. This curve appeared to follow the same basic pattern as those for 7 February and 10 February with the exception that this took on a different shape from either of the previous two for apertures less than the bottoming out diameter of about 5 mm. In

TABLE II

D (mm)	$\sigma_{\ell I}[V(D,t)]$	$\sigma_{\ell I}[F(D_o,t)]$	G(D)	$G(D)/[G(D)]_{min}$
22.6	.431	.431	1.000	1.55
17.0	.465	.433	.930	1.44
12.0	.541	.401	.740	1.14
7.0	.579	.398	.686	1.06
6.0	.701	.454	.647	1.00
5.0	.676	.441	.651	1.01
4.0	.599	.426	.710	1.10
3.0	.716	.426	.594	.92

order to see better how this run compared with the previous two, G(D) values were recomputed using the 20 mm diameter as D_o. The result is shown in Figure 14. $[G(D)]_{min}$ for (7-9) April is still well below that of 7 and 10 February. The average $\sigma_{\ell I}$ for the fixed aperture system for this run was $\langle\sigma_{\ell I}[F(D_o,t)]\rangle$ = .08 which is much lower than the average values for 7 and 10 February as is $[G(D)]_{min}$. Table III gives a comparison of the average signal variance with $[G(D)]_{min}$ for the three experiments conducted in the same manner, with the same equipment, but with different turbulence conditions present as indicated by $\langle\sigma_{\ell I}\rangle$.

TABLE III

Date	$\langle\sigma_{\ell}[F(D_o,t)]\rangle$	$[G(D)]_{min}$	$\Delta\langle\sigma_{\ell I}\rangle$	$\Delta[G(D)]_{min}$
10 Feb	.428	.647	--	--
7 Feb	.330	.468	.098	.179
(7-9) Apr	.084	.223	.246	.245

It appears that $[G(D)]_{min}$ increases with $\langle\sigma_{\ell I}\rangle$ for low values of $\langle\sigma_{\ell I}\rangle$, and that in general, for a given D_o, the value of $[G(D)]_{min}$ is dependent upon the level of turbulence. The higher the turbulence level, the higher the $[G(D)]_{min}$ value.

b. Aperture Diameter Normalization

Examination of Figure 14 shows that the shapes and slopes of the plots are similar from the largest aperture size down to about 5 mm where three different forms of

the curve then emerge. Following previous theoretical models [Refs. 1, 20 and 21], it is expected that D_{min}, the aperture best approximating the "vanishingly small" receiver, should be directly related to the intensity transverse correlation length, ρ_{ℓ}. This quantity is given in the three models as:

(1) $(\lambda Z)^{1/2}$, [Tatarski, Ref. 20]

(2) $(\frac{4Z}{k})^{1/2}$, [Fried, Ref. 21]

(3) $(\frac{Z}{k})^{1/2}$, [Lutomirski and Yura, Ref. 1].

Aperture diameters for the three corridor experiments were scaled according to the three models, the results of which are shown in Figures 15, 16 and 17, respectively. The three curves bottom out at approximately the value of $D = (\frac{Z}{k})^{1/2}$ predicted by Lutomirski and Yura.

c. Over Land Experiment (2128-2347, 20 April 1976)

Aperture diameters examined were 40, 30, 20, 15, 10, 7, 5 and 3 millimeters. The Fan-Scan was set at a divergence of 7 milliradians and no neutral density filter was used to decrease the signal intensity. The laser was situated about 2 meters and the detectors 2.5 meters off the ground. The sky was clear, temperature averaged 10°C and winds were negligible (0-2 m/sec).

"G(D) vs. $\frac{D}{(Z/k)^{1/2}}$" was plotted to locate the bottoming out point. Although able to test only a few aperture sizes, previous runs conducted outside the corridor

laboratory (discussed in section d below) indicated that the $(Z/k)^{1/2}$ normalization factor was accurate in predicting the bottoming out point of the graph at $D/(Z/k)^{1/2} = 1.0$. Figure 18 shows the graph for the experiment conducted on 20 April. The bottoming out occurs for the aperture size nearest, but not less than, $D/(Z/k)^{1/2} = 1.0$. Note, for this path length $(Z/k)^{1/2} \approx 5.8$ mm, and although the 5 mm aperture size is nearer to $(Z/k)^{1/2}$ than the 7 mm size, previous runs have shown that the behavior of G(D) below $D/(Z/k)^{1/2} = 1.0$ is erratic. Thus, the 7 mm size is nearer to the minimum G(D) value that corresponds to the bottoming out point at $D = (Z/k)^{1/2}$ than is the 5 mm size. As a further comparison, the corridor runs conducted on 7 February and (7-9) April at a path length of 280 m were plotted with this run of 20 April at the path length of 336 m, shown in Figure 19. It appears that the bottoming out point occurs very close to $D/(Z/k)^{1/2} = 1.0$.

$[G(D)]_{min}$ for this experiment, with respect to a 20 mm D_o, was .666 and the average $\sigma_{\ell I}$ was $\langle\sigma_{\ell I}[F(D_o,t)]\rangle = .162$. This does not fit in with the results given in Table III; however, the propagation path and turbulence conditions were different. To verify a predictable increase of $[G(D)]_{min}$ with $\langle\sigma_{\ell I}\rangle$ would require repetition of the experiment under identical experimental conditions and over the same propagation path where the turbulence would have the same characteristics. Time considerations precluded this procedure.

d. Over Water (Land to Land)

(1) 2220, 5 March - 0345, 6 March 1976 (Spanagel Roof to Coast Guard Parking Lot)

Due to the irregular propagation path used and corresponding turbulence conditions over a long distance, this entire sequence was conducted under saturation conditions for $\sigma_{\ell I}$. $\langle\sigma_{\ell I}[F(D_o,t)]\rangle$ was 1.01 and $[G(D)]_{min}$ was .8808 with respect to a D_o of 24.3 mm. The graph of "G(D) vs. Aperture Diameter, D" is shown in Figure 20. For this path length, $(Z/k)^{1/2}$ = 15.3 mm. The main item of interest for this run is that, under saturation conditions, the maximum difference in G(D) values observed was only $[\Delta G(D)]_{max}$= .167, which included comparisons of aperture sizes of 24.3, 20, 16, 12, 7, 6, 5, 4, 3 and 2 millimeters. This indicates that aperture averaging has only a small effect on the measured signal variance under saturation conditions for aperture sizes less than 24.3 mm.

(2) 1550-1640, 11 March 1976 (Monterey Holiday Inn to Hopkins Marine Laboratory)

Due to the limited time available for conducting the experiment on this day, only aperture sizes of 41.7, 24.3 and 14.0 millimeters were examined. A plot of "G(D) vs. Aperture Diameter, D" is shown in Figure 21. The path length was 4230 m, giving a $(Z/k)^{1/2}$ of 20.6 mm. Figure 21 contains insufficient data to draw definite conclusions. The same data is plotted again in Figure 24 in terms of the normalized diameter, and will be discussed

at that point. $[G(D)]_{min}$ and $\langle\sigma_{\ell I}[F(D_o,t)]\rangle$ for this run should not be compared with other experiments in this section since a different source and fixed aperture detector system was used and $\sigma_{\ell I}$ is wavelength dependent for identical turbulence conditions.

3. Propagation in the Marine Boundary Layer (R/V ACANIA Experiments)

a. 1840-1930, 30 March 1976

The winds during the time of this experiment varied from 8 to 12 m/sec in a direction of about 10 degrees off the normal to the propagation path. The sky was partly cloudy, temperature about 7°C, sea conditions were moderate with average wave heights of about 1 meter, and swell heights of about 2 to 3 meters moving in a direction normal to the propagation path. The motion of the R/V ACANIA at anchor made maintenance of gyro lock-on difficult. This undoubtedly caused intensity variances to be greater than would be observed normally. The path length on this day was 1600 m. The detectors were located about 7 meters and the source about 5 meters above the ocean surface. Aperture sizes compared were 38, 31, 24.3, 17 and 10 millimeters. For this path length, $(Z/k)^{1/2}$ = 12.7 mm. The "G(D) vs. Aperture Diameter, D" curve is shown in Figure 22. This is not typical of past aperture averaging results, but resembles those obtained under saturated conditions. However, $\langle\sigma_{\ell I}[F(D_o,t)]\rangle$ for this experiment was .149, well below the saturation region. It is felt that the sea

conditions, rapid ship movements, and inability of the gyroscope lock-on system to work effectively in moderate seas may have obscured any detectable aperture averaging effects.

b. 1340-1415, 2 April 1976

Wind and sea conditions on this day were identical to those of 30 March. The sky being clear was the only difference in weather conditions. The sea state was still moderate and there was still considerable ship motion. The path length on this day was 1600 m. The gyroscope lock-on system had been improved slightly by readjusting the existing circuitry; all other experimental conditions were as described for 30 March. Aperture sizes used for this run were 40, 30, 20 and 10 mm. Figure 23 shows "G(D) vs. Aperture Diameter, D" and Figure 24 compares "G(D) vs. $D/(Z/k)^{1/2}$" for this run with the data taken over water with a path length of 4229 m on 11 March. Once again, it appears the normalization factor $(Z/k)^{1/2}$ successfully predicts the diameter of the aperture that best approximates a vanishingly small receiver.

c. 1445-1657, 27 April 1976

The sky was clear at 1445 but became overcast at about 1545. Winds were 8 to 10 m/sec blowing normal to the propagation path; waves also moved normal to the path with a height of about 1 meter and swells about 2 meters high. The ship rolled considerably in the swells and once again gyroscope lock-on was difficult. The ship was anchored, path length was 1650 m, and aperture diameters

examined were 40, 35, 30, 25, 20, 16, 13, 10, 5 and 4 millimeters. "G(D) vs. $D/(Z/k)^{1/2}$" for this run is shown in Figure 25. G(D) values seem erratic; this is attributed to difficulty in stabilizing the detector and tracking the ACANIA from shore.

d. 1830-2024, 29 April 1976

The sky was clear, wind speed throughout the experiment was 3 to 4 m/sec, and path length was reduced to 1442 m. Sea conditions improved slightly with wave heights down to about .7 m and swells of about 1.5 m. The wave direction was about 15 degrees off the normal to the propagation path as was the wind. Aperture sizes of 40, 35 30, 25, 20, 16 and 13 millimeters were used. "G(D) vs. $D/(Z/k)^{1/2}$" is plotted in Figure 26. The 35 mm aperture size was used as D_o for the G(D) calculations since it appeared to give more credible overall values based on past experiments. The G(D) value for the 40 mm aperture is plotted relative to the 35 mm aperture as D_o. With the exception of the 40 mm aperture $[\frac{D}{(Z/k)^{1/2}} = 3.33]$ and the 16 mm aperture $[\frac{D}{(Z/k)^{1/2}} = 1.33]$, the curve appears to parallel results of past runs, i.e., reaches a minimum at $\frac{D}{(Z/k)^{1/2}} \approx 1.0$ and shows a nearly linear decrease of G(D) with decreasing aperture diameter to this point. For this run, $[G(D)]_{min} = .721$ and $\langle \sigma_{\ell I}[F(D_o,t)] \rangle = .145$.

e. 1044-1311, 30 April 1976

The sea state was relatively calm with wave heights of about .5 m and no apparent swells. The sky was clear, temperature about 21°C and winds were 3 to 4 m/sec. The calm sea state enabled the gyroscope tracking system to work well in the automatic mode and results more consistent with past sequences were obtained on this day. The ship was at anchor and the propagation path length was 1625 m. Aperture sizes examined were 40, 16, 13, 10 and 5 millimeters and $(Z/k)^{1/2}$ for this path length was 12.8 mm. The plot is shown in Figure 27. Bottoming out occurs near $D/(Z/k)^{1/2} = 1.0$, $[G(D)]_{min} = .766$, and for this run $\langle\sigma_{\ell I}[F(D_o,t)]\rangle = .264$. A comparison of $[G(D)]_{min}$ and $\langle\sigma_{\ell I}\rangle$ for the three R/V ACANIA experiments is given in Table IV.

TABLE IV

Date	$[G(D)]_{min}$	$\langle\sigma_{\ell I}[F(D_o,t)]\rangle$
2 Apr	.792	.726
30 Apr	.766	.264
29 Apr	.721	.145

From the data of Table IV it appears again that in general $[G(D)]_{min}$ increases with $\langle\sigma_{\ell I}\rangle$.

4. Comparison of Theoretical Aperture Averaging Factors with Experimental Results

a. Lutomirski and Yura Model [Ref. 1]

For aperture diameters on the order of the intensity correlation length, as utilized during these experiments, Lutomirski and Yura "recommend" an aperture averaging factor of

$$A = \frac{1}{1 + \left(\frac{D}{2\rho_{\ell}}\right)^2} . \tag{46}$$

Table V lists Lutomirski and Yura's theoretical value of A computed for our experiments and the observed value of A. A, theoretically defined as $\sigma_s^2/\sigma_{s_o}^2$, is equivalent to our $[G(D)]_{min}/[G(D_o)]$ where D_o replaces D in equation (46). The theoretical values do not correlate well with the empirical values. Further, Lutomirski and Yura's theoretical model does not contain any turbulence dependence which appears to be necessary in view of the apparent dependence of $[G(D)]_{min}$ on $\langle\sigma_{\ell I}\rangle$ seen empirically.

b. Fried's Model [Ref. 21]

To compare empirical results with Fried's theoretically derived plot of "Θ vs. $D/(4Z/k)^{1/2}$," (Figure 4), whose curves are based on an aperture diameter of $D = .1(4Z/k)^{1/2}$ as representing a vanishingly small receiver, it was necessary to use the experimental aperture

TABLE V

DATE/LOCATION	A (THEORY)	A (EMPIRICAL)
7 Feb/Corridor	.180	.219
(7-9) Apr/Corridor	.066	.021
11 Mar/Hopkins-Holiday	.495	.646
20 Apr/Navy Annex	.347	.284
2 Apr/ACANIA	.288	.627
29 Apr/ACANIA	.322	.520
30 Apr/ACANIA	.290	.587

size for each run that gave the minimum G(D) value as the vanishingly small aperture diameter. The effect of this is to shift the empirical curves to the right of the theoretical curve. Figures 28 and 29 show Fried's theoretical plot for log amplitude variance $C_\ell(0) = 2^{-5}$ as compared with experimental values for various runs. For this graph, aperture diameters were appropriately normalized for comparison by the $(4Z/k)^{1/2}$ factor. Using equation (45), Θ was calculated as

$$\Theta = \frac{\sigma_s^2[V(D,t_o)]}{\sigma_s^2[V(D',t_o)]}, \tag{47}$$

where $\sigma_s^2[V(D',t_o)]$ is the signal variance measured at time t_o and with variable aperture diameter D', which corresponds to the aperture diameter that best approximated a vanishingly small receiver, i.e., corresponded to $[G(D)]_{min}$. $\sigma_s^2[V(D,t_o)]$ is the signal variance that would have been measured at time t_o had aperture size D been used, and was found from the relation

$$\sigma_s^2[V(D,t_o)] = \sigma_s^2[V(D,t)] \cdot \frac{\sigma_s^2[F(D_o,t_o)]}{\sigma_s^2[F(D_o,t)]}, \tag{48}$$

where again, F is the fixed aperture detector.

Empirical results appear to follow Fried's theoretical model generally well. In contrast with

Lutomirski and Yura's aperture averaging model, Fried acknowledges the dependence of the aperture averaging factor on the turbulence conditions, as represented by different curves for particular values of $C_{\ell}(0)$ in Figure 4. Fried's model indicates that as $C_{\ell}(0)$ increases, θ increases for a specific aperture diameter, or the inverse of the aperture averaging factor decreases. This is in agreement with empirical results noted in Sections 2.a.(3) and 3.e. above. From Figure 28 it is evident that the aperture averaging curve for 7 February lies below that of 10 February and above that of (7-9) April. The θ values are therefore in general larger for 10 February than for 7 February, i.e., the ratio of $\sigma_s^2/\sigma_{s_o}^2$ is larger, and the inverse of the aperture averaging factor is less, as predicted by Fried's theory.

B. APERTURE AVERAGING EFFECTS ON THE RELATIVE TEMPORAL-FREQUENCY POWER SPECTRUM

1. General Results

The spectrum analyzer frequency limits were selected to examine frequencies within the range 10 Hz to 2.56 KHz. The demodulator in the signal processing system eliminates frequencies above 2 KHz, coinciding with the original estimate of the Fan-Scan frequency. The bandwidth is further reduced to a maximum frequency of 1 KHz for experiments conducted using the Sanborn HP-3914 Recorder. Power spectra from all frequency analysis experiments show the

actual Fan-Scan frequency to be 1.92 KHz, clearly evident as a noise spike in Figures 34, 35 and 36. Previous work at NPS by Schroeder [Ref. 28] examined frequencies from 20 Hz to 1 KHz.

Results of the experiments conducted on (7-9) April, 20 April and (29-30) April, under varying turbulence conditions, all indicate that aperture averaging has a discernable effect on the observed power spectrum. Empirical results support the theoretical prediction that a corresponding reduction in high frequency power results as aperture diameter is increased. The reduction in power, however, appears to occur over a large portion of the frequency range, not solely on the high frequency end. Figures 30, 31, 32 and 33 show the effect of aperture averaging on the relative power spectrum.

2. Turbulence-Dependent Forms of the Frequency Spectrum

As previously remarked, the three frequency analysis experiments were conducted at different locations and under different turbulence conditions. The resulting power spectra for each run were similarly different. Typical spectra for the corridor experiment (inhomogeneous turbulence), the Navy Annex run (over land in homogeneous turbulence), and the R/V ACANIA data (over water in homogeneous turbulence), are shown in Figures 34, 35 and 36, respectively. The significant item of note in Figure 34 is the uniformity of the spectrum below .85 KHz. The prevalence of noise spikes at 110 Hz and 120 Hz intervals in Figure 35 is believed due

to the extremely noisy, gas-powered portable generator used to provide power to the electronic equipment during this experiment. Also peculiar to this experiment were characteristically low magnitude power spectra. Figure 36 shows an approximately linear decrease in power with increasing frequency.

Eliminating the noise spikes in Figure 35, it appears that the spectrum assumes the same general form as that of Figure 34. A significant difference in the experimental conditions for 9 April and 20 April as opposed to those of 30 April was the average wind speed present. On 9 April and 20 April winds were negligible. On 30 April, conducted at sea on board the ACANIA, average wind speeds were about 4 m/sec. Further experiments need to be conducted to examine the effect of wind speed on the shape of the power spectrum.

3. Comparison with Clifford's Theoretical Model

Clifford's theoretical model for the temporal-frequency power spectrum for spherical and plane waves are given by equations (32) through (35). The values of f_o for 9 April, 20 April and 30 April, based upon respective average wind speeds of 1 m/sec, 1.5 m/sec and 4 m/sec are 30 Hz, 41 Hz and 53 Hz, respectively. For comparison with the theoretical model (Figure 3), typical spectra for these experiments were plotted vs. "Log Ω" and are shown in Figure 37. The vertical axis is the percentage of power

at a particular frequency compared to the maximum power attainable as determined by the spectrum analyzer's "Y-axis" voltage setting.

There appear to be two significant differences between the empirical results of Figure 37 and Clifford's theoretical spectra of Figure 3. First, Clifford indicates that the rapid downward slope of the spectrum begins at $\log \Omega \approx -0.1$ for plane waves and $\log \Omega \approx 0.2$ for spherical waves. Empirical results show the drop occurring at $\log \Omega \approx 3.0$ for the (7-9) April and 20 April experiments. The spectrum of (29-30) April shows an overall negative slope for all frequencies. Secondly, the slope appears to decrease less rapidly than the theoretical $(f)^{-8/3}$. The slope for (7-9) April is of the order of $(f)^{-6/11}$ and for 20 April and (29-30) April, $(f)^{-2/13}$. Further data collection is necessary to examine if, and to what extent, various turbulence parameters affect the magnitude of the negative slope. It does appear, however, that Clifford's $(f)^{-8/3}$ is too rapid a decrease.

4. Differences in Magnitude of the Aperture Averaging Effect

Examination of Figures 30 through 33 indicates that there are significant differences between aperture averaging effects on the relative power spectrum as seen under the various experimental conditions. In an attempt to determine a factor common to the variances and to the power reductions which were not directly proportional to

aperture diameter, parameters such as wind speed, $\langle\sigma_{\ell I}\rangle$, C_N, $\sigma_{\ell I}$ and G(D) were examined. No factor was found that individually accounts for the variations. A detailed analysis of all factors concurrently was not undertaken due to time limitations.

V. SUMMARY AND CONCLUSIONS

A. APERTURE AVERAGING EFFECTS ON SCINTILLATION

The variance of log-amplitude fluctuations that would theoretically be observed if using a vanishingly small receiver can best be approximated by an aperture of diameter $(Z/k)^{1/2}$. A diameter of this size eliminates aperture averaging effects present when using apertures larger than $(Z/k)^{1/2}$, and that may be present when using aperture diameters smaller than $(Z/k)^{1/2}$. Experiments conducted in an enclosed laboratory in inhomogeneous turbulence and field experiments conducted in homogeneous turbulence, both over land and in the marine boundary layer, support this prediction from the theoretical model of Lutomirski and Yura [Ref. 1].

Fried's theoretical model of aperture averaging [Ref. 21] predicts that Θ, the aperture averaging factor, increases continuously as aperture size is decreased from an arbitrarily large aperture diameter. Empirical results indicate that the aperture averaging factor does not increase continuously as aperture size is reduced to a vanishingly small diameter, but increases continuously until an aperture diameter $(Z/k)^{1/2}$ is reached. A further reduction in aperture diameter [below $(Z/k)^{1/2}$] causes Θ to (1) reverse direction and decrease or (2) remain near the same value of Θ.

In general, the value of the aperture averaging factor increases as $\langle\sigma_{\ell I}\rangle$ increases. Put another way, for an aperture of diameter larger than $(Z/k)^{1/2}$, the aperture averaging correction factor decreases as the amount of turbulence increases. Under weak turbulence conditions, the effect of aperture averaging is quite significant. For strong scintillation conditions, the aperture averaging effect is decreased and becomes less significant.

The ratio $G(D')/[G(D)]_{min}$ gives the factor by which the measured signal variance (or other turbulence parameter), measured with an aperture of diameter D', $D' > (Z/k)^{1/2}$, must be multiplied to represent the value that would have been measured had a vanishingly small receiver been used. It is important to note that the value of $[G(D)]_{min}$ is a function of the largest aperture diameter used (D_o), and should not be viewed as an absolute value for a particular set of turbulence parameters. In general, the value of $[G(D)]_{min}$ decreases as D_o is increased.

B. APERTURE AVERAGING EFFECTS ON THE TEMPORAL-FREQUENCY POWER SPECTRUM

An increase in aperture diameter appears to decrease the magnitude of power in the frequency range $.5\ KHz < f < 2\ KHz$ of the temporal-frequency power spectrum for scintillation measurements. The difference in power at a particular frequency for two given aperture diameters differed significantly for different experimental and turbulence conditions. The reason for the disparity was not determined due to time considerations.

Spectra obtained from experiments in the corridor laboratory, over land, and in the marine boundary surface layer indicate a negative sloped decrease in power at higher frequencies for the temporal-frequency power spectrum less rapid than the $(f)^{-8/3}$ predicted by Clifford [Ref. 19]. Further investigation is required to determine the effect changes in certain turbulence parameters have on the form of the power spectrum.

C. EXTENSION OF PROJECT

Comparisons of $[G(D)]_{min}$ with $\langle\sigma_{\ell I}\rangle$ indicated that, for a given aperture size larger than that which approximates a vanishingly small receiver, the aperture averaging correction factor is not a constant, but is dependent upon the level of turbulence present. Further experimentation is needed to compare $[G(D)]_{min}$ values, for a given maximum reference diameter D_o, with $\langle\sigma_{\ell I}\rangle$ values, to determine the relationship between the level of turbulence and the aperture averaging correction factor for a given aperture diameter D_o.

It seems clear from this report and other published data that aperture averaging reduces the high frequency power content in the temporal-frequency power spectrum and eliminates certain high frequencies proportional to increasing aperture diameter. However, experiments conducted under different turbulence conditions and over different propagation paths indicate that the power spectrum assumes different general shapes. This needs further investigation

through the examination of power spectra obtained over the same propagation path under various turbulence conditions, and under the same turbulence conditions over various propagation paths. In conjunction with this, Clifford's theoretical model of the temporal-frequency power spectrum for plane and spherical waves should be examined for validity more thoroughly through empirical study.

D. SUMMARY MATRIX OF EXPERIMENTS CONDUCTED

Date	Location	Path Length (m)	Detectors	1(Apt Ave) 2(W/Freq Anal)	Aperture Diameters (mm)
(7-8) Feb 76	Corridor	280	(V)Avalanche/ (F)PIN-5DP (No Field Lens)	1	22.6, 20, 17, 14, 12, 10, 7, 6, 5, 4, 3, 2
10 Feb 76	Corridor	280	"	1	22.6, 20, 17, 14, 12, 10, 7, 6, 5, 4, 3, 2
(5-6) Mar 76	Spanagel Roof-Coast Guard	2335	(V)Avalanche/ (F)PIN-5DP (W/Field Lenses)	1	24.3, 20, 16, 12, 7, 6, 5, 4, 3, 2
11 Mar 76	Holiday Inn-Hopkins Lab	4230	(V)Avalanche/ (F)HgCdTe (No Field Lens)	1	41.7, 24.3, 14
30 Mar 76	Pt. Pinõs-ACANIA	1600	(V)Avalanche/ (F) PIN-5DP (W/Field Lenses)	1	38, 31, 24.3, 17, 10
2 Apr 76	Pt. Pinõs-ACANIA	1600	"	1	40, 30, 20, 10
(7-9) Apr 76	Corridor	280	"	1,2	40, 30, 20, 15, 10, 7, 5, 3, 2, 1.5
20 Apr 76	Navy Annex	336	"	1,2	40, 30, 20, 15, 10, 7, 5, 3

Date	Location	Path Length (m)	Detectors	1(Apt Ave) 2(W/Freq Anal)	Aperture Diameters (mm)
27 Apr 76	Pt. Pinõs-ACANIA	1650	"	1	40, 35, 30, 25, 20, 16, 13, 10, 5, 4
29 Apr 76	Pt. Pinõs-ACANIA	1442	"	1,2	40, 35, 30, 25, 20, 16, 13
30 Apr 76	Pt. Pinõs-ACANIA	1625	"	1,2	40, 16, 13, 10, 5

Figure 1

Illustration of Kolmogorov Turbulence Model

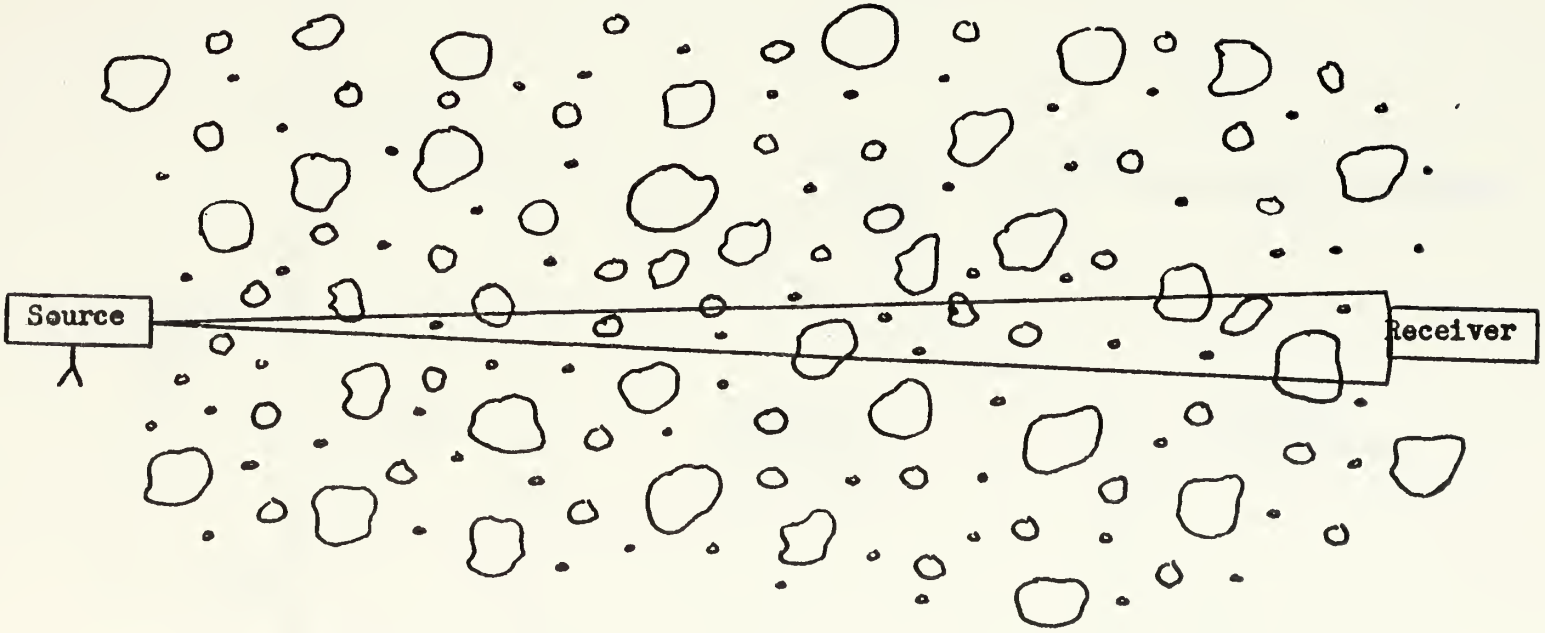

Figure 2

Kolmogorov Turbulence Power Spectrum

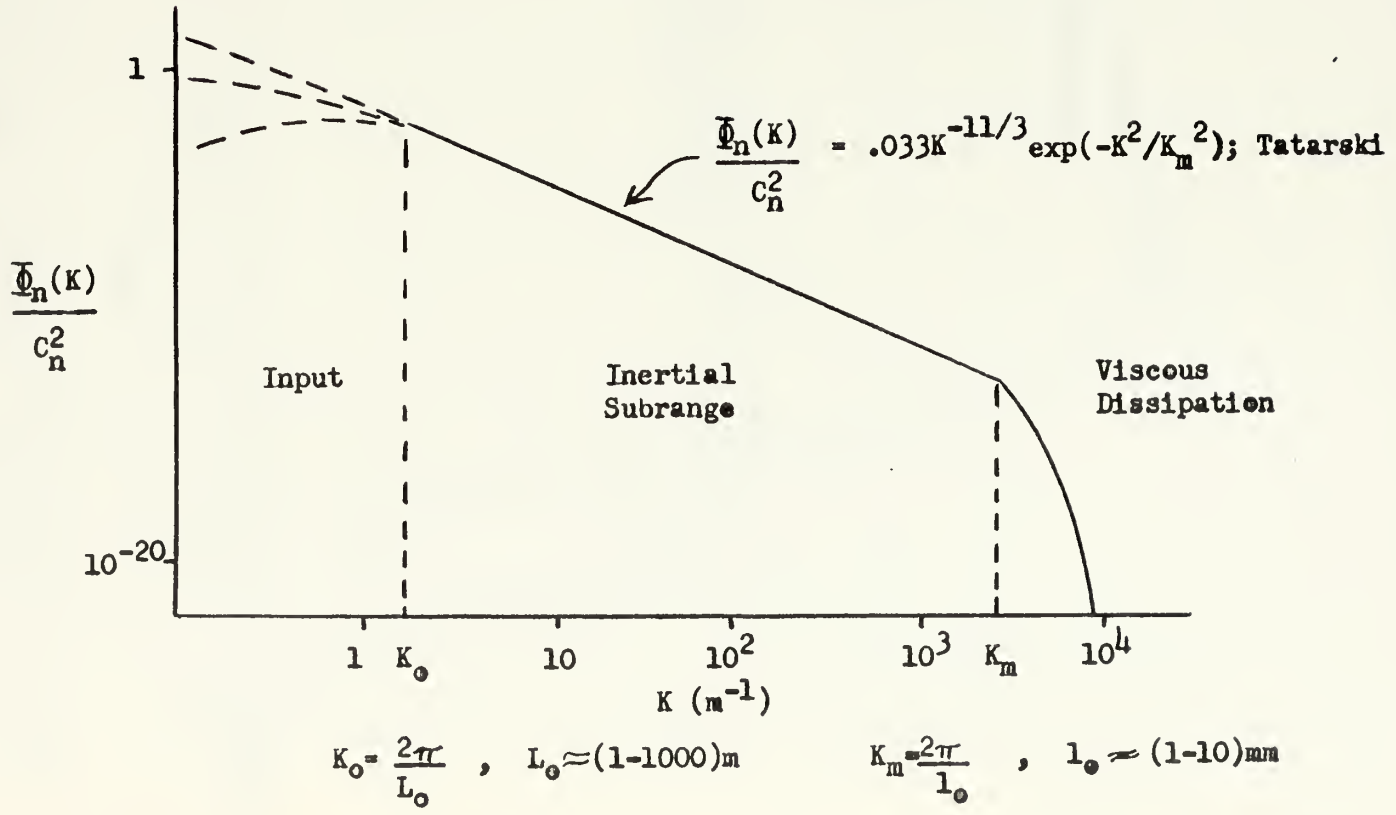

Figure 3

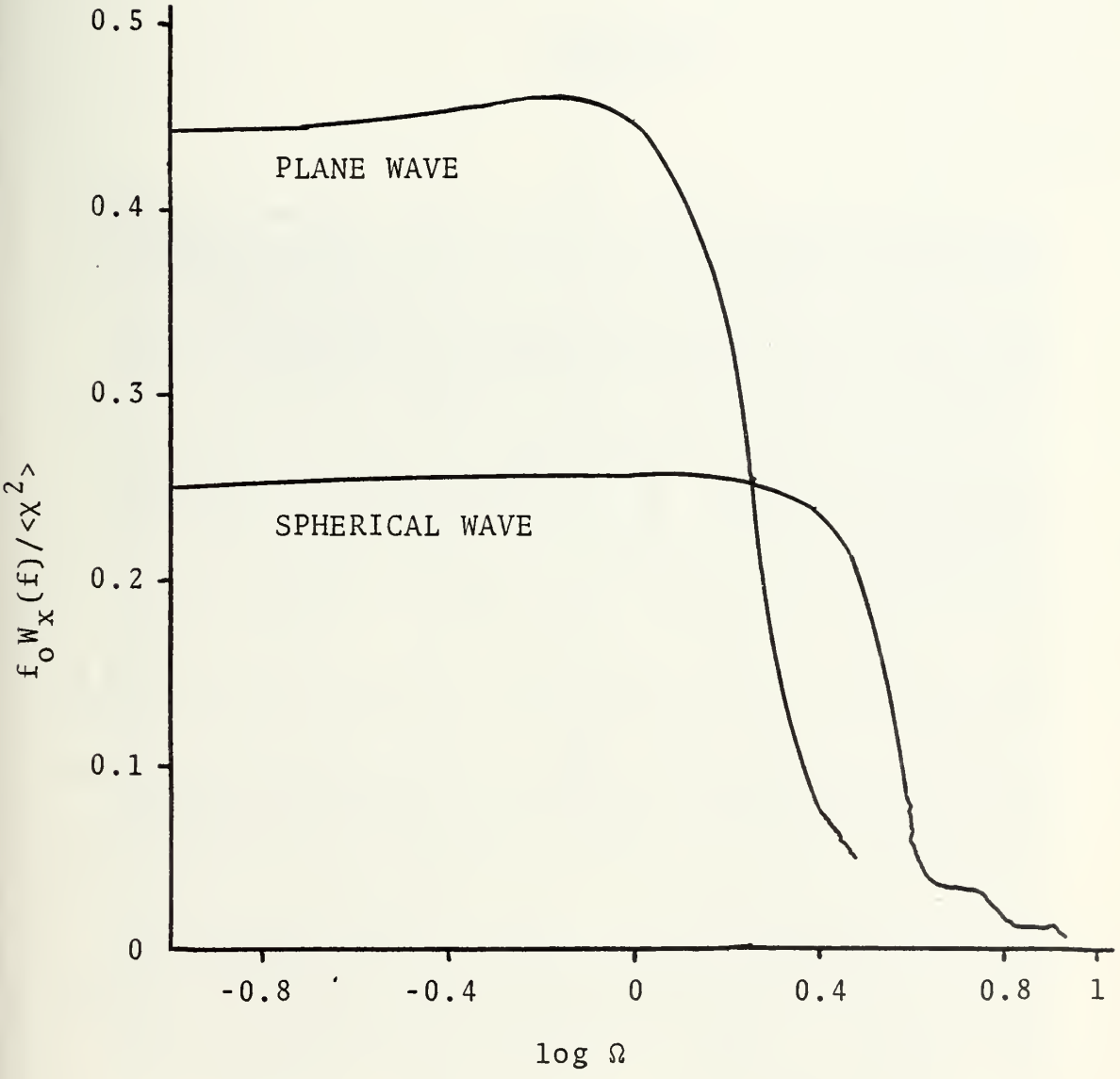

Clifford's theoretical temporal power spectrum of log-amplitude fluctuations for plane- and spherical-wave propagation.

Figure 4

Fried's Theoretical "Θ vs. $\frac{D}{(4Z/k)^{1/2}}$"

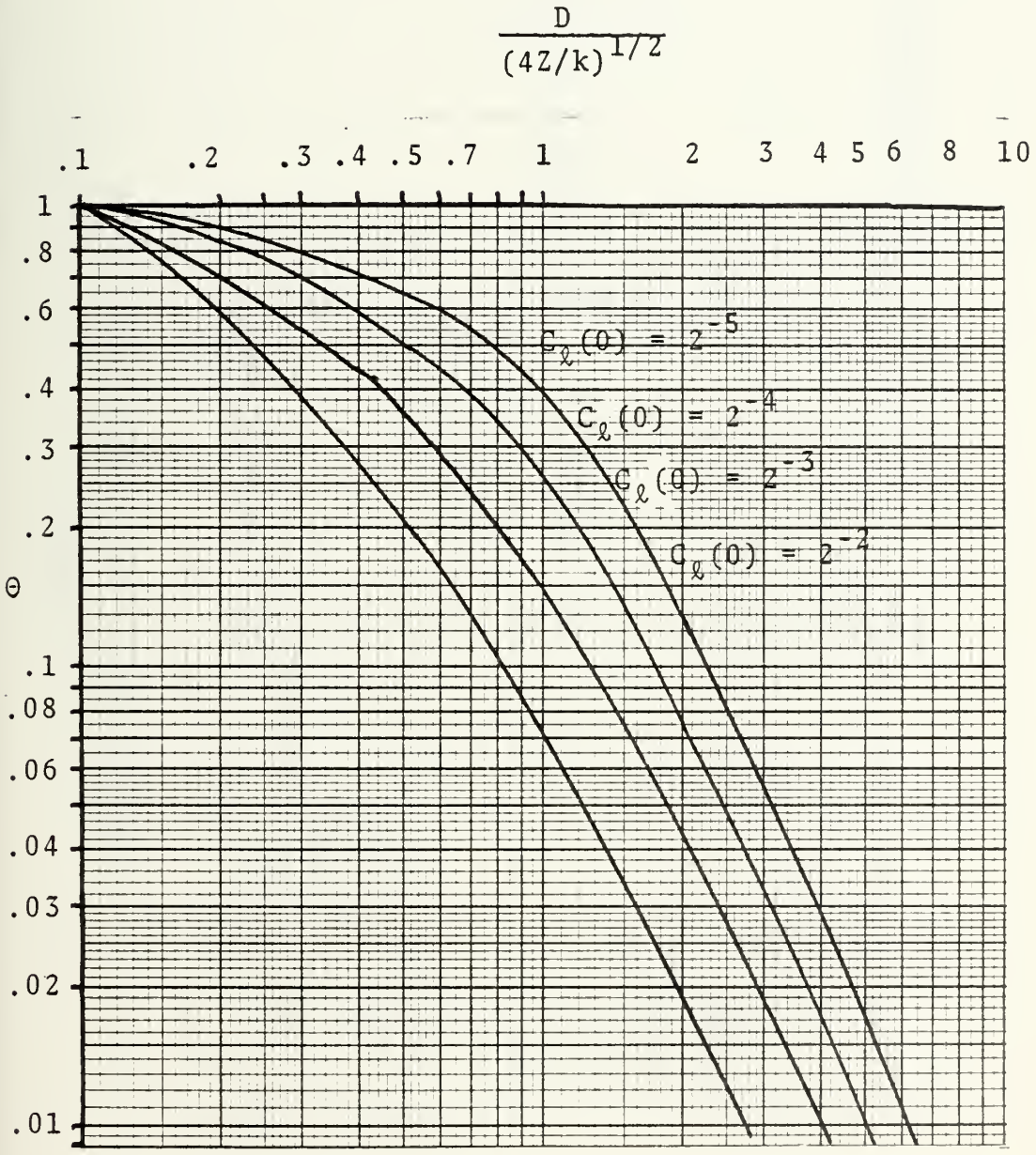

Figure 5

PIN-5DP Photodiode Detector Circuit

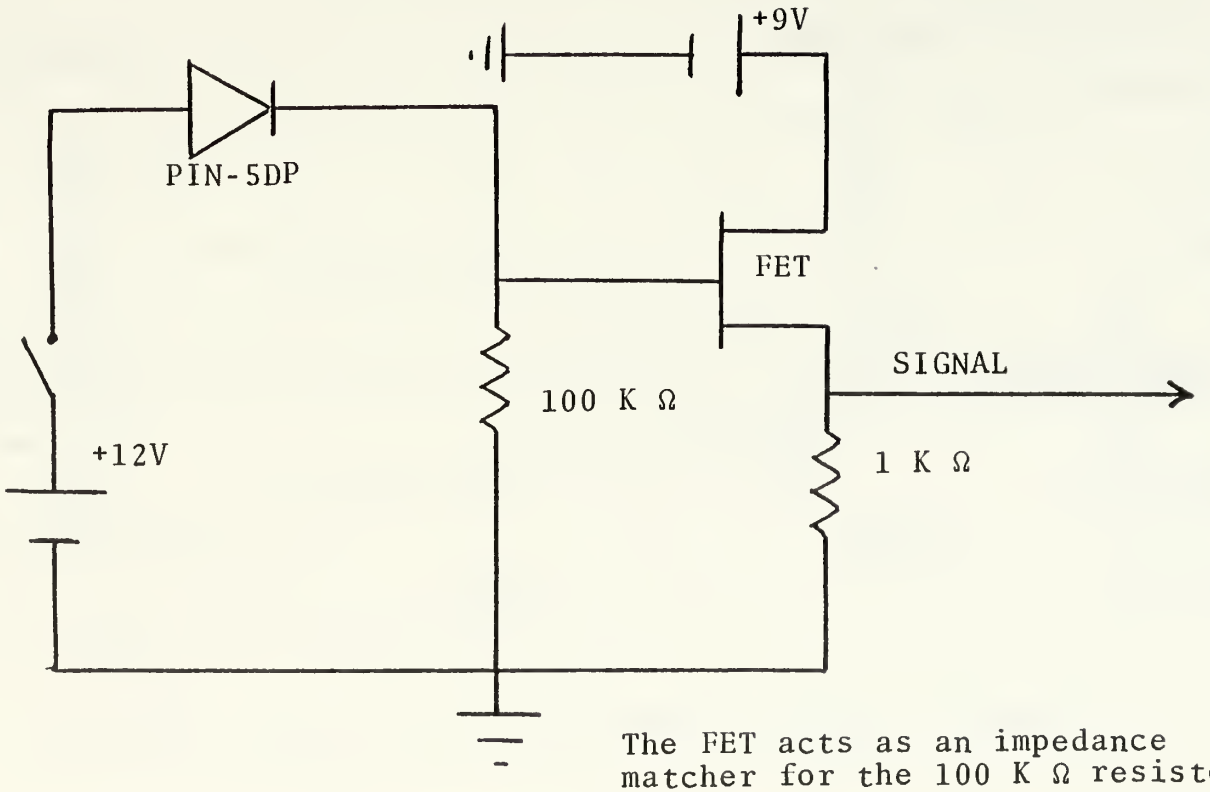

The FET acts as an impedance matcher for the 100 K Ω resistor.

Figure 6

Field Lens System for Avalanche Photodiode Detector

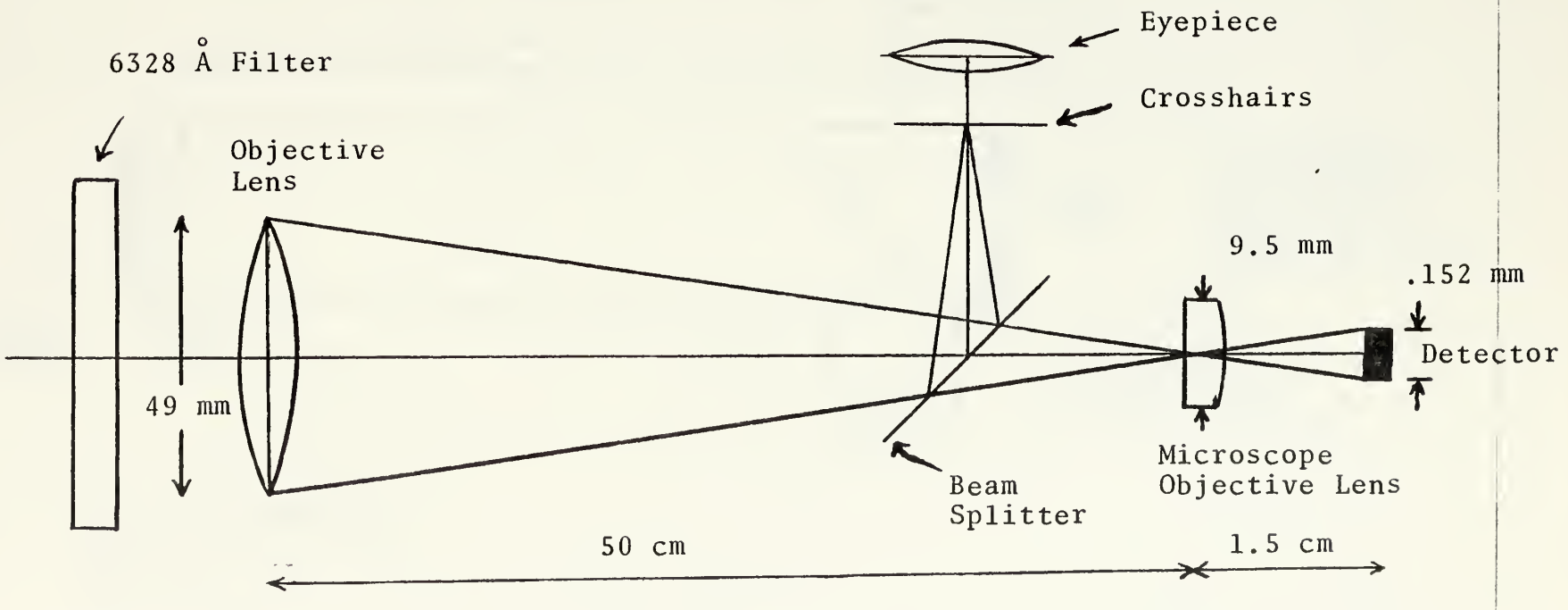

System is encased in a thin-walled aluminum cylinder.

Figure 7

Field Lens System for PIN-5DP Photodiode Detector

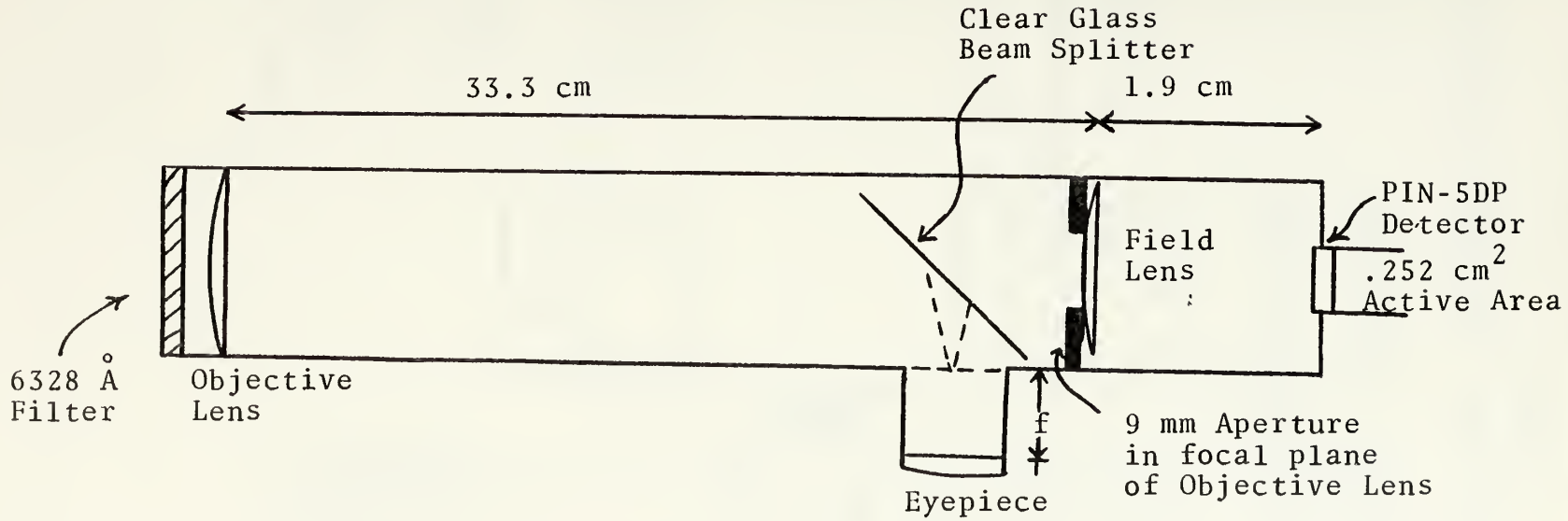

Optical Properties:

Objective Lens: D_o = 2.5 cm; f_o = 33.3 cm

Field Lens: D_o = .9 cm; f_o = 1.8 cm

Convergence Angle: 4.3°. Acceptance Angle = $\frac{D_{field}}{f_{obj}}$ = 2.7×10^{-2} rad = 1.54°

Image distance from field lens = 1.90 cm

Image size = .143 cm diameter

Field lens required to fill detector (.252 cm diam.) = 3.04 cm

Figure 8

Electronic Components: Aperture Averaging Experiment

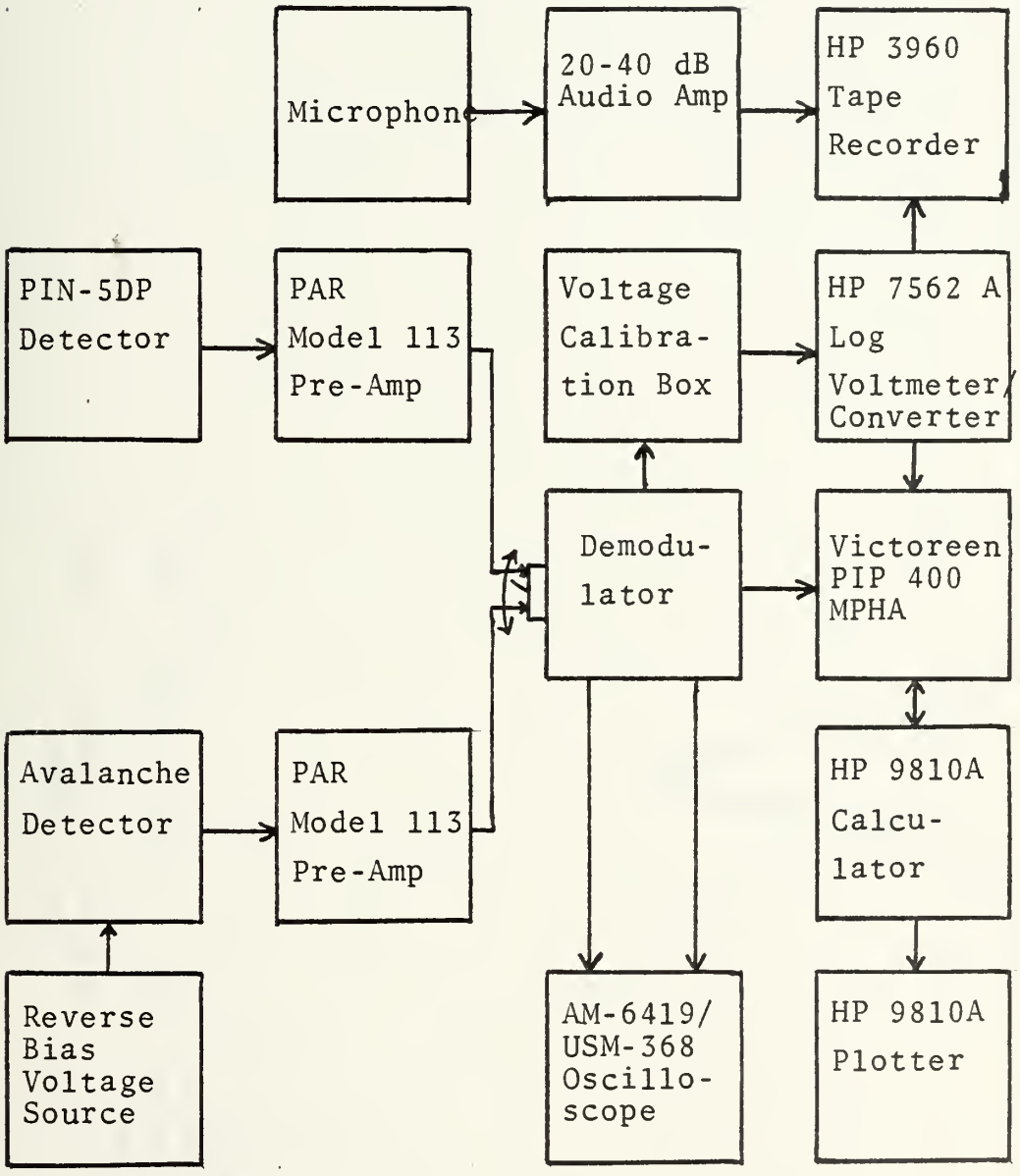

Figure 9

Corridor Experiment Log-Intensity Distribution

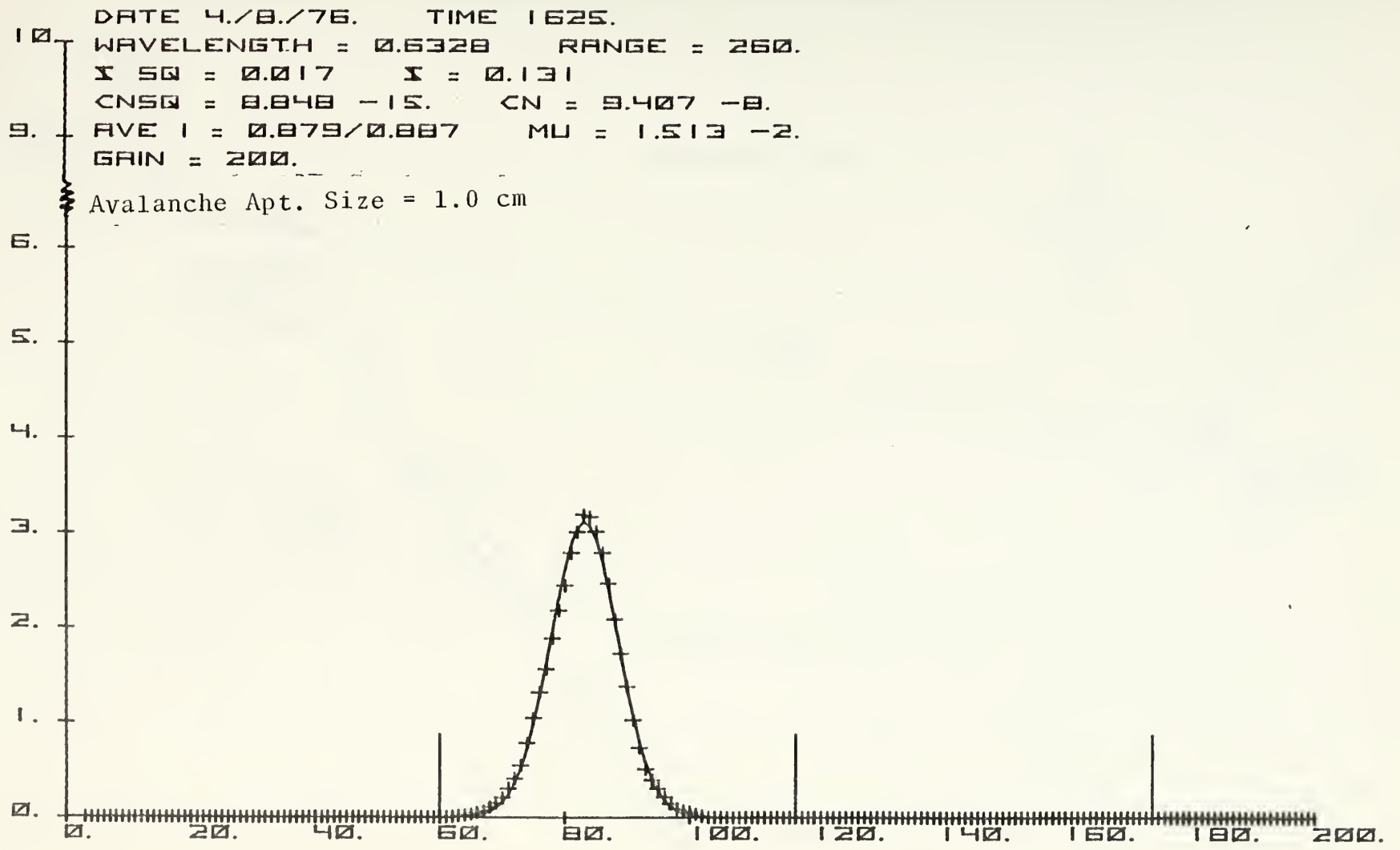

Figure 10
Propagation Paths over Monterey Bay

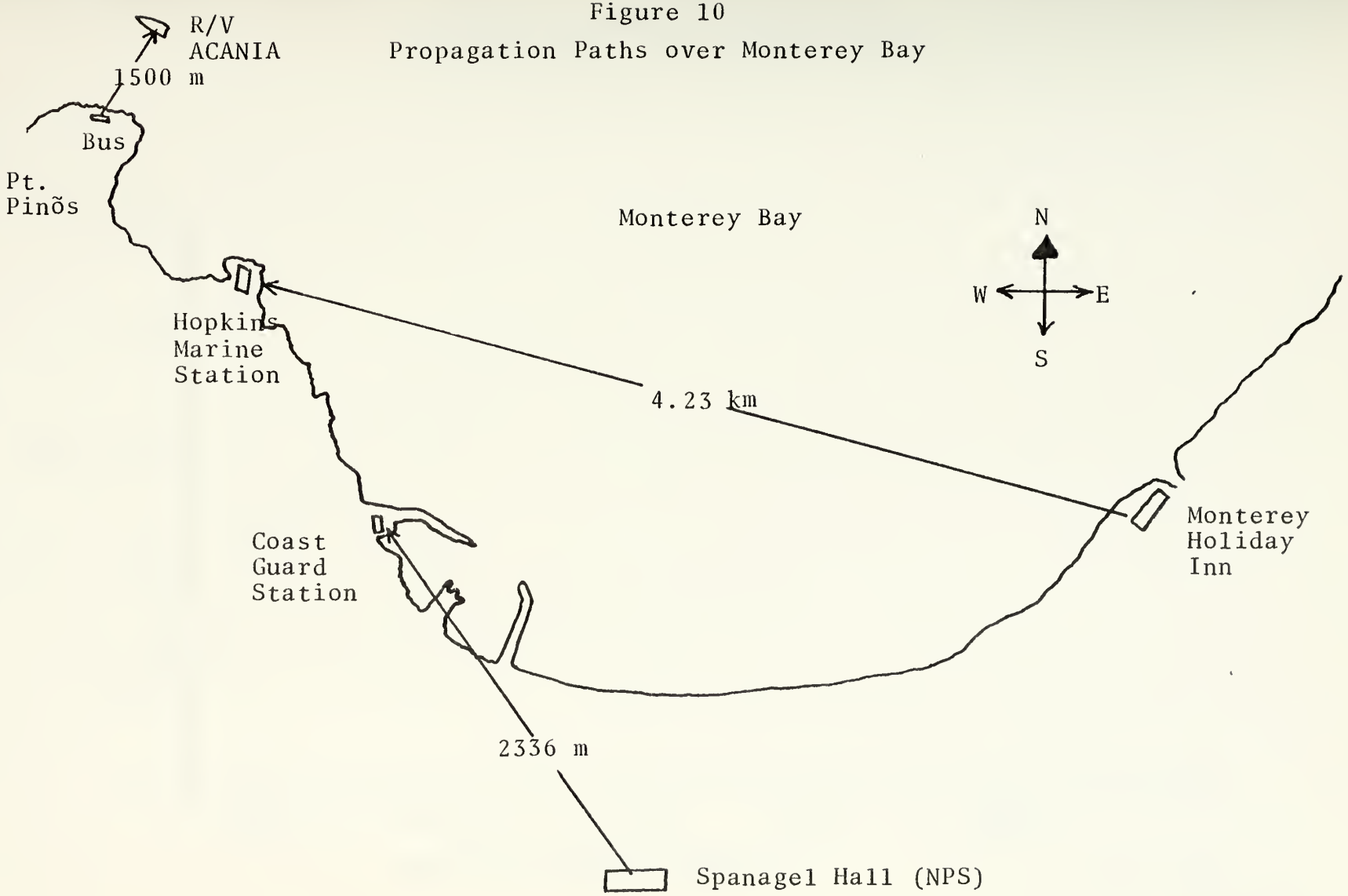

Figure 11

G(D) vs. Aperture Diameter D
Corridor Run, (7-8) February 1976

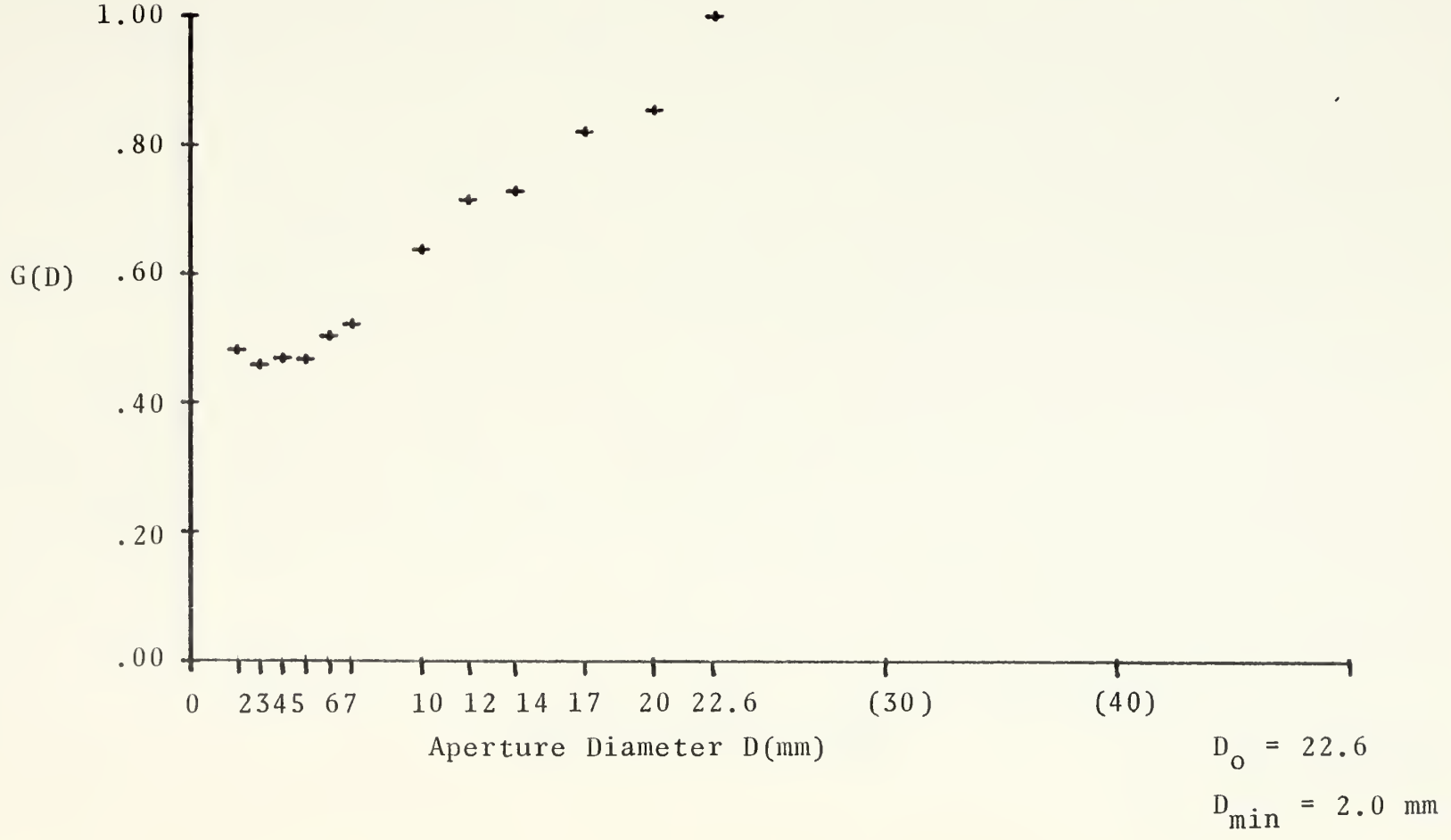

Figure 12

G(D) vs. Aperture Diameter D
Corridor Run, 10 February 1976

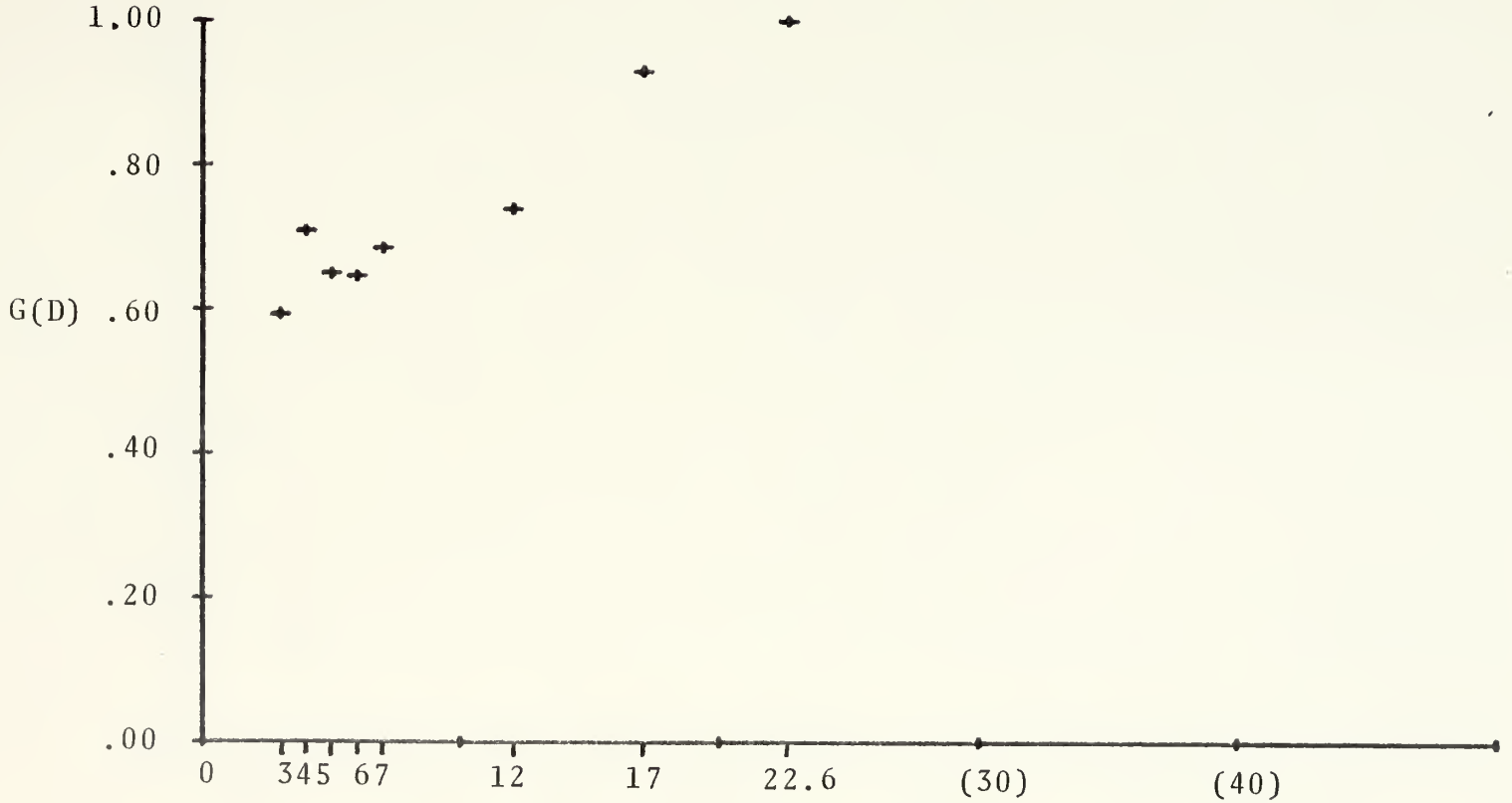

D_o = 22.6 mm

D_{min} = 3.0 mm

Figure 13

G(D) vs. Aperture Diameter D
Corridor Run (7-9) April 1976

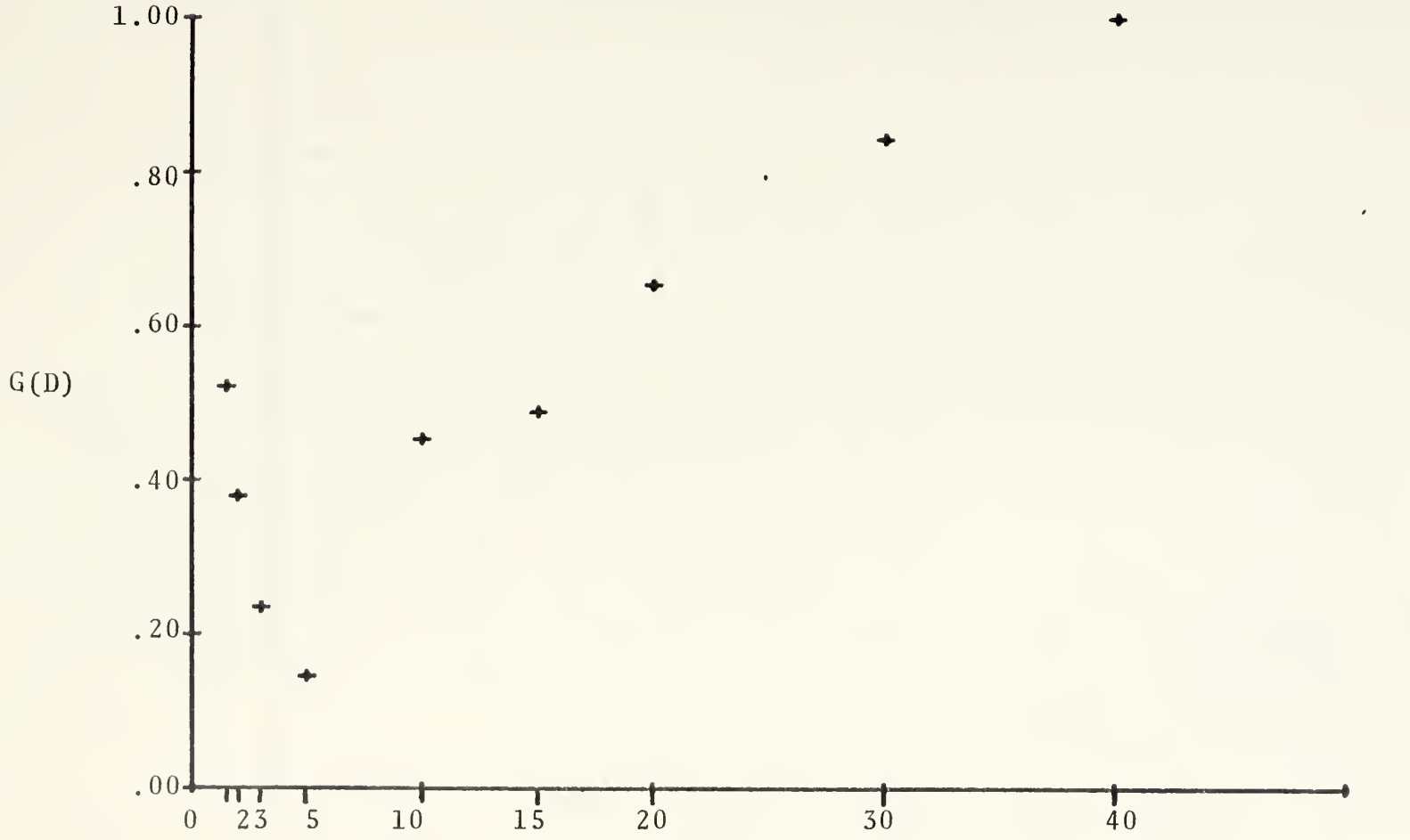

D_o = 40 mm

D_{min} = 1.5 mm

Figure 14

Comparison of Corridor Runs of
7 February, 10 February and (7-9) April

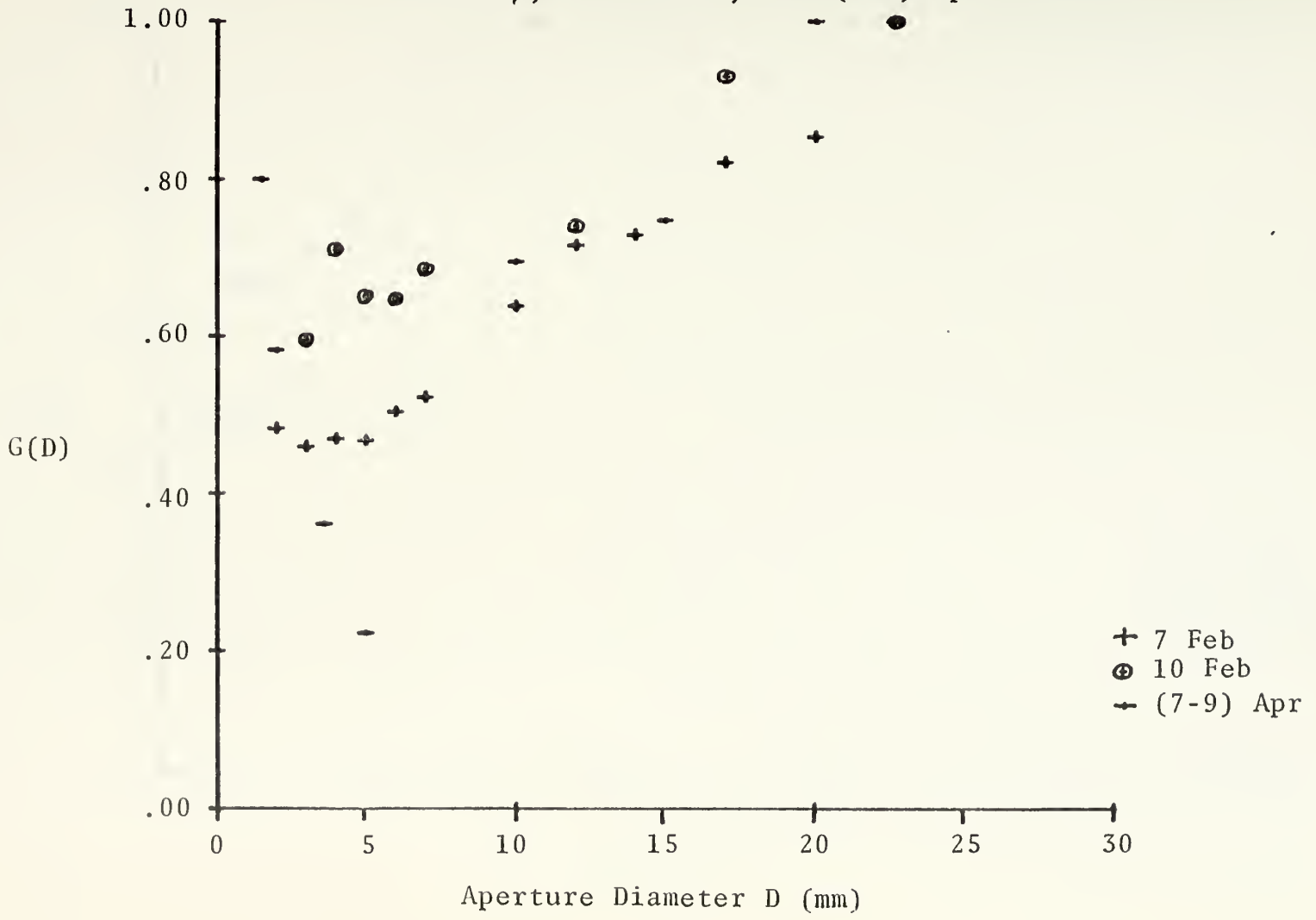

Figure 15
G(D) vs. $D/(\lambda Z)^{1/2}$: Tatarski Model

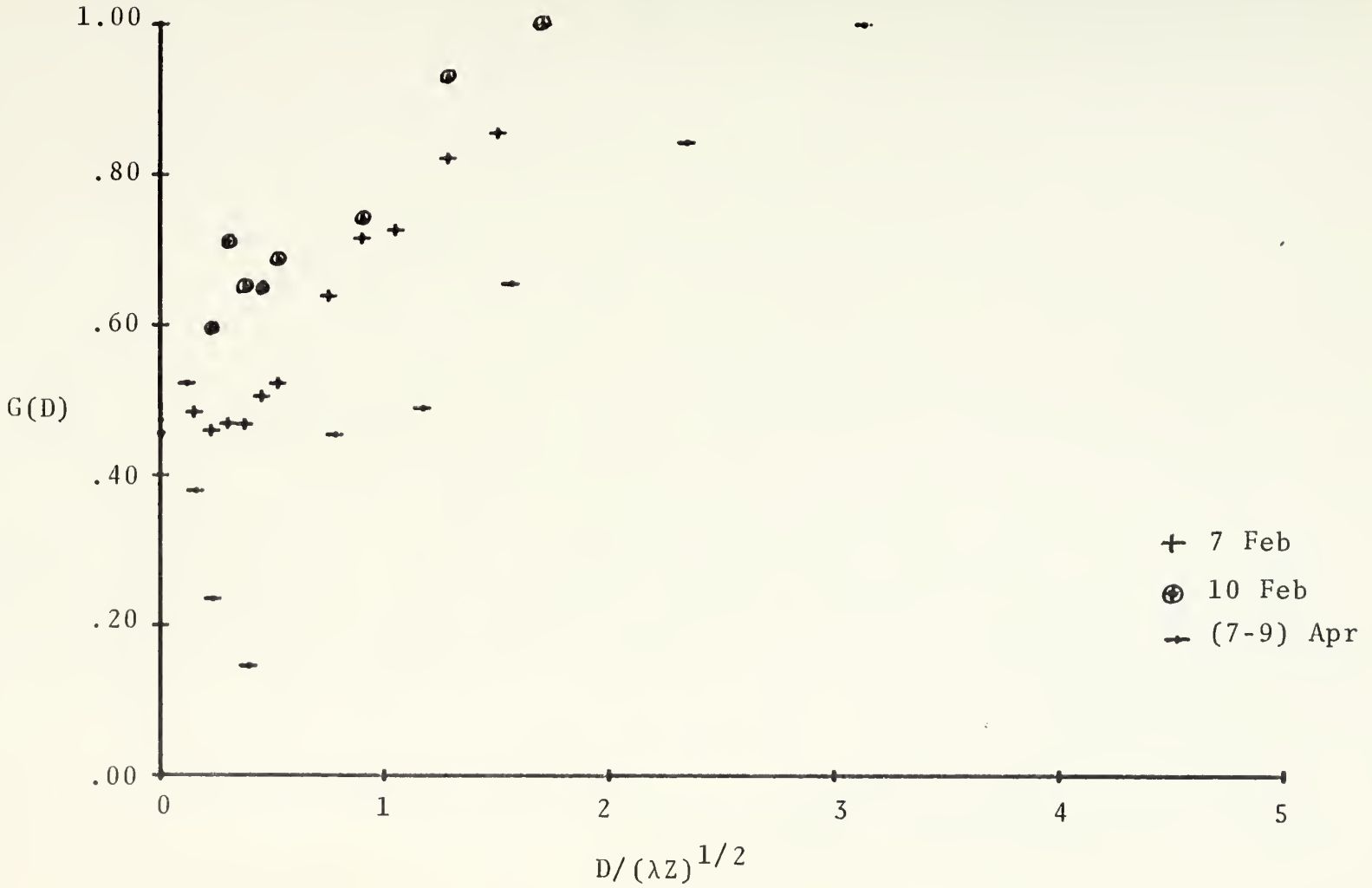

Figure 16
G(D) vs. $D/(4Z/k)^{1/2}$: Fried Model

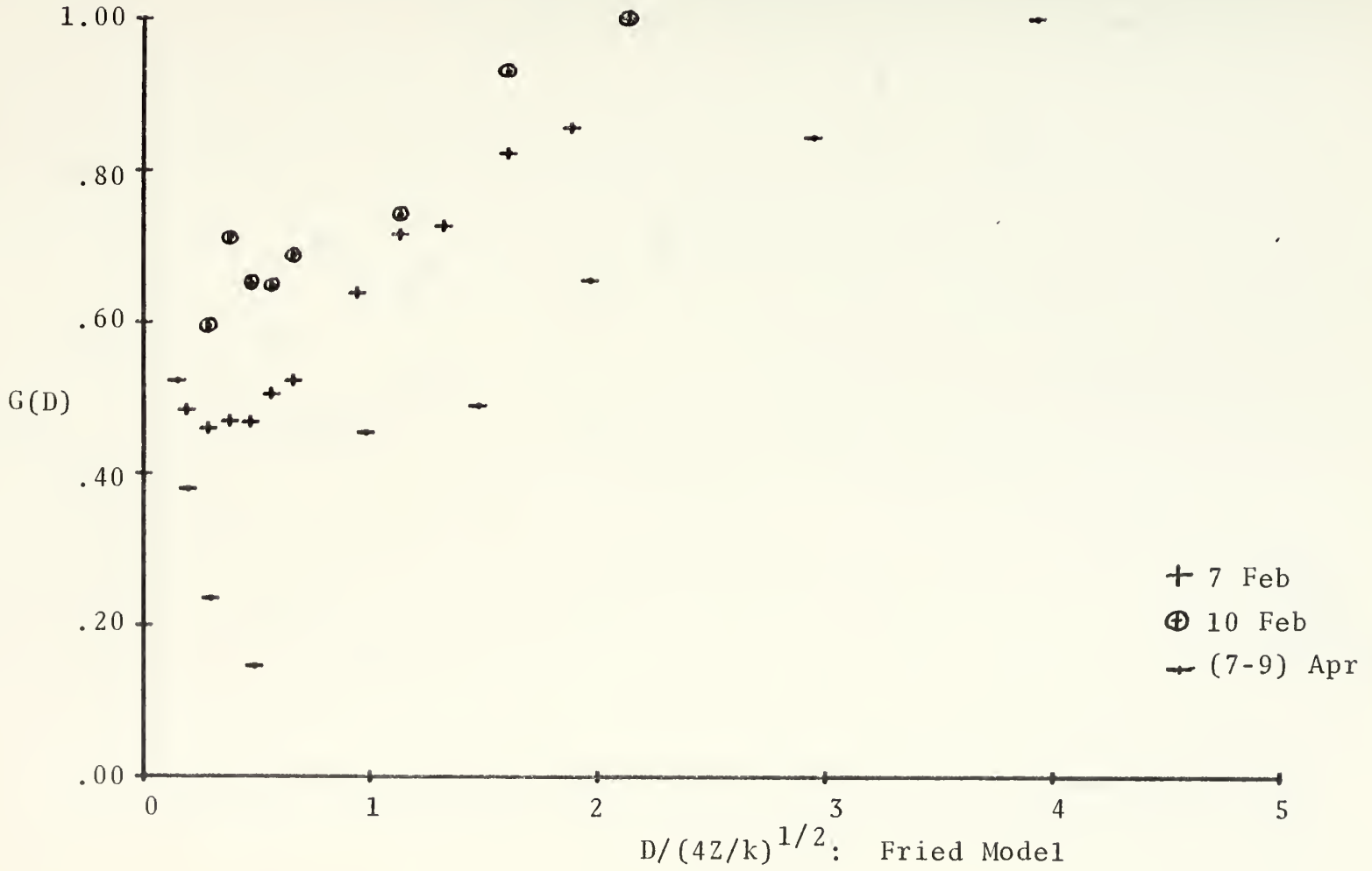

Figure 17

G(D) vs. $D/(Z/k)^{1/2}$: Lutomirski and Yura Model

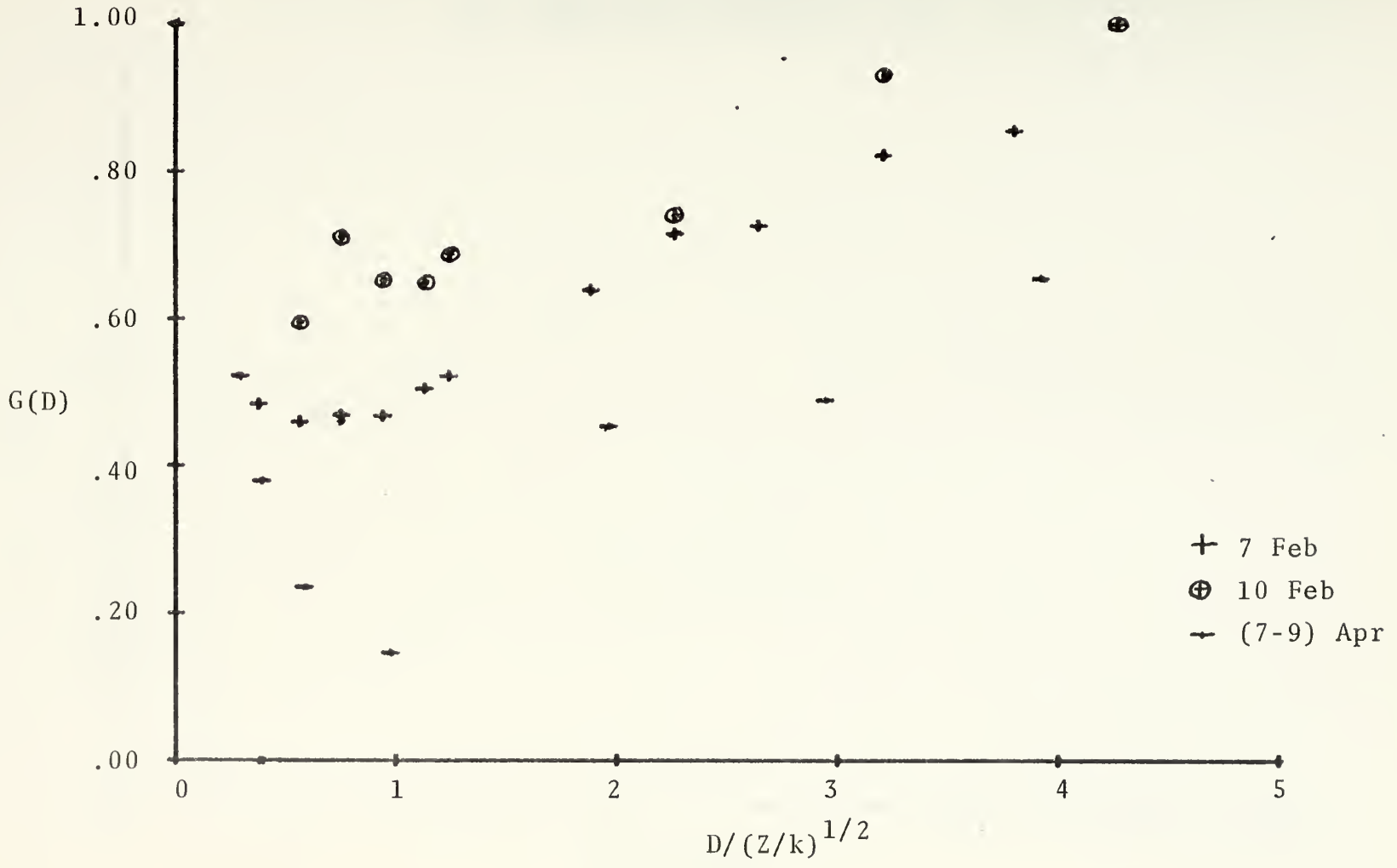

Figure 18

$G(D)$ vs. $D/(Z/k)^{1/2}$

Navy Annex Run, 20 April 1976

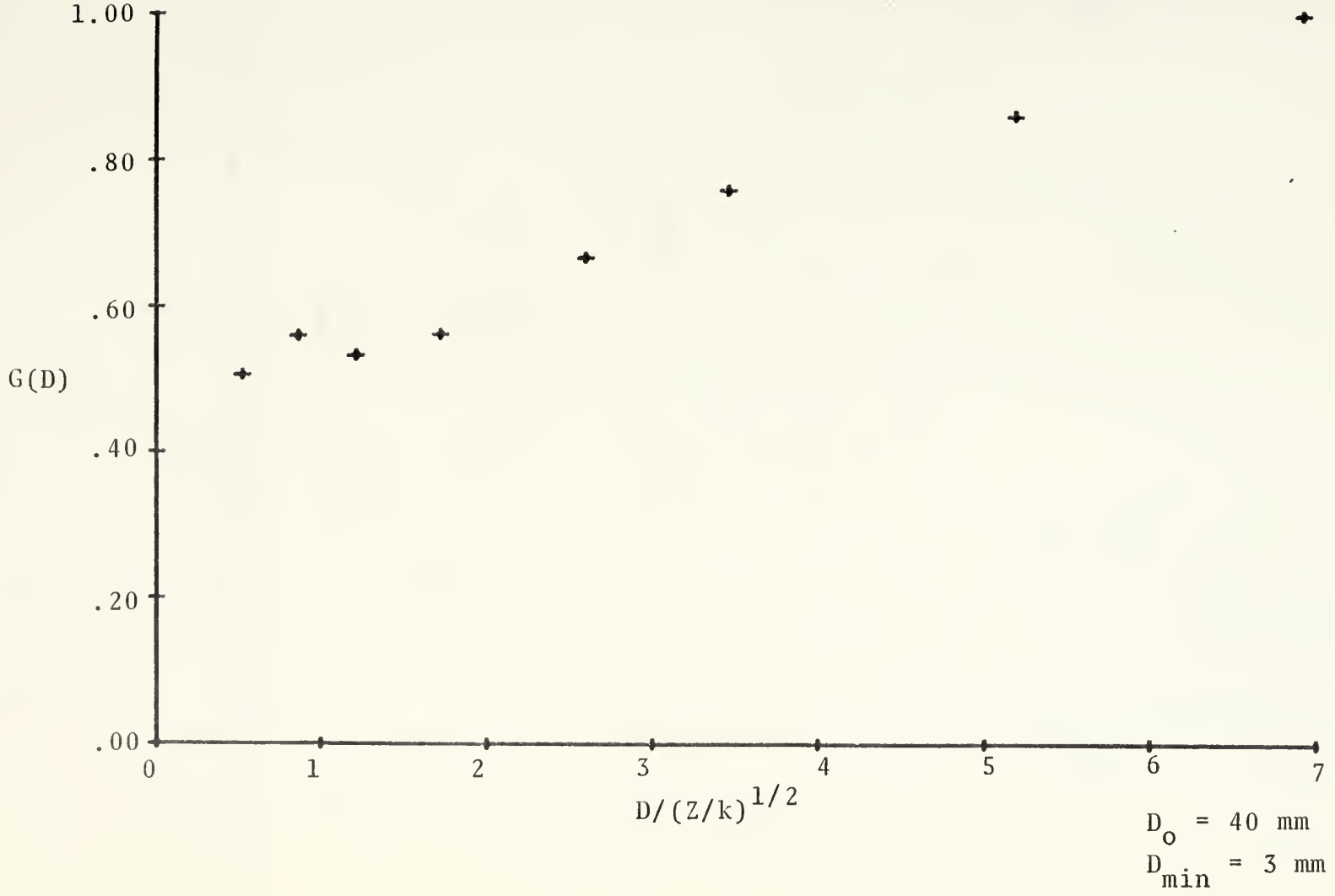

Figure 19

$G(D)$ vs. $D/(Z/k)^{1/2}$

Corridor, 7 Feb and (7-9) Apr; Navy Annex, 20 Apr

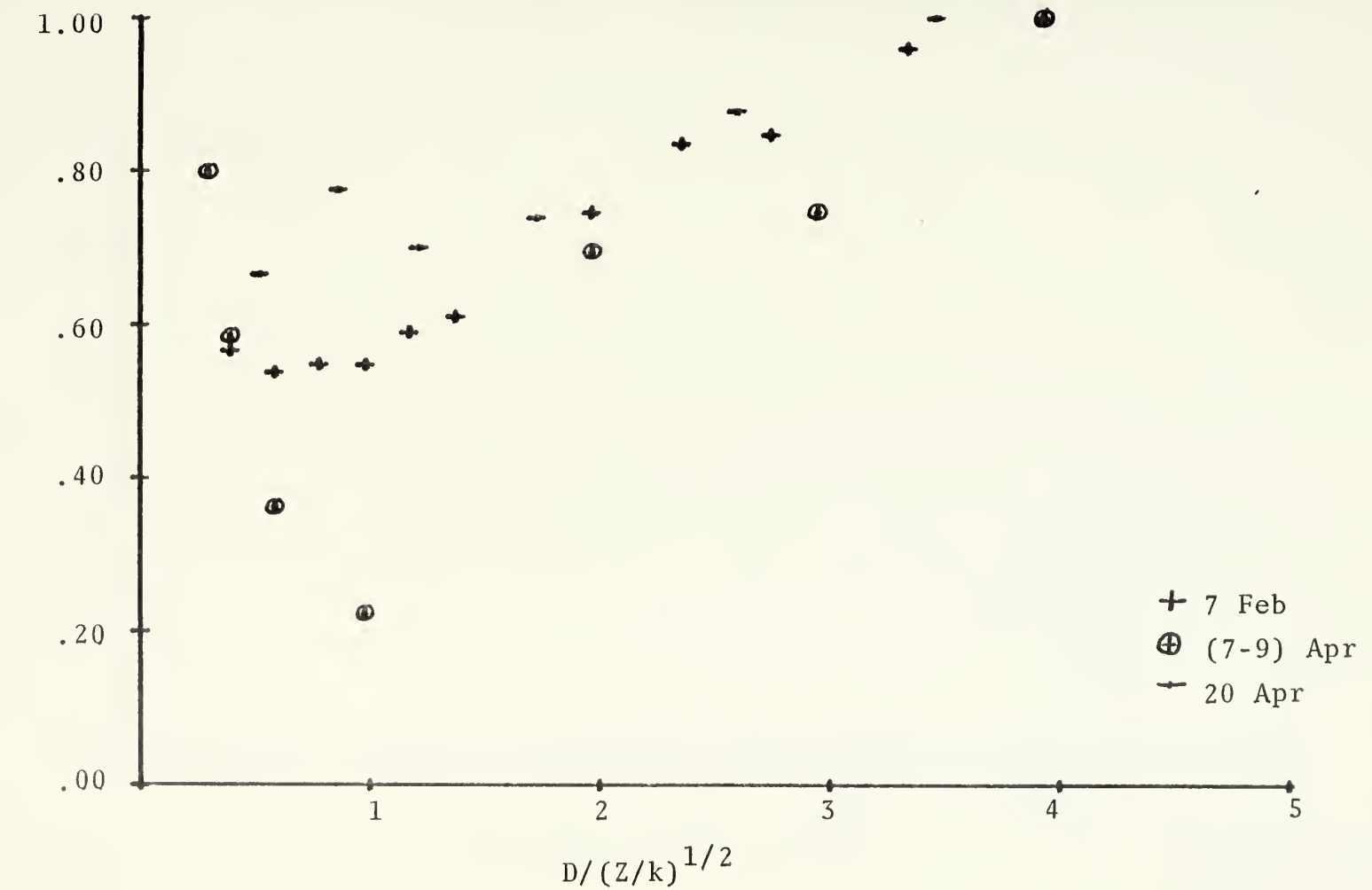

Figure 20

G(D) vs. Aperture Diameter D
Spanagel Roof to Coast Guard Parking Lot, (5-6) March 1976
Saturation Conditions for $\sigma_{\ell I}$

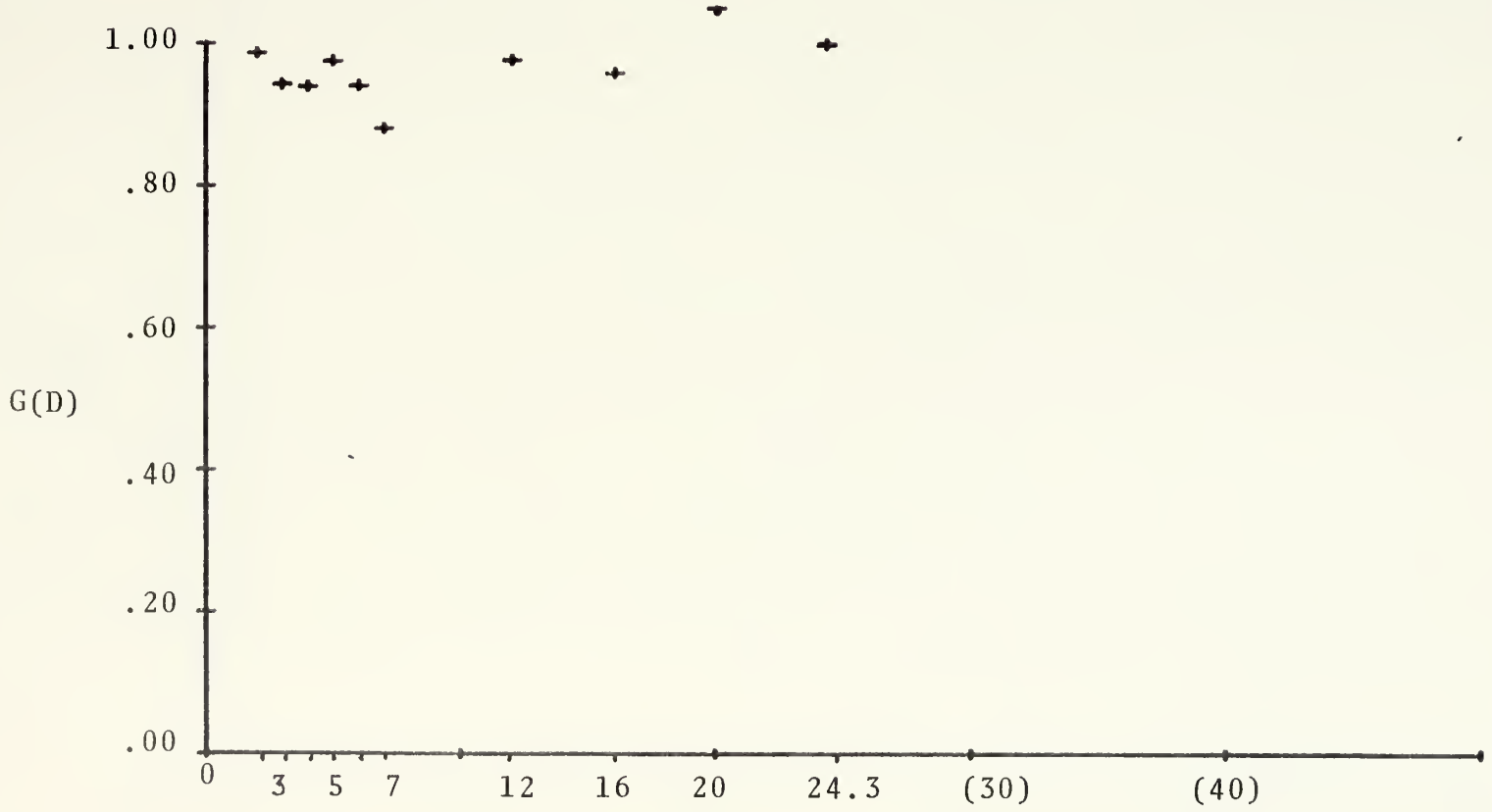

D_o = 24.3 mm

D_{min} = 2 mm

Figure 21

G(D) vs. Aperture Diameter, D
Monterey Holiday Inn to Hopkins Marine Station, 11 March 1976

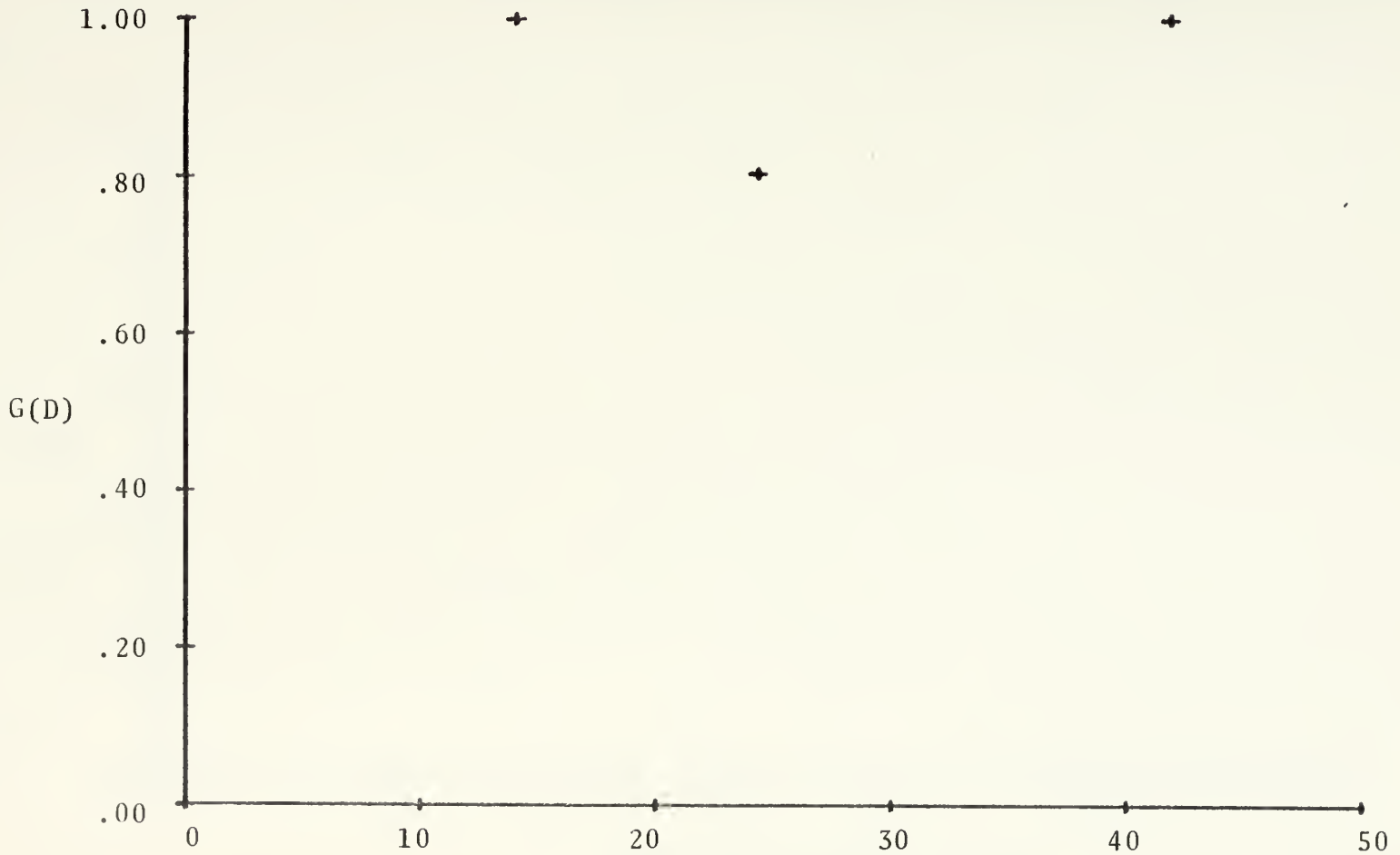

D_o = 40 mm

D_{min} = 14 mm

Figure 22

G(D) vs. Aperture Diameter D
R/V ACANIA, 30 March 1976

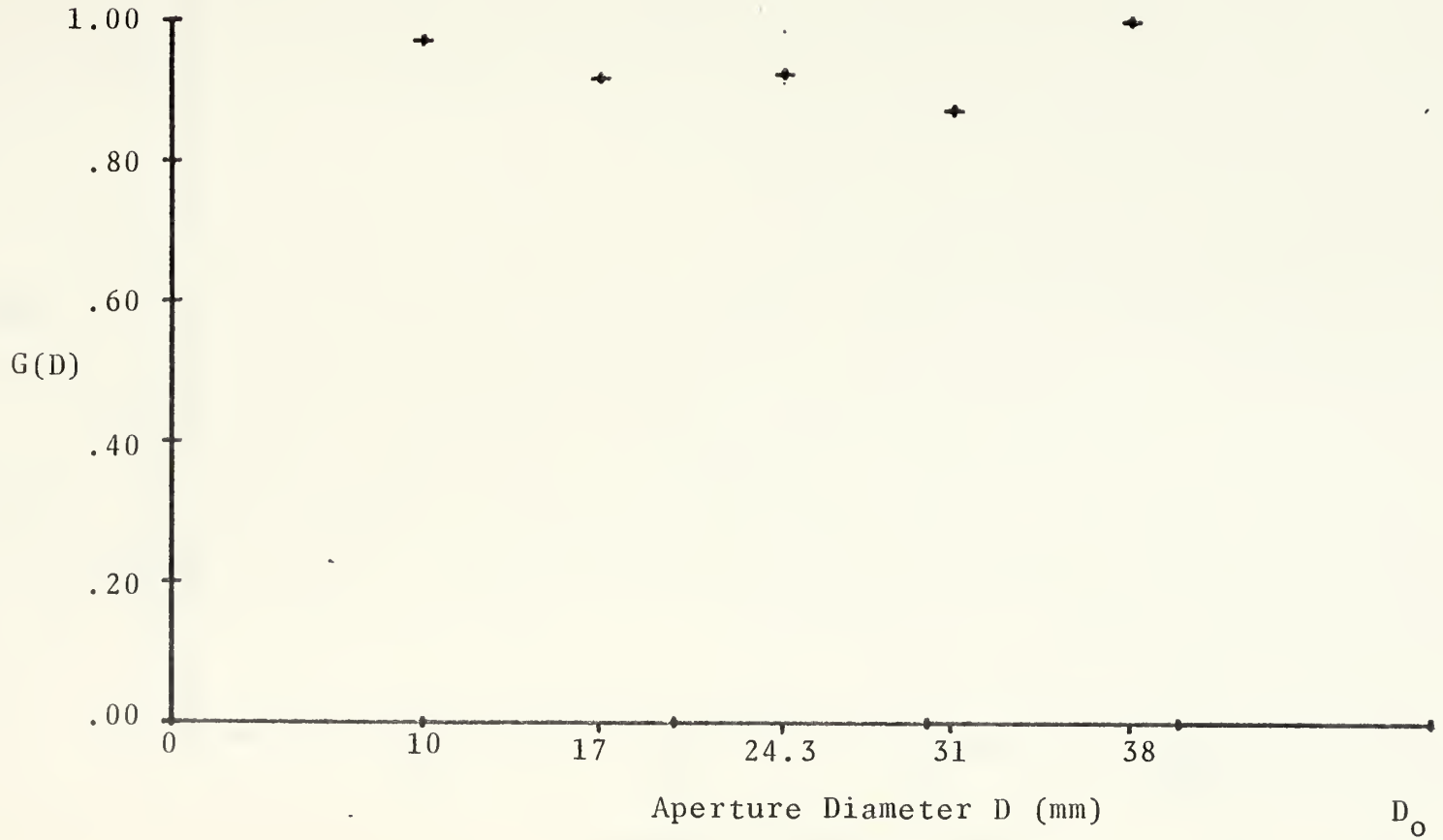

D_o = 38 mm

D_{min} = 10 mm

Figure 23

G(D) vs. Aperture Diameter D
R/V ACANIA, 2 April 1976

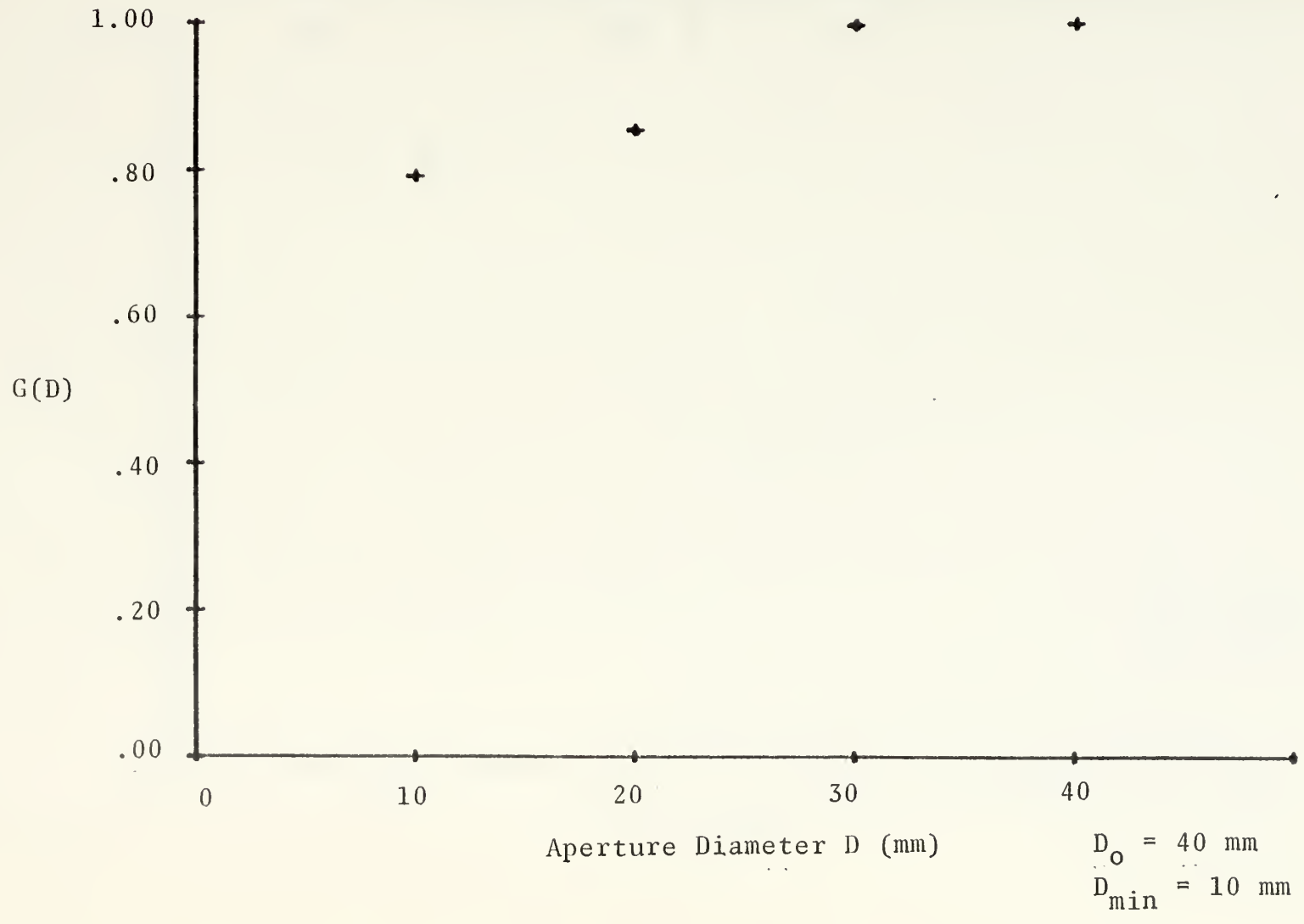

Figure 24

$G(D)$ vs. $D/(Z/k)^{1/2}$

R/V ACANIA, 2 April, and Holiday to Hopkins, 11 March 1976

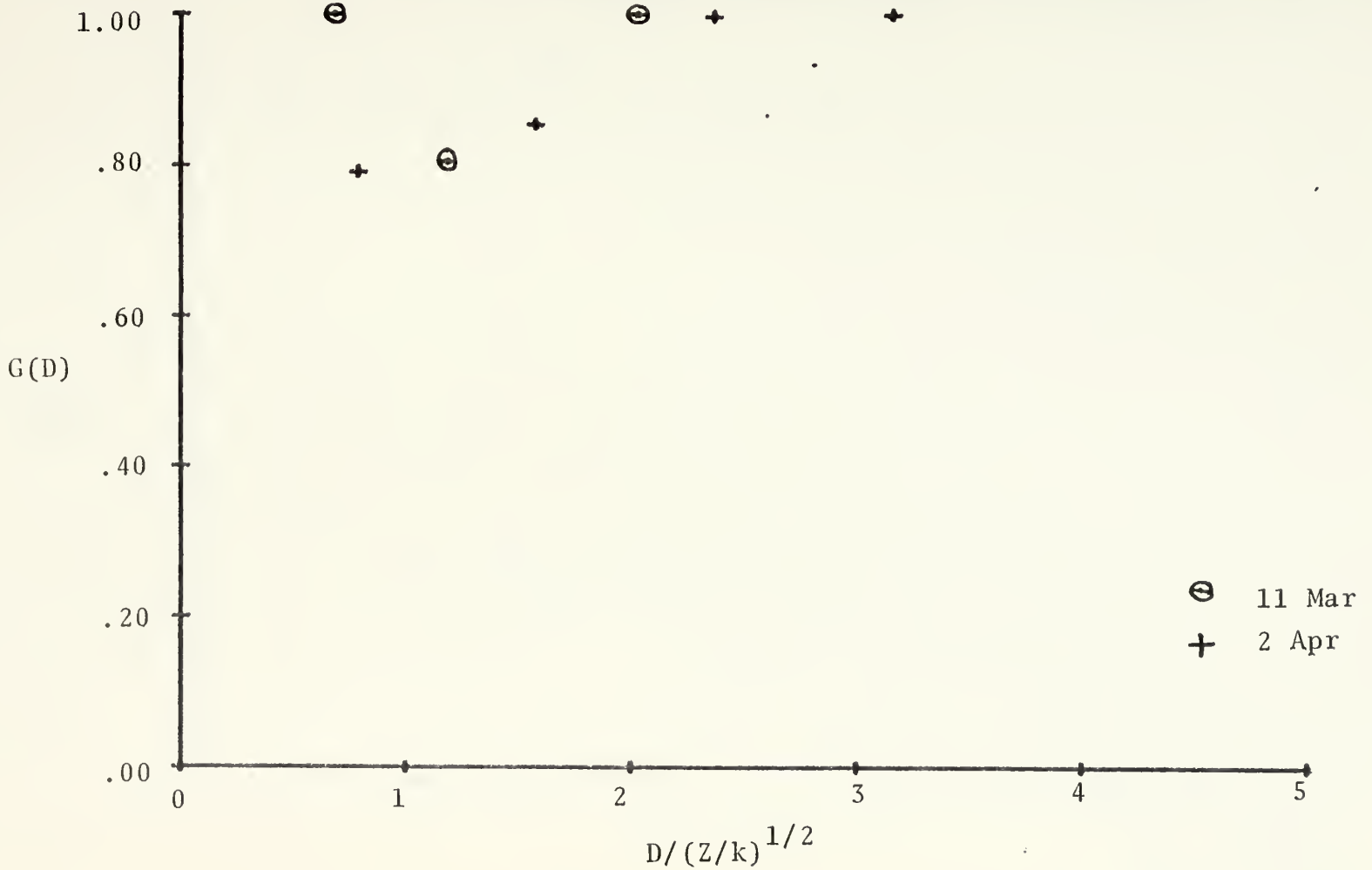

Figure 25
G(D) vs. $D/(Z/k)^{1/2}$
R/V ACANIA, 27 April 1976

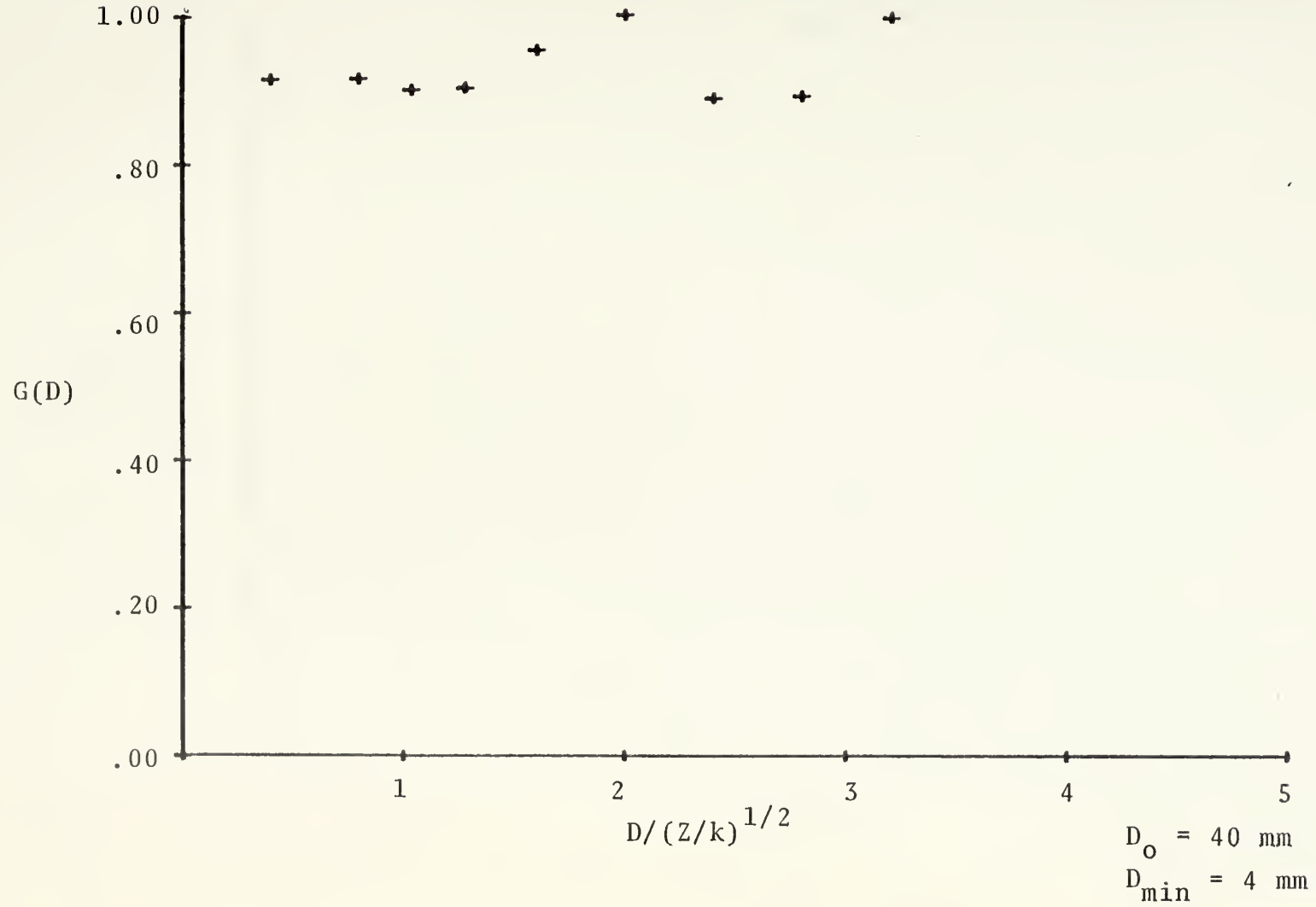

Figure 26
$G(D)$ vs. $D/(Z/k)^{1/2}$
R/V ACANIA, 29 April 1976

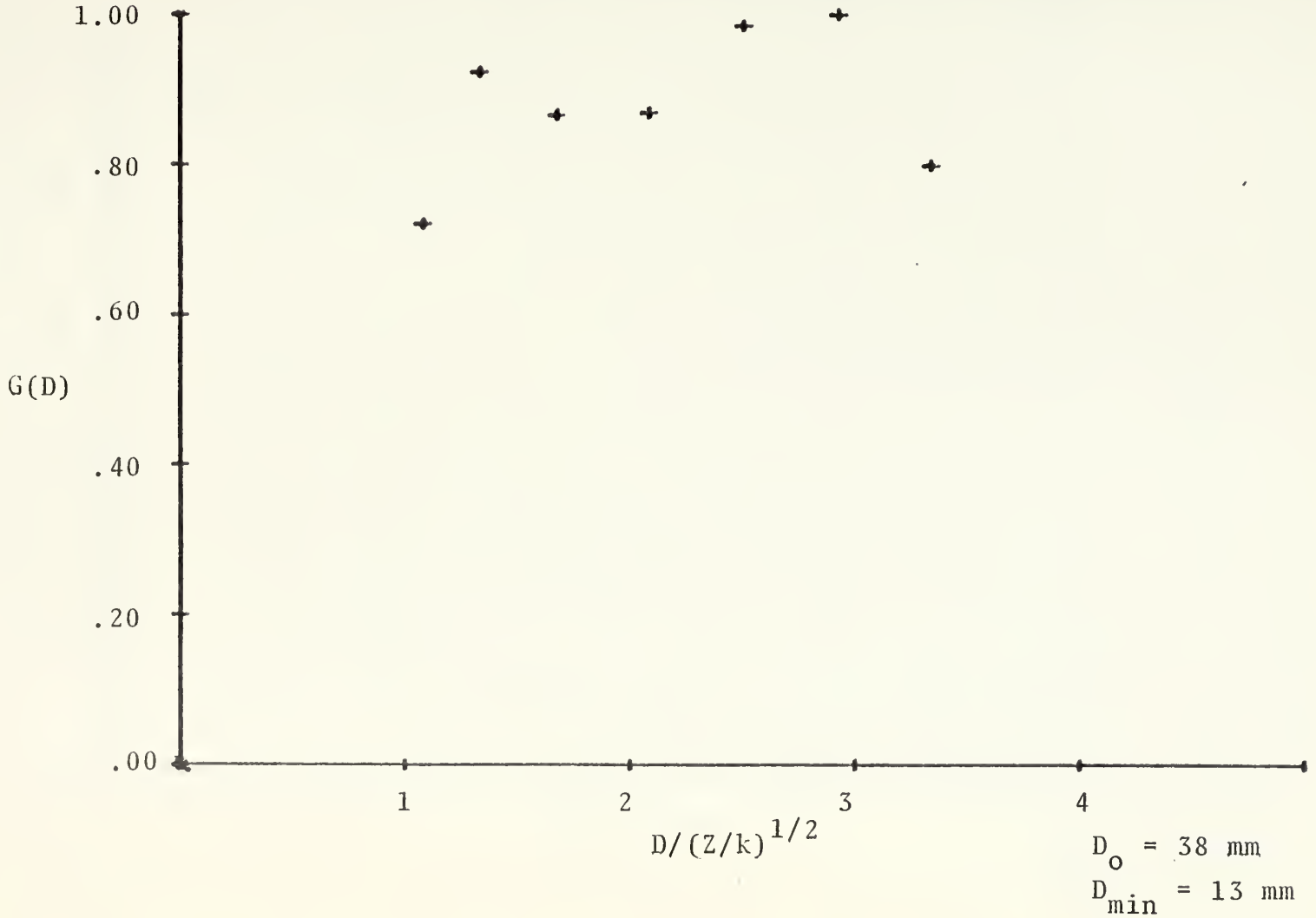

Figure 27

G(D) vs. $D/(Z/k)^{1/2}$

R/V ACANIA, 30 April 1976

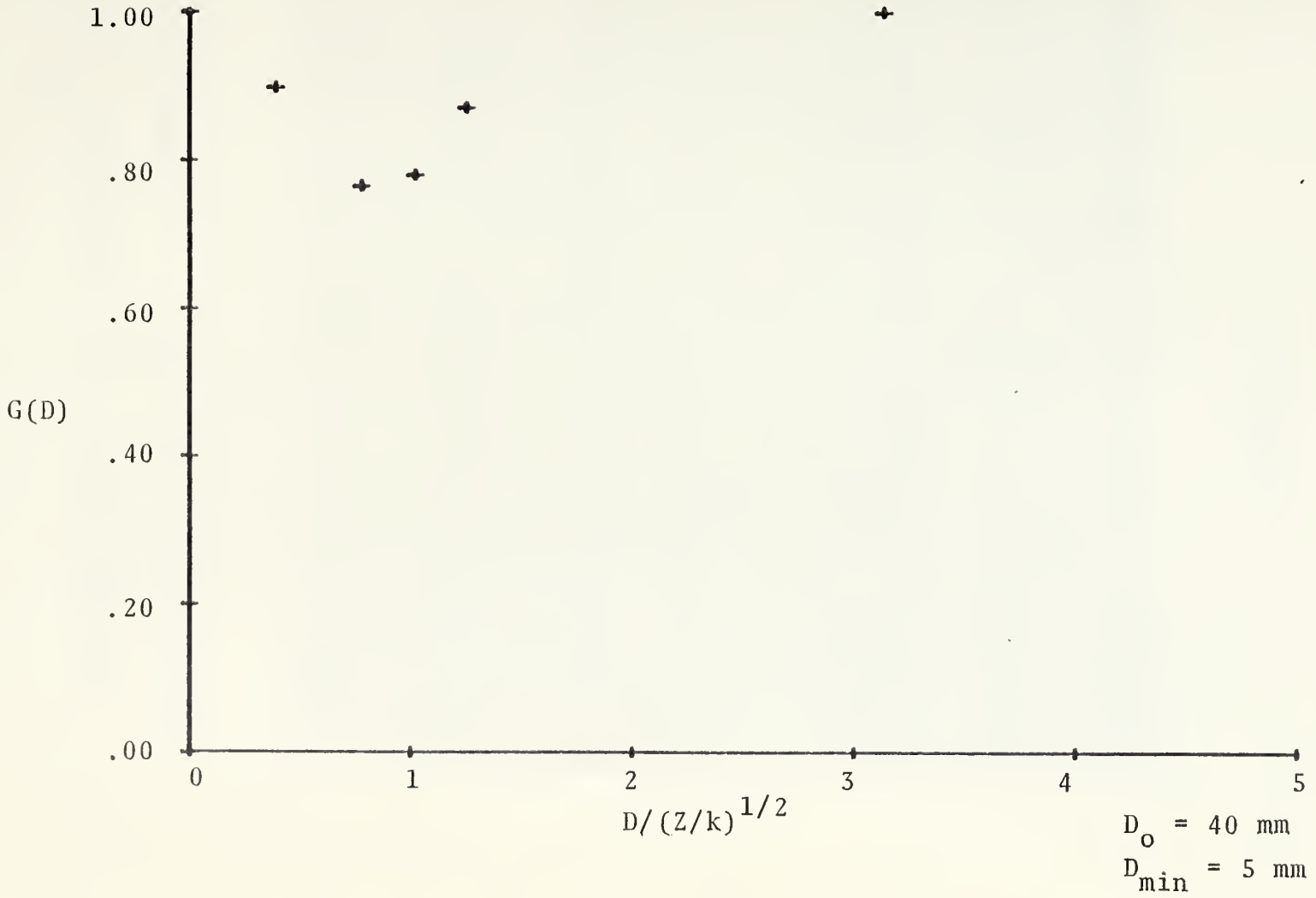

Figure 28

Empirical and Theoretical "Θ vs. $\frac{D}{(4Z/k)^{1/2}}$"

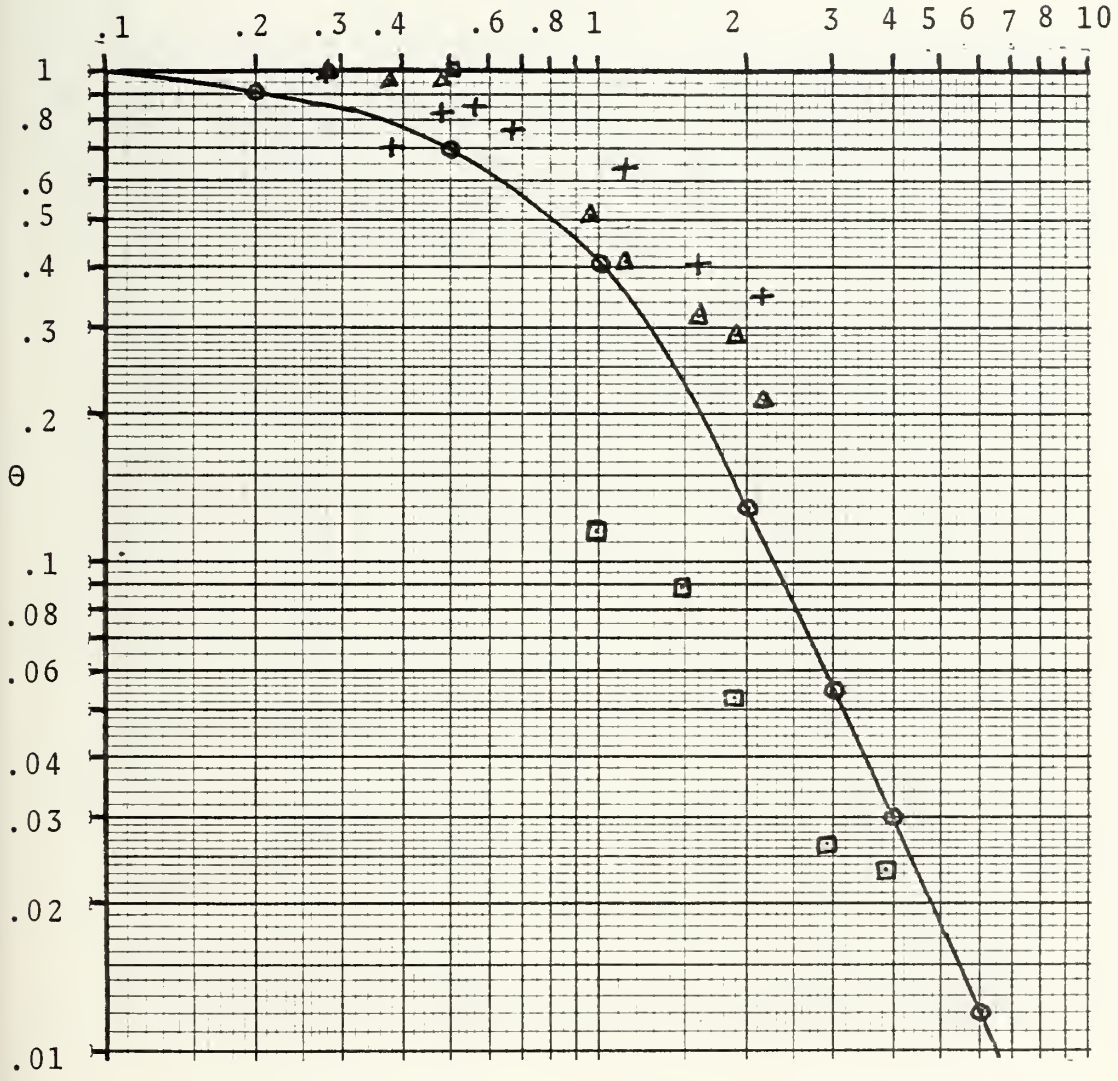

△ 7 Feb (Corridor)

⊡ (7-9) Apr (Corridor)

⊙ Fried's Theoretical for $C_{\ell}(0) = 2^{-5}$

\+ 10 Feb (Corridor)

Figure 29

"Θ vs. $\frac{D}{(4Z/k)^{1/2}}$": ACANIA Experiments

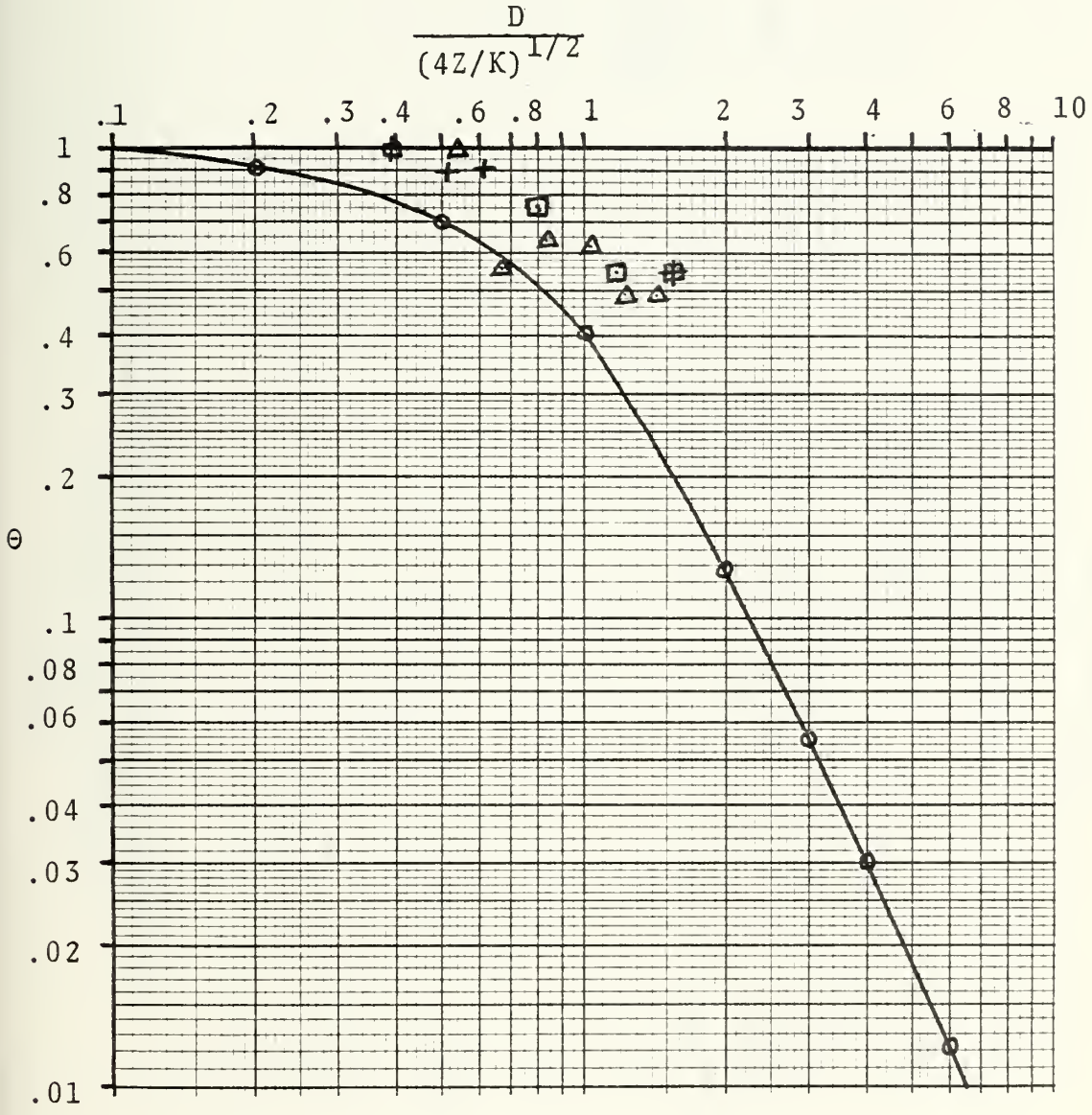

⊙ Fried's Theoretical + 30 April 1976

△ 29 April 1976 ⊡ 2 April 1976

Figure 30

Relative Power Spectra
(7-9) April 1976, Corridor Experiment

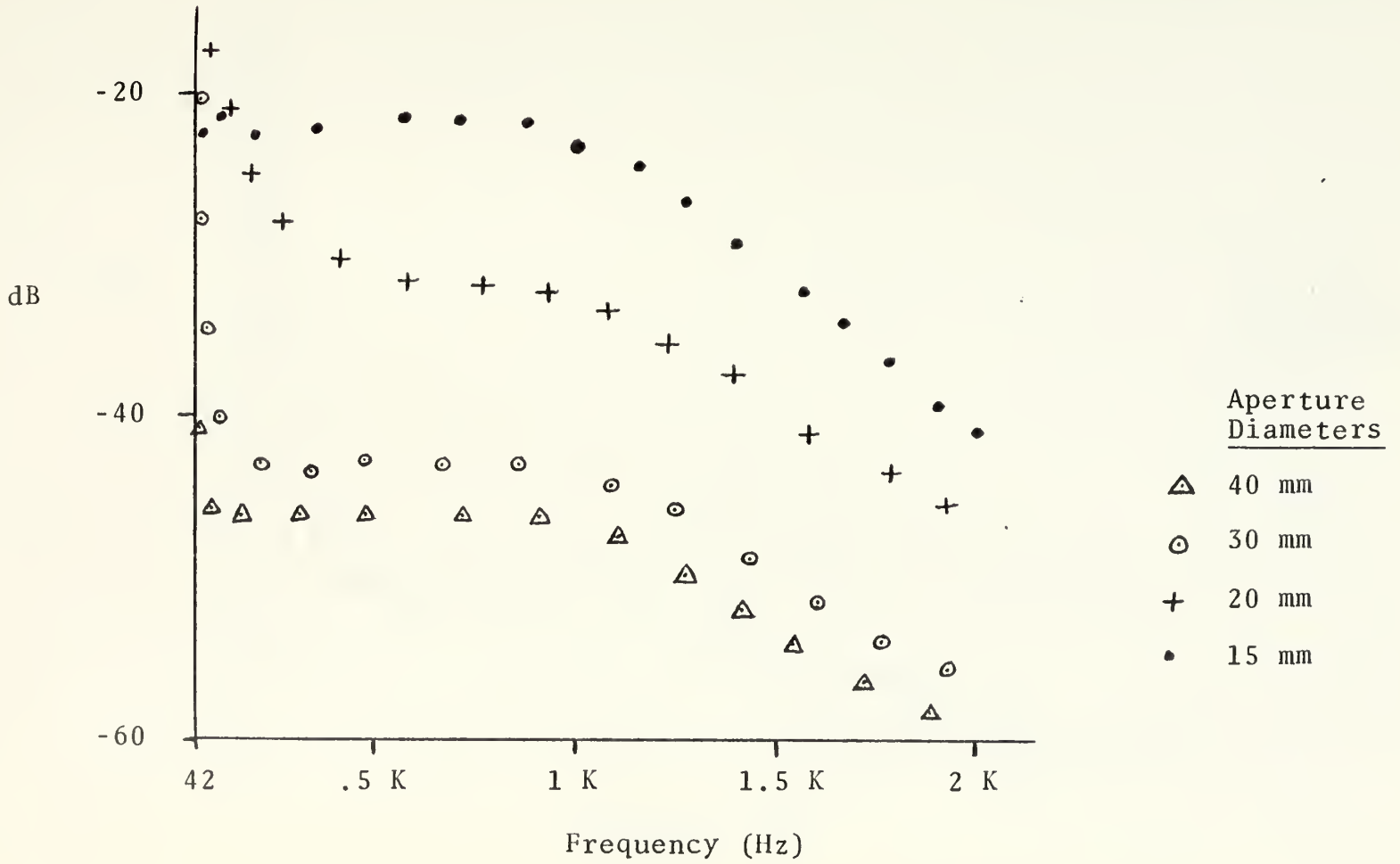

Figure 31

Relative Power Spectra
20 April 1976, Over Land Experiment

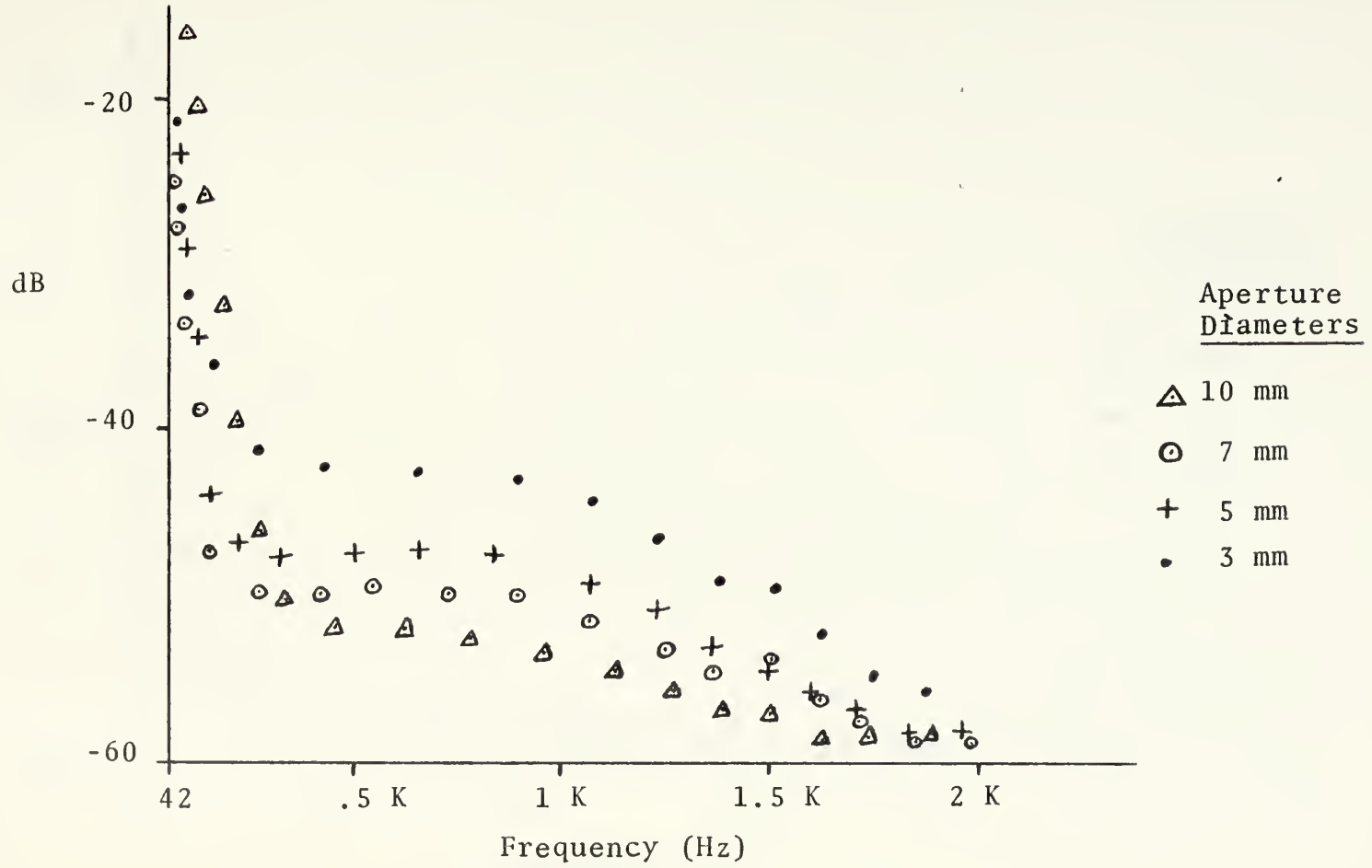

Figure 32

Relative Power Spectra
20 April 1976, Over Land Experiment

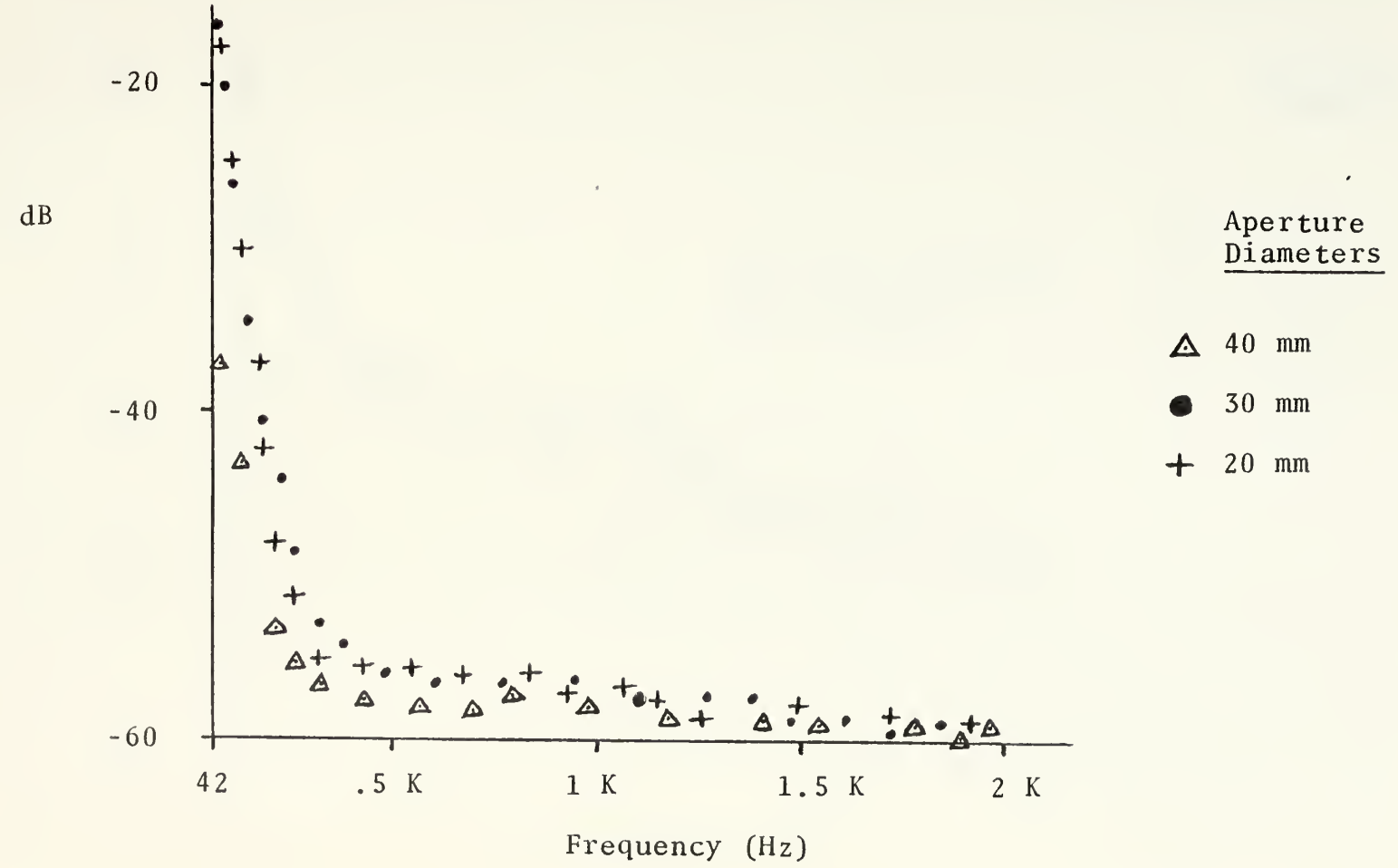

Figure 33

Relative Power Spectra
(29-30) April 1976, R/V ACANIA Experiment

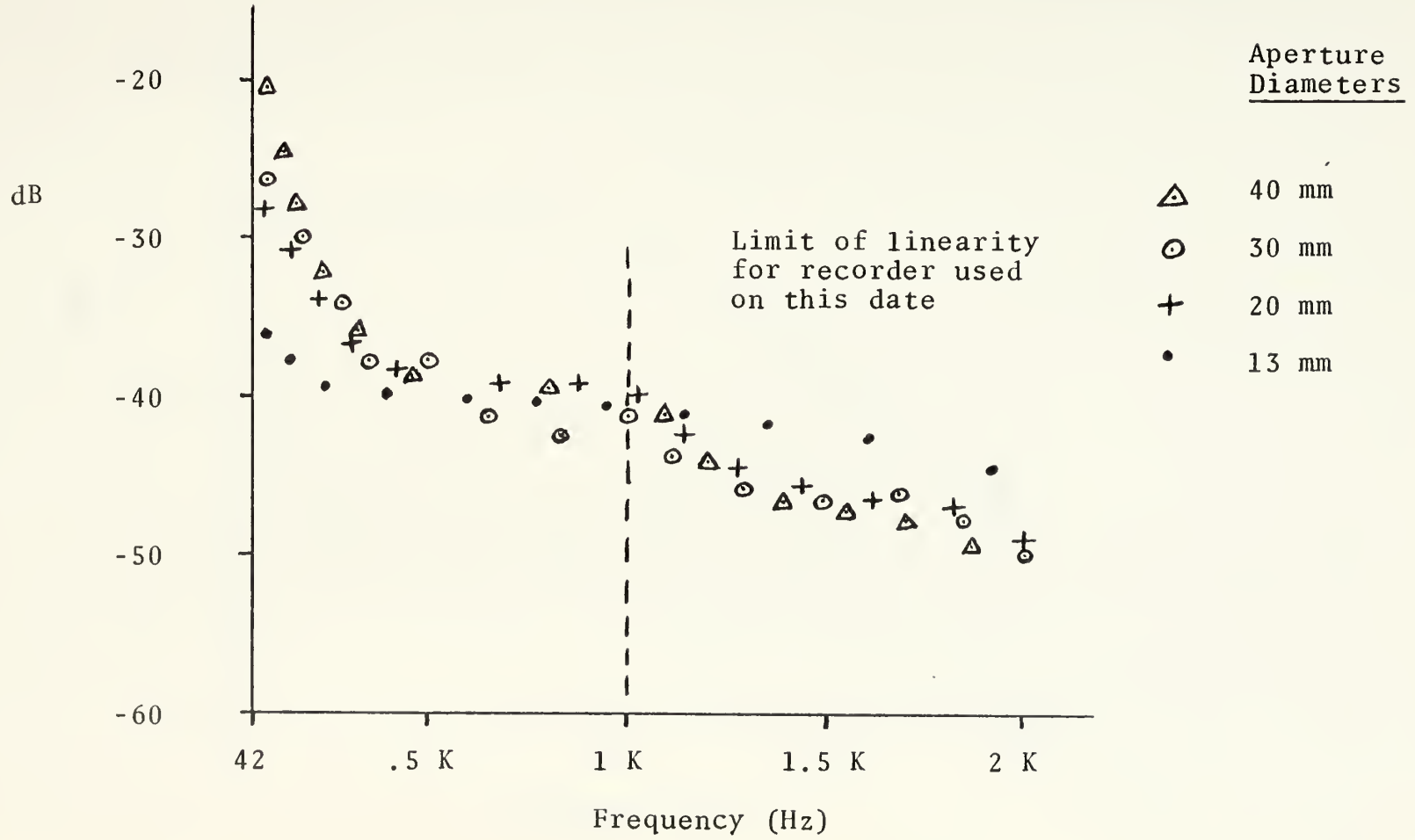

Figure 34

Typical Power Spectrum
9 April 1976, Corridor Experiment
Aperture Diameter = 24.3 mm

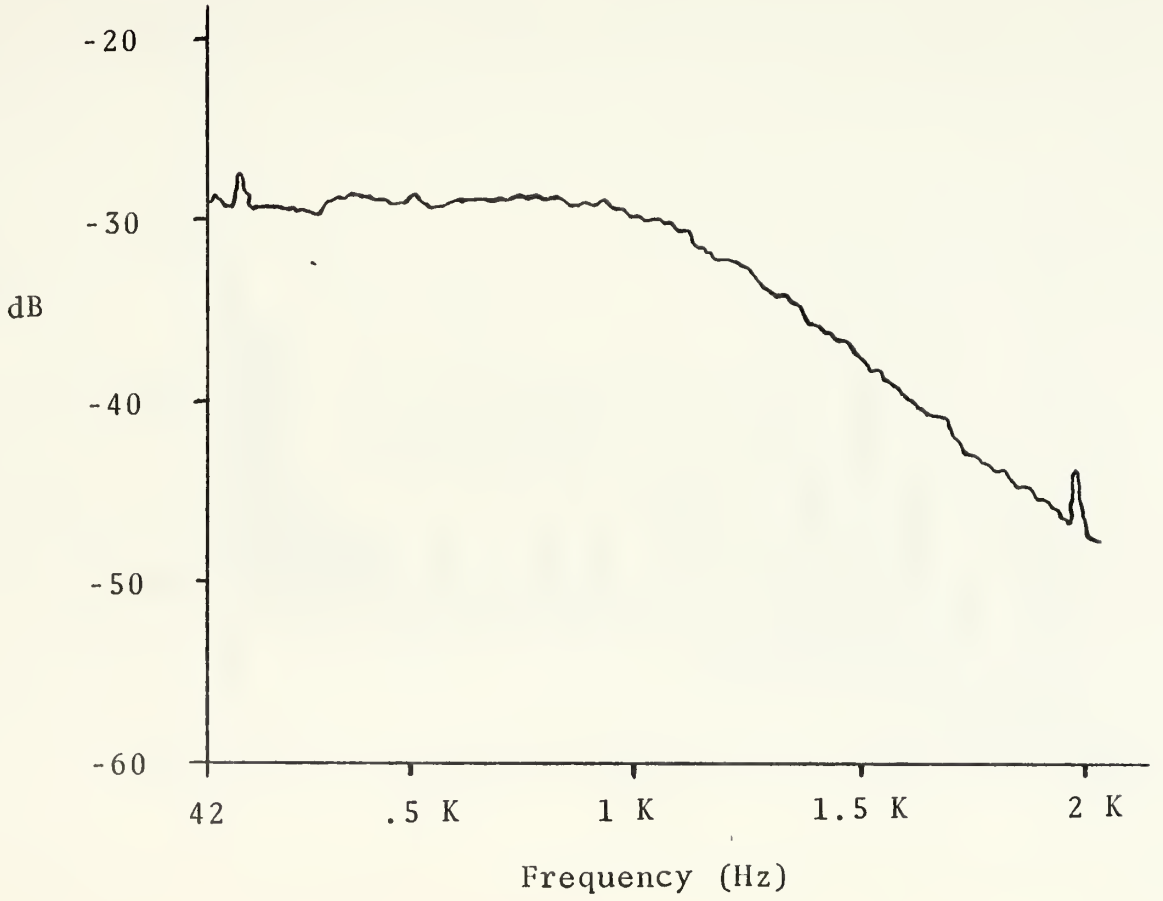

Figure 35

Typical Power Spectrum
20 April 1976, Over Land Experiment
Aperture Diameter = 24.3 mm
Peak frequencies recorded from spectrum analyzer digital readout.

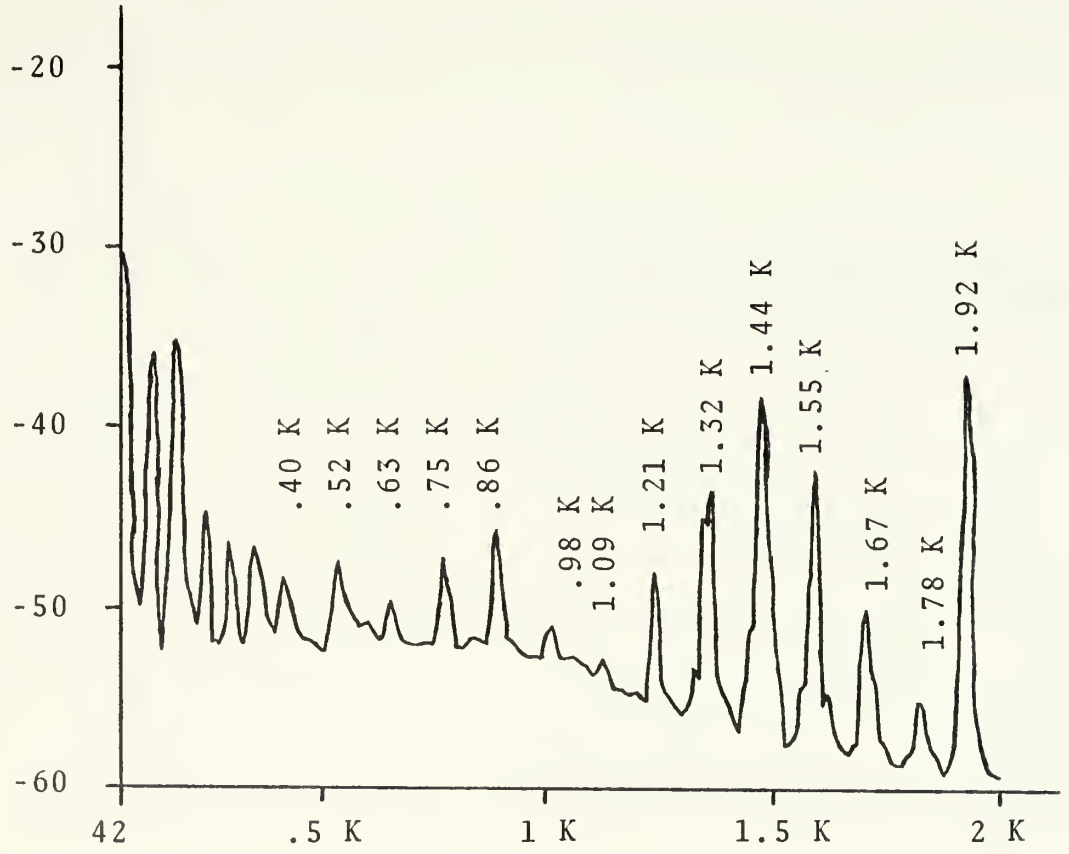

Figure 36

Typical Power Spectrum
(29-30) April 1976, R/V ACANIA Experiment
Aperture Diameter = 25 mm

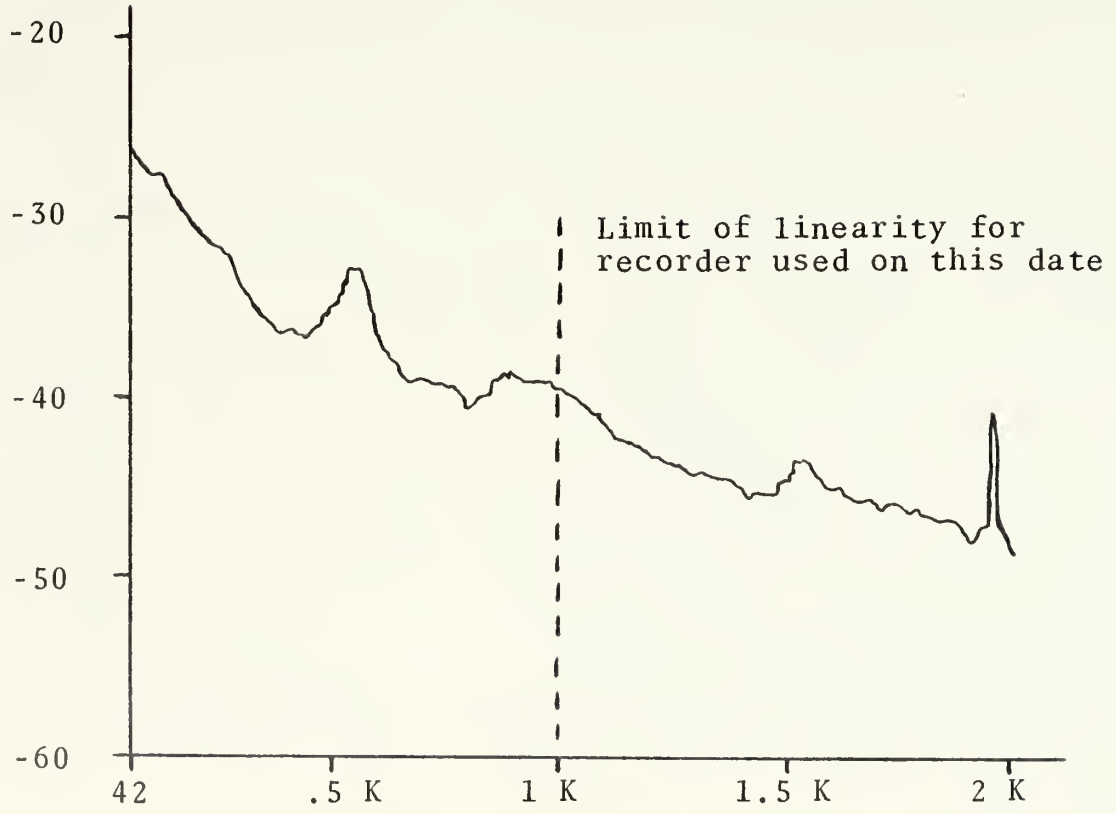

Figure 37

Log Ω vs. % of Maximum dB Scale Setting

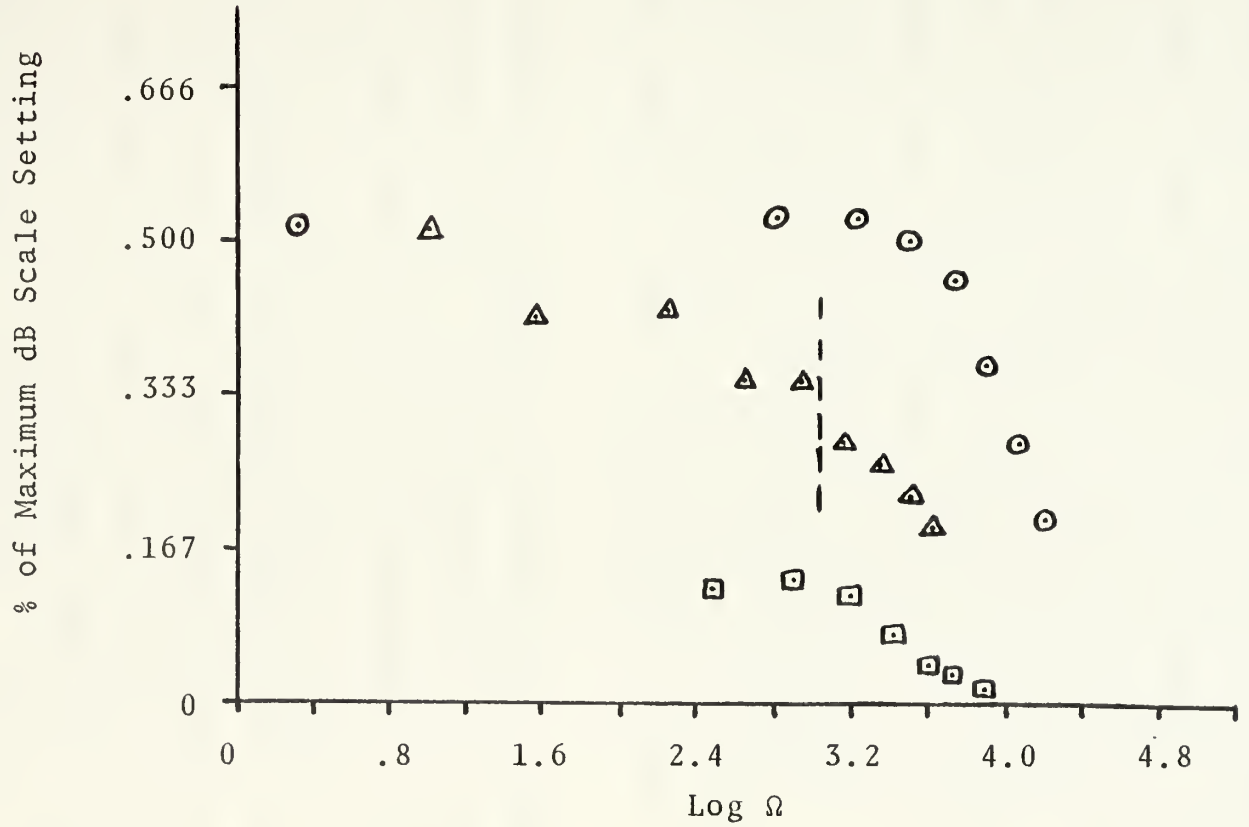

⊙ (7-9) Apr ⊡ 20 Apr △ (29-30) Apr (Dashed line: Recorder linearity limit)

APPENDIX B

TEST PROCEDURE AND PERFORMANCE CHARACTERISTICS OF THE TEXAS INSTRUMENTS TYPE TIXL69 LARGE-AREA SILICON AVALANCHE PHOTODIODE

A series of tests was conducted to evaluate the detection capabilities and performance characteristics of the TIXL69 avalanche photodiode detector and to compare them with that of the PIN-5DP photodiode detector. The two detectors were evaluated at a signal intensity comparable to that anticipated during a typical at-sea data run, i.e., about $1.4X10^{-9}W/cm^2$ (the intensity of a 5 mW He-Ne (6328Å) laser source at a distance of about .8 nautical miles and with a beam divergence of 7 milliradians).

The circuit used with the avalanche detector is illustrated in Figure B1(a). The reverse bias voltage source was a Hewlett Packard Harrison 6515A DC Power Supply.

Dark current as a function of reverse bias voltage was measured first to see if it compared with the manufacturer's stated values of $3.5X10^{-9}A$ minimum to $1.1X10^{-7}A$ maximum. The test circuit used is shown in Figure B1(b). During this experiment the avalanche detector was covered by black cloth to keep light from hitting the detector surface. There were no windows in the enclosed room, all room lights were out, and the room was completely dark. A flashlight was used for recording data. To ensure that

the voltage applied was actually occurring as a voltage drop across the avalanche photodiode, a Hewlett Packard 419A Null Voltmeter was connected to the circuit as shown. The voltmeter indicated that the avalanche photodiode was indeed receiving the full potential drop. Using a Keithley Instruments 600B Electrometer to measure the current, it appeared that values in the nanoamp region were occurring. However, the current indicator was not stable and repetitive current readings at the same reverse bias voltage fluctuated greatly. It was decided that a more accurate ammeter was needed and a Keithley Instruments 410 Micro-Microammeter was obtained. Steady, repeatable values of current were now attained for specific reverse bias voltages.

As shown in Figure B2, dark current was linear with applied reverse bias voltage from 20 volts through 157.5 volts, then increased by a factor of about 10^3 at an applied voltage of 160 volts. Dark current values were higher than that stated by the manufacturer by a factor of 10^2 at low applied reverse bias voltages, decreasing to a factor of 10 higher at high values. For this particular detector, breakdown occurs at a reverse bias voltage of 160 volts vice the manufacturer's indicated 166 volts.

The HP Harrison 6515A DC voltage source was then replaced by a battery box consisting of a series of seven 22.5 volt and one 1.5 volt batteries to be used with the avalanche detector during actual aperture averaging

experiments. The "Dark Current vs. Reverse Bias Voltage" experiment was repeated. The same equipment and circuit as described above was used and dark current values obtained with the battery box were identical to those obtained with the HP Harrison 6515A DC source.

With the breakdown voltage known, the next test was to examine the "Signal-to-Noise Ratio vs. Reverse Bias Voltage" at signal intensities similar to those previously described under at-sea conditions. The experimental setup was as shown in Figure B3. The signal source was a .5 mW He-Ne (6328Å) laser. The laser beam was passed through a +8 cm focal length lens followed by a signal chopper located just beyond the focal point of the lens, then proceeded a distance of 3.35 meters to the avalanche detector. The avalanche detector was mounted on a stand that permitted horizontal and vertical movement in order to maximize signal intensity appearing on the oscilloscope. The signal from the detector was sent to a PAR (Princeton Applied Research) Model 113 Pre-Amp, then to a Monsanto AM-6419/USM-368 oscilloscope for display. External triggering was used on the oscilloscope. To obtain the desired signal intensity, a Jodon Model PM-550 Digital Optical Power Monitor, placed at the location of the avalanche detector, measured signal intensity directly. With the uninterrupted laser beam incident on the Jodon detector at close range (about 10 cm), the Power Monitor indicated a maximum power output of .39 mW. The diameter of the laser beam was 6 mm wide while the diameter

of the active detection area of the Jodon detector is 3 mm. Since the laser beam is theoretically (and appeared to be from visual inspection) Gaussian, roughly 87% of the output intensity was incident on the Jodon detector active area, covering it completely, and giving a source power output of $5.5X10^{-3}W/cm^2$. At the position of the avalanche detector, the intensity had decreased, due to beam expansion from the unfocused optics of the source output, to $1.0X10^{-3}W/cm^2$. With the chopper added and running at normal operating speed, the intensity reduced further to $5.7X10^{-4}W/cm^2$. With the diverging lens in place, to complete the setup, intensity decreased to $3X10^{-5}W/cm^2$. To reduce the intensity further, neutral density filters (Kodak Wrattan Filter (in B glass) N.D.4, N.D.3 and N.D.2) were used singly and in combination. With the N.D.4 filter inserted (reduces intensity by 10^{-4}) between the laser and the +8 cm lens, signal intensity was reduced to $3X10^{-9}W/cm^2$, as desired.

When using the PAR, it was found that a saturated signal occurred on the oscilloscope if PAR Gain setting was too high. A saturated signal was identifiable as a rectangular-shaped 8.75 volt signal with normally visible scintillation absent.

On 26 January 1976 an experiment comparing "S/N vs. Reverse Bias Voltage" at a given signal intensity for the avalanche detector was conducted followed by a comparison of "S/N of Avalanche Detector vs. S/N of PIN-5DP Detector" at varying intensities. In both experiments the equipment

setup of Figure B3 was used. PAR settings were: L-F ROLL OFF--100, H-F ROLL OFF--300K, Gain--Variable. The Harrison 6515A DC Power Supply was used to supply reverse bias voltage to the avalanche detector and a 6328Å filter was used in front of the avalanche and PIN photodiode detectors. No lens system was used to focus the incoming light onto the detector active area for either detector. Table BI gives data collected during the "S/N vs. Reverse Bias Voltage" for the avalanche detector, shown graphically in Figure B4. In Table BI, note (1) the lower PAR Gain settings required to avoid saturation as V_{bias} increases beyond 120 volts, and (2) the increase in noise voltage as V_{bias} increases. From Figure B4 it can be seen that S/N increases fairly linearly from a reverse bias voltage of 80 volts through 159 volts. Table BII is a comparison of the performance of the PIN photodiode detector and the avalanche photodiode detector. Both detectors were located at the same distance from the signal source and both used the same PAR and oscilloscope for signal output. It is evident that the avalanche detector, when set at its optimum reverse bias voltage, gives a significant improvement in performance over the PIN photodiode detector, especially at the weaker intensities characteristic of actual field experiments.

A responsivity curve was plotted to compare experimental results with the manufacturer's stated performance characteristics. From Figure B5 it can be seen that experimental

results follow very closely the predicted values with the following exceptions: (1) actual signal gains corresponding to manufacturer's highest predictions were not attained and (2) the maximum reverse bias voltage that could be applied was less than manufacturer indications.

In summary, the TIXL69 avalanche detector proved to give a significant improvement over the PIN-5DP photodiode detector for low intensity signal detection, as anticipated. The maximum (and optimum) reverse bias voltage that can be applied is 159 volts, slightly less than previously expected. Measurements of responsivity agree with manufacturer's stated values but do not attain the highest values predicted.

Figure B1(a)
Circuit Diagram: Avalanche Photodiode Detector

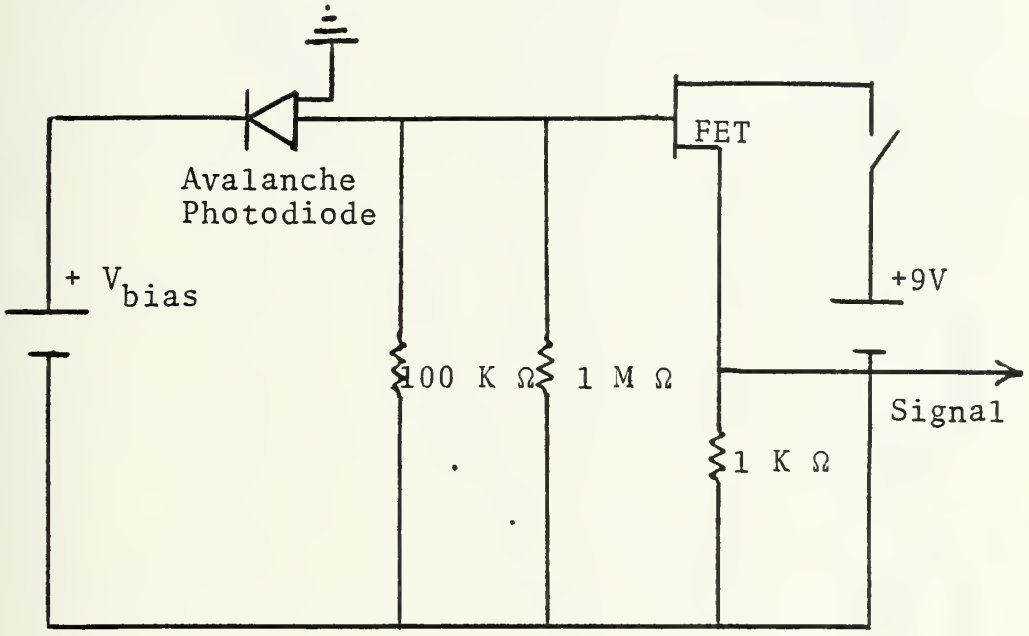

Figure B1(b)
Test Setup: Dark Current Experiment

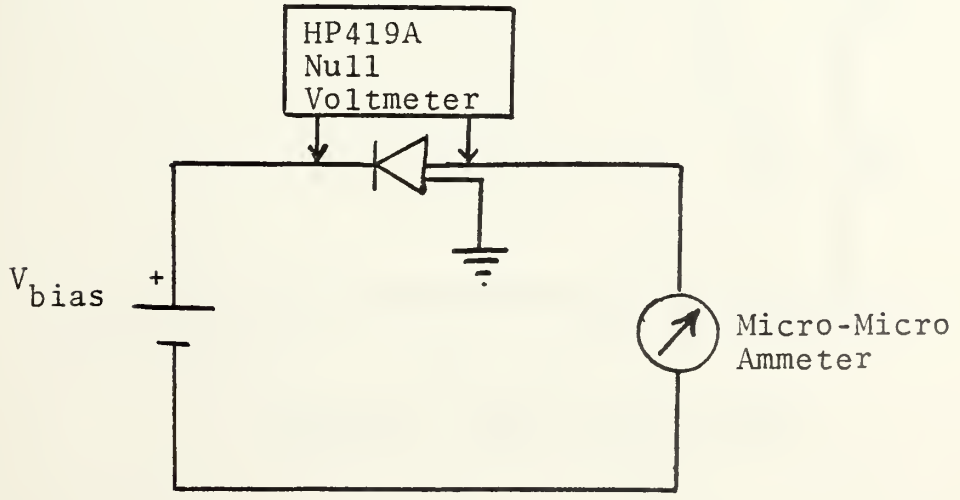

Figure B2

Dark Current vs. Reverse Bias Voltage
21 January 1976

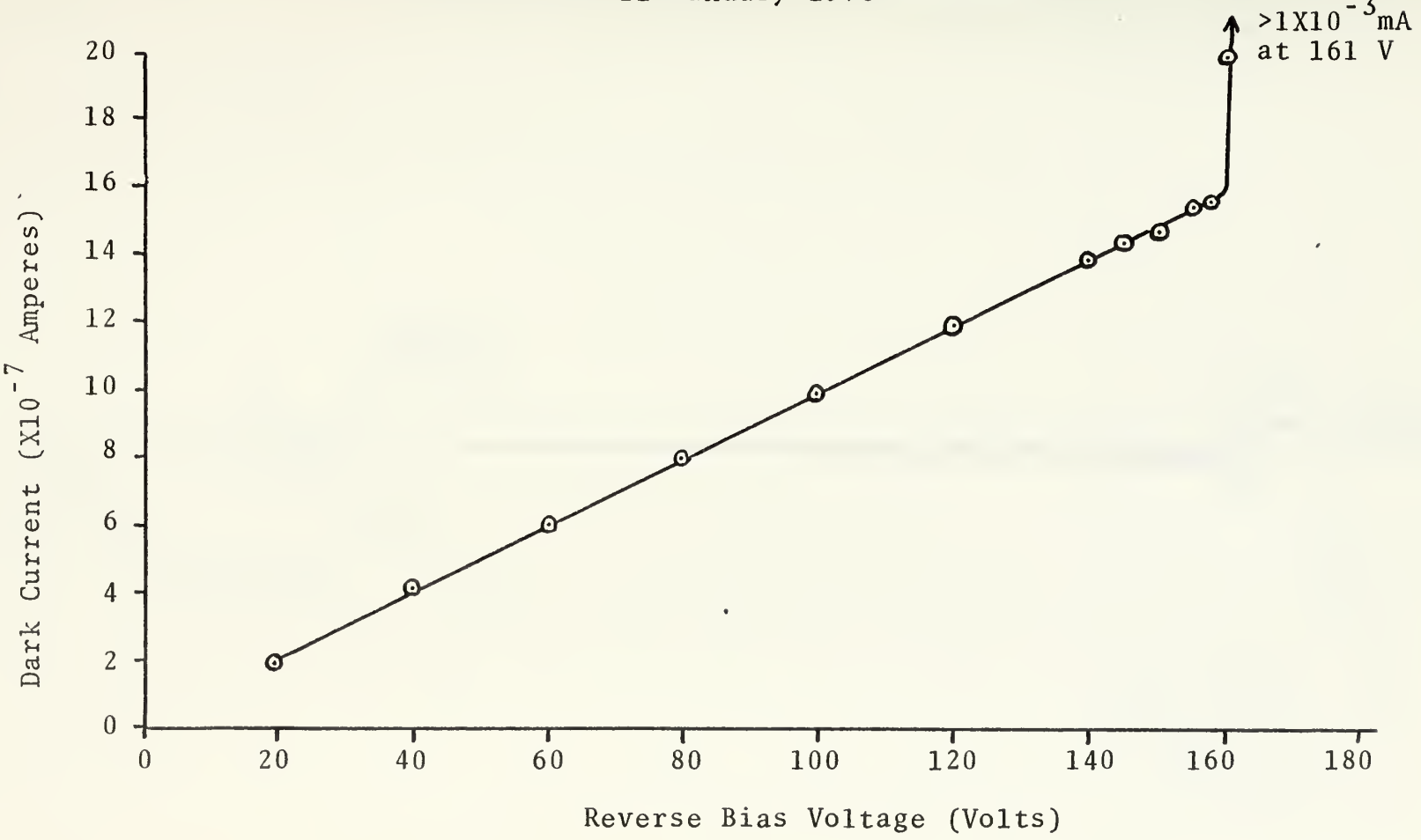

Figure B3

S/N Experimental Setup for Comparing Avalanche and PIN-5DP Photodiode Performance

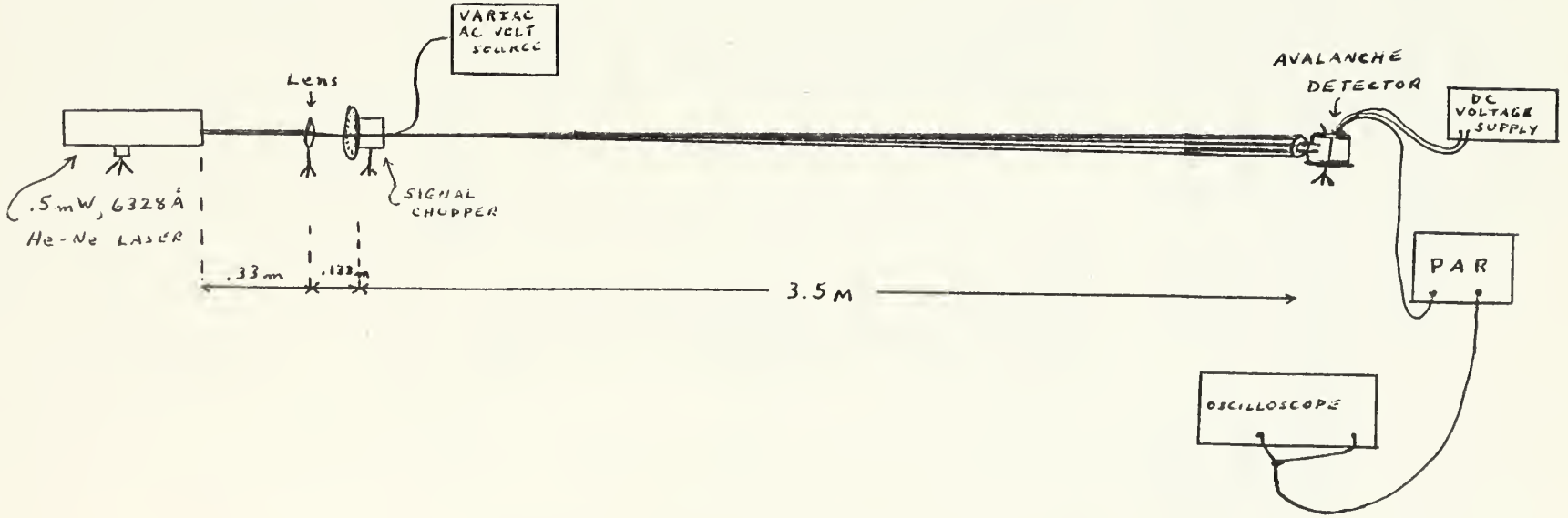

TABLE BI

S/N VS. V_{BIAS}

FOR AVALANCHE DETECTOR

26 January 1976, Source: .5mW, 6328 Å He-Ne laser. Using chopped signal and diverging lens, as shown in Figure B3, signal intensity using N.D.F 4 ≈ $3X10^{-9}W/cm^2$.

V_{BIAS}	PAR GAIN	$V_{(NOISE)}$	$V_{(SIGNAL)}$	S/N
20V	10K	.55V	1.4V	2.5
50V	10K	.60V	1.55V	2.6
80V	10K	.65V	1.9V	2.9
100V	10K	.70V	2.75V	3.9
120V	10K	1.05V	5.25V	5.0
140V	5K	1.25V	7.0V	5.6
150V	2K	1.10V	6.5V	5.9
155V	1K	1.00V	6.0V	6.0
159V	200	.70V	4.35V	6.2
160V	NO SIGNAL			

Figure B4

S/N vs. V_{bias} for Avalanche Detector

26 January 1976

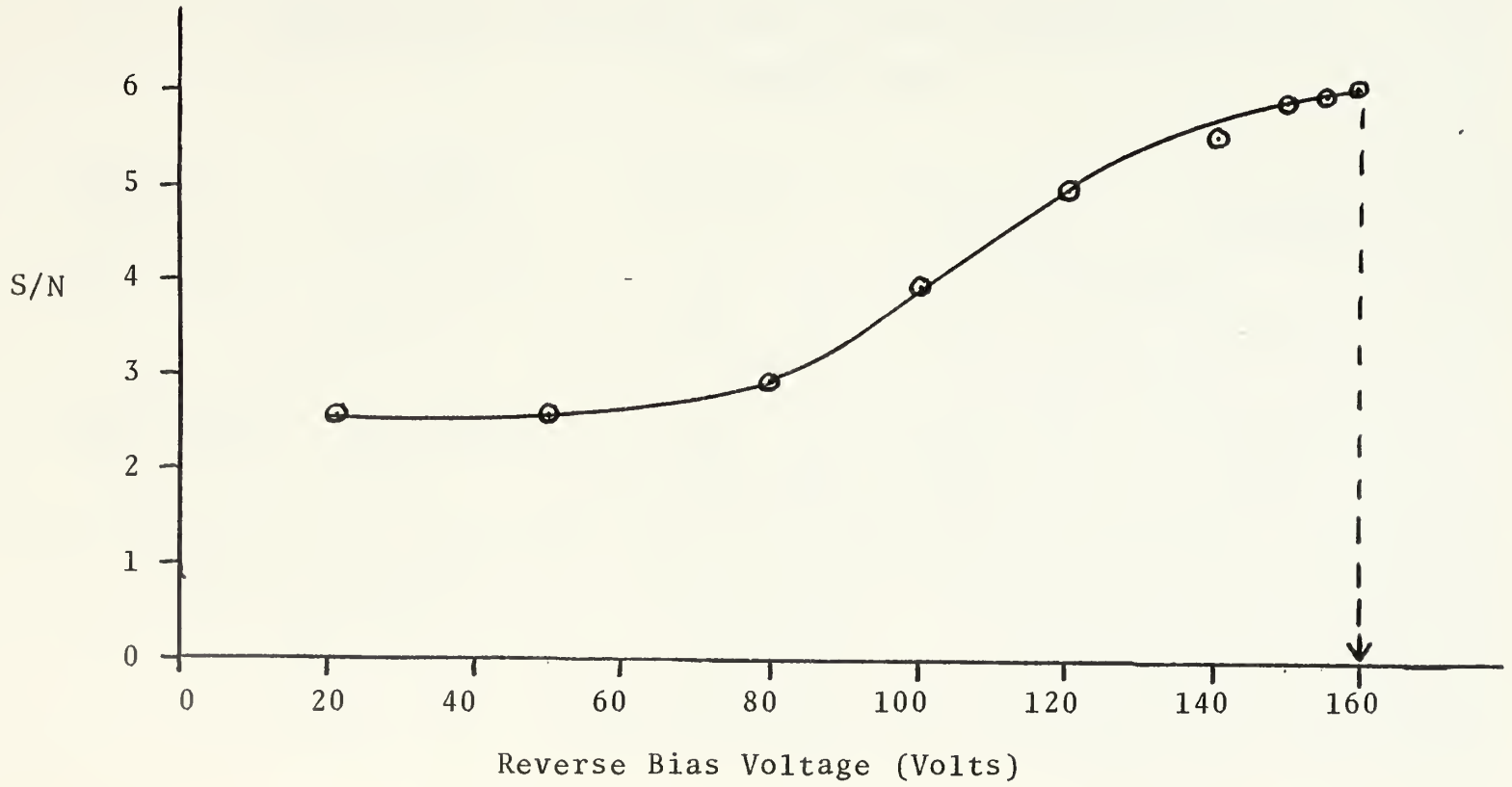

TABLE BII

COMPARISON OF AVALANCHE AND PIN-5DP PHOTODIODE DETECTORS

26 JANUARY 1976

INTENSITY	DETECTOR	PAR GAIN	$V_{(NOISE)}$	$V_{(SIGNAL)}$	S/N
$1X10^{-9}W/cm^2$	Avalanche	200	Saturated Signal		> 17.5
	PIN	10K	1.1V	5.0V	4.5
$1X10^{-10}W/cm^2$	Avalanche	200	0.7V	4.35V	6.2
	PIN	10K	1.0V	1.0V	1.0

Figure B5

Comparison of Manufacturer's Predicted and Empirical Responsivities

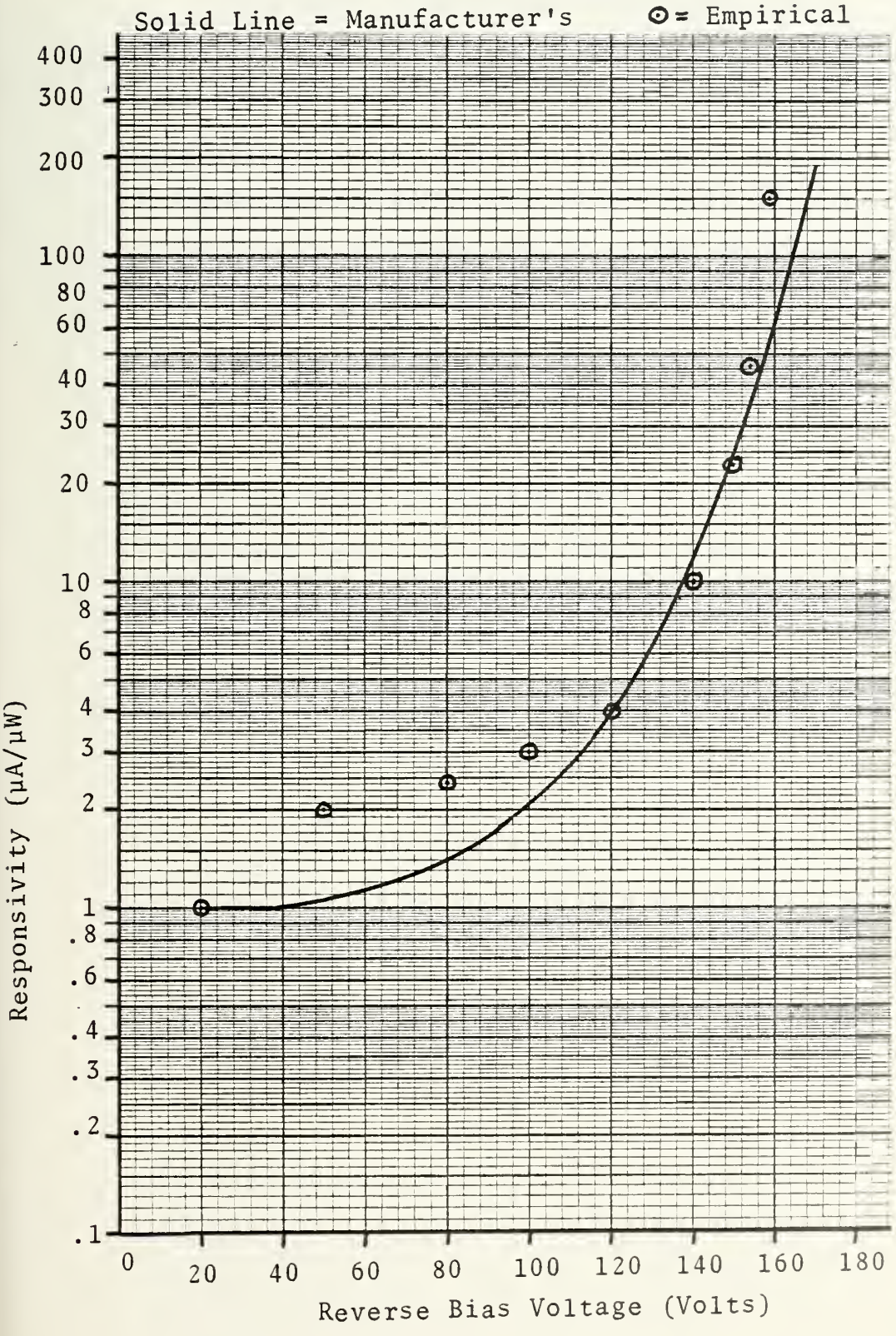

APPENDIX C

EQUIPMENT PERFORMANCE CHARACTERISTICS

1. Precision Instruments, Model No. PI-6204, four-channel recorder:

   Input sensitivity, .05 to 10 volts rms;

   Frequency response, DC to 10 KHz $\pm$3 dB at 37.5 ips on FM Record;

   Signal to Noise Ratio, 35 dB at 37.5 ips, 300 Hz to 100 KHz.

2. Sanborn HP-3914, 14-channel Analog Tape Recorder:

   Maximum Input, 5 volts (peak to peak);

   Gain, unity from 0 to 850 Hz, -.23 dB at 1 KHz;

   Tape Speed 7.5 ips.

LIST OF REFERENCES

1. Lutomirski, R.F, and Yura, H. T., Degradation of Laser Systems by Atmospheric Turbulence, The Rand Corporation, p. 1-64, R-1171-ARPA/RC, June 1973.

2. Strohbehn, J. W., "Line-of-Sight Wave Propagation through the Turbulent Atmosphere," Proceedings of the IEEE, p. 1301-1317, Aug. 1968.

3. Wheelon, A. D., "Radio Wave Scattering by Tropospheric Irregularities," J. Res. NBS (Radio Propagation), Vol. 63D, p. 205-233, 1959.

4. Wheelon, A. D., "Radio Scattering by Tropospheric Irregularities," J. Atmospheric Terrest. Phys., Vol. 15, p. 185-205, 1959.

5. De Wolf, D. A., "Wave Propagation through Quasi-Optical Irregularities," Journal of the Optical Society of America, Vol. 55, p. 812-817, 1965.

6. Heidbreder, G. R., "Multiple Scattering and the Method of Rytov," Journal of the Optical Society of America, Vol. 57, p. 1477-1479, 1967.

7. Tatarski, V. I., Propagation of Waves in a Turbulent Atmosphere (in Russian), Moscow, Nauka, p. 280-285, 1967.

8. Tatarski, V. I., IZV. VUZ. RADIOFIZ, Vol. 5, p. 490-507, 1962.

9. Brown, W. P., Jr., "Validity of the Rytov Approximation in Optical Propagation Calculations," Journal of the Optical Society of America, Vol. 56, p. 1045-1052, 1966.

10. Strohbehn, J. W., "Comments on Rytov's Method," Journal of the Optical Society of America, Vol. 58, p. 139-140, 1958.

11. Tatarski, V. I., op. cit. [7], p. 326-333.

12. De Wolf, D. A., "Multiple Scattering in a Random Continuum," Radio Science, Vol. 2, p. 1379-1392, 1967.

13. De Wolf, D. A., "Saturation of Irradiance Fluctuations due to Turbulent Atmosphere," Journal of the Optical Society of America, Vol. 58, p. 461-466, 1968.

14. Gracheva, M. E. and Gurvich, A. S., "On Strong Fluctuations of the Intensity of Light when Propagating in the Lower Layer of the Atmosphere," IZV. VUZ. RADIOFIZ, Vol. 8, p. 717-724, 1965.

15. Gracheva, M. E., "Research into the Statistical Properties of the Strong Fluctuations of Light when Propagated in the Lower Layer of the Atmosphere," IZV. VUZ. RADIOFIZ, Vol. 10, p. 775-787, 1967.

16. Fried, D. L., Mevers, G. E., and Keister, M. P., "Measurements of Laser Beam Scintillations in the Atmosphere," Journal of the Optical Society of America, Vol. 57, p. 787-797, 1967.

17. Yura, H. T., "Temporal-Frequency Spectrum of an Optical Wave Propagating under Saturation Conditions," Journal of the Optical Society of America, Vol. 64, 0. 357-359, March 1974.

18. De Wolf, D. A., "Strong Irradiance Fluctuations in Turbulent Air: Plane Waves," Journal of the Optical Society of America, Vol. 63, p. 171-179, February 1973.

19. Clifford, S. F., "Temporal-Frequency Spectra for a Spherical Wave Propagating through Atmospheric Turbulence," Journal of the Optical Society of America, Vol. 61, p. 1285-1292, October 1971.

20. Tatarski, V. I., The Effects of the Turbulent Atmosphere in Wave Propagation, National Science Foundation, 1971.

21. Fried, D. L., "Aperture Averaging of Scintillation," Journal of the Optical Society of America, Vol. 57, p. 169-175, February 1967.

22. Homstad, G. E., and Heneghan, J. M., "Aperture-Averaging Effects for Weak Scintillations," Journal of the Optical Society of America, Vol. 64, p. 162-165, February 1974.

23. Kerr, J. R., "Experiments on Turbulence Characteristics and Multiwavelength Scintillation Phenomena," Journal of the Optical Society of America, Vol. 62, p. 1040-1049, September 1972.

24. Dunphy, J. R. and Kerr, J. R., "Scintillation Measurements for Large Integrated-Path Turbulence," Vol. 63, p. 981, August 1973.

25. Brown, W. P., Jr., "Fourth Moment of a Wave Propagating in a Random Medium," Journal of the Optical Society of America, Vol. 62, p. 966, August 1972.

26. Clifford, S. F., JOSA, p. 471, Vol. 63 (1973).

27. Strohbehn, J. W., and Homstad, G., "Probability Distribution and Aperture Averaging Effects in Optical Scintillation," Digest of Technical Papers, Topical Meeting on Optical Propagation through Turbulence.

28. Schroeder, A. F., Jr., Laser Scintillation Properties in the Marine Boundary Layer, M. S. Thesis, Naval Postgraduate School, Monterey, December 1973.

29. Höhn, D. H., "Effects of Atmospheric Turbulence on the Transmission of a Laser Beam at 6328 Å II - Frequency Spectra," Applied Optics, Vol. 5, p. 1433-1436, September 1966.

30. Kerr, J. R., Multiwavelength Laser Propagation Study, Vols. I-IV, Oregon Graduate Center, Portland, Oregon (ARPA), 1970 to present.

31. Plett, J. L., Pulse Height Analyzer Interfacing and Computer Programming in the Environmental Laser Propagation Project, M. S. Thesis, Naval Postgraduate School, Monterey, June 1976.

32. Johnson, W. B., Evans, W. E. and Uthe, E. E., Atmospheric Effects upon Laser Eye Safety, Part I, Stanford Research Institute, April 1970.

33. Dabberdt, W. F. and Johnson, W. B., Atmospheric Effects upon Laser Eye Safety, Part II, Stanford Research Institute, May 1971.

34. Ochs, G. R., Bergman, R. R. and Snyder, J. R., "Laser Beam Scintillation over Horizontal Paths from 5.5 to 145 km," Journal of the Optical Society of America, Vol. 59, No. 2, 1969, p. 231.

35. Gracheva, M. E., IZV. VYSSH. UCHEB. ZAVED. RADIOFIZ, Volume 13, No. 55, 1970.

36. Ochs, G. R., "Measurements of 0.63 μm Laser Beam Scintillation in Strong Atmospheric Turbulence," ESSA Tech. Report. No. ERL. 154-WPL10 (U.S. Government Printing Office, Washington, D. C., 1970).

INITIAL DISTRIBUTION LIST

		No. Copies
1.	Defense Documentation Center Cameron Station Alexandria, Virginia 22314	2
2.	Library, Code 0212 Naval Postgraduate School Monterey, California 93940	2
3.	Department Chairman, Code 61 Department of Physics and Chemistry Naval Postgraduate School Monterey, California 93940	2
4.	Professor A. W. Cooper, Code 61 Cr Department of Physics and Chemistry Naval Postgraduate School Monterey, California 93940	6
5.	LT Howard R. Hall, USN 300 Glenwood Circle, Apt. 283 Monterey, California 93940	2

166528

Thesis
H1478 Hall
c.1

Aperture averaging effects on scintillation and the temporal-frequency power spectrum.